On local panel distortions due to hot-curing adhesive

On local panel distortions due to hot-curing adhesives

antin Pr

Konstantin Priesnitz

ISBN 978-94-6295-359-8





ON LOCAL PANEL DISTORTIONS DUE TO HOT-CURING ADHESIVES



ON LOCAL PANEL DISTORTIONS DUE TO HOT-CURING ADHESIVES

Proefschrift

ter verkrijging van de graad van doctor aan de Technische Universiteit Delft, op gezag van de Rector Magnificus prof. ir. K. C. A. M. Luyben, voorzitter van het College voor Promoties, in het openbaar te verdedigen op vrijdag 2 october 2015 om 12:30 uur

door

Konstantin Priesnitz

Diplom-Ingenieur der Physikalischen Ingenieurwissenschaft, Technische Universität Berlin, Duitsland, geboren te Berlijn, Duitsland. Dit proefschrift is goedgekeurd door de promotor:

Prof. dr. ir. R. Benedictus

Copromotor: Ir. J. Sinke

Samenstelling promotiecommissie:

Rector Magnificus, voorzitter

Prof. dr. ir. R. Benedictus, Technische Universiteit Delft, promotor Ir. J. Sinke, Technische Universiteit Delft, copromotor

Onafhankelijke leden:

Prof. dr. ir. R. Marissen, Technische Universiteit Delft Prof. Dr. rer. nat. W. H. Müller, Technische Universität Berlin Prof. dr. ir. I.M. Richardson. Technische Universiteit Delft Dr. ir. K.M.B. Jansen, Technische Universiteit Delft

Andere leden:

Prof. dr. W.A. Groen, Technische Universiteit Delft

Ir. J. Sinke heeft als begeleider in belangrijke mate aan de totstandkoming van het proefschrift bijgedragen.





This research was carried out under project number M22.8.10384 in the framework of the Research Program of the Materials innovation institute M2i (www.m2i.nl).

Keywords: adhesive bonding, automotive, bond-line readout, bond-line read-

through, chemical shrinkage, cure, distortion, residual stress, sur-

face defect

Printed by: Uitgeverij BOXPress || Proefschriftmaken.nl, 's-Hertogenbosch

Front & Back: Uitgeverij BOXPress || Proefschriftmaken.nl, 's-Hertogenbosch

Copyright © 2015 by K. Priesnitz

ISBN 978-94-6295-359-8

An electronic version of this dissertation is available at

http://repository.tudelft.nl/.





SUMMARY

For many joining applications, adhesive bonding is the favoured method. It provides the ability to join dissimilar materials such as metals and plastics. Adhesive bonds can be formed over large flange areas subsequently increasing the overall stiffness of the assembly. In some cases, however, the bonding process can lead to distortions, *i.e.* unwanted visible deformations, especially if thin-walled structures such as car body panels are involved. These deviations from the intent shape might not affect the structural integrity of a part, but, if visible to customers on a product's surface, they can be considered an aesthetic flaw. Distortions can be divided in local ones, which occur close to the bond line, and global ones, which affect the geometry of the entire assembly.

In this thesis, the development of local panel distortions that occur in a hot-cure cycle of an adhesive is studied. A laboratory sample is exposed to temperature cycles with different heating rates and cure temperatures; the displacement of a steel strip is monitored. The panel curvatures are measured after cure cycles with and without a dwelling step at elevated temperature before the cure temperature is reached. A simulation model is developed that takes thermal and chemical volume changes, the cure evolution, the liquid-solid transition and stress relaxation of the adhesive into account. Mechanical properties and expansion coefficients were measured and integrated in the simulation model. Simulation results are compared with data from the experiments. The sensitivity of the predictions of distortions to changing material properties is investigated.

Distortions can arise early in the cure cycle. Even during the heating phase, panels can start to deform. The model predicts well the development of distortions. The influence of the temperature cycle on distortions is also reproduced by the model due to the hypo-elastic formulation of the stress-strain relation during cure. A pre-cure step can be used to reduce distortions. The model can reproduce that. Improvements, however, might be in a range in which also other effects play a role, such as deviations of adherends from an intended shape before the bonding process. Predictions showed different sensitivities to changing material constants. In a set-up where the adhesive is not confined, the bulk modulus did not show any significant influence on the predictions of distortions, so that an estimate for it may suffice. Chemical shrinkage, however, needs to be measured in-situ or should be corrected from measurements at room temperature

viii Summary

to fit the real behaviour at elevated temperatures, since the influence on distortions is strong. The gel point, as the transition point from liquid to solid, has also a significant influence on predictions of distortions and should be determined with sufficient accuracy.

SAMENVATTING

Voor vele verbindingstoepassingen is lijmen de geprefereerde methode. Het biedt de mogelijkheid om verschillende materialen te verbinden, zoals metalen en plastics. Lijmverbindingen kunnen worden gevormd over grote flensoppervlakken, wat de algehele stijfheid van de assemblage vergroot. Echter, in sommige gevallen kan het lijmproces leiden tot vertekeningen, d.w.z. ongewenste zichtbare vervormingen, vooral als er sprake is van dunwandige constructies zoals autocarrosseriepanelen. Deze afwijkingen van de gewenste vorm beïnvloeden wellicht niet de structurele integriteit van een onderdeel, als ze op het oppervlak van een product zichtbaar zijn voor klanten kunnen ze worden gezien als een esthetische tekortkoming. Vertekeningen kunnen worden verdeeld in lokale vertekeningen, die plaatsvinden dicht op de verbindingslijn, en globale, die de geometrie van de gehele assemblage beïnvloeden.

In dit proefschrift wordt de ontwikkeling bestudeerd van lokale paneelvertekeningen die plaatsvinden in een hete-uithardingscyclus van een lijm. Een laboratoriummonster wordt blootgesteld aan temperatuurcycli met verschillende opwarmingssnelheden en uithardingstemperaturen. Daarbij wordt de verplaatsing van een stalen strip gemeten. De paneelkrommingen worden gemeten na uithardingscycli met en zonder een verblijftijd op verhoogde temperatuur, voordat de uithardingstemperatuur is bereikt. Een simulatiemodel wordt ontwikkeld dat rekening houdt met thermische en chemische volumeveranderingen, de evolutie van de uitharding, de vloeibaar-vast overgang en de spanningsloslating van de lijm. Mechanische eigenschappen en expansie-coëfficiënten werden gemeten en geïntegreerd in het simulatiemodel. Resultaten van de simulatie worden vergeleken met data van de experimenten. De gevoeligheid voor veranderende materiaaleigenschappen van de voorspellingen van vertekeningen wordt onderzocht.

Vertekeningen kunnen vroeg in de uithardingscyclus de kop opsteken. Zelfs tijdens de opwarmfase kunnen panelen beginnen te vervormen. Het model voorspelt goed de ontwikkeling van vertekeningen. De invloed van de temperatuurscyclus op vertekeningen wordt ook door het model gereproduceerd dankzij de hypo-elastische formulering van de spannings-rek relatie tijdens uitharding. Een voor-uithardingsstap kan worden gebruikt om vertekeningen te verminderen. Het model kan dat reproduceren. Echter, verbeteringen zouden in een bereik kunnen zijn waarin ook andere effecten een rol spe-

x Samenvatting

len, zoals afwijkingen van een gewenste vorm van de te lijmen onderdelen, voor het lijmproces. Voorspellingen lieten verschillende gevoeligheden voor veranderende materiaalconstanten zien. In een opstelling waarin de lijm niet ingesloten is, vertoonde de compressiemodulus geen significante invloed op de voorspellingen van vertekeningen. Een schatting van de compressiemodulus kan dus volstaan. Chemische krimp moet echter in-situ gemeten worden of moet gecorrigeerd worden van metingen bij kamertemperatuur om het gedrag bij verhoogde temperaturen te passen, aangezien de invloed ervan op vertekeningen groot is. Het gel punt heeft als omslagpunt van vloeibaar naar vast ook een significante invloed op voorspellingen van vertekeningen en moet met voldoende nauwkeurigheid vastgesteld worden.

NOMENCLATURE

ROMAN LETTERS

Symbol	Description	Units
a	Adhesive layer thickness	m
A	Material constant	J/mol
a(T)	Shift factor	-
b_1	Material constant	-
b_2	Material constant	-
C	Tait constant	-
C_0	Material constant	1/K or 1/°C
C_1 , C_2	Constants of the Williams-Landel-Ferry equation	-, K
$C_{ijkl}(t)$	Relaxation tensor	Pa
d	Measured out-of-plane displacement	m
E	Young's modulus	Pa
E(t)	Relaxation function	Pa
$E_{ m a}$	Material constant	J/mol
E_{∞}	Equilibrium modulus	Pa
E_m	mth modulus in Prony series	Pa
E'	Storage modulus	Pa
E''	Loss modulus	Pa
G(t)	Shear relaxation modulus	Pa
G(q)	Cure-dependent equilibrium modulus	Pa
$G^{ ext{ inn}}$	Equilibrium shear modulus after complete cure	Pa
$G_{\!\scriptscriptstyle \mathrm{g}}$	Glassy (instantaneous) shear modulus	Pa
G_{∞}	Equilibrium shear modulus	Pa
G'	Storage shear modulus	Pa
G''	Loss shear modulus	Pa
$h_{{\scriptscriptstyle m L170}}$, $h_{{\scriptscriptstyle m M170}}$,	Heating period in a cure cycle	s
$h_{{\scriptscriptstyle \mathrm{H}170}}$, $h_{{\scriptscriptstyle \mathrm{L}155}}$,		
$h_{\scriptscriptstyle{ ext{M155}}}$, $h_{\scriptscriptstyle{ ext{H155}}}$		

xii Nomenclature

H_{∞}	Total heat of reaction	J/g
H(t)	Accumulated released heat at time <i>t</i>	J/g
J	Jacobi determinant	-
K	Bulk modulus	Pa
K(T)	Temperature-dependent bulk modulus	Pa
K(t)	Bulk relaxation modulus	Pa
k_0	Material constant	1/s
k_1	Material constant	1/K or 1/°C
k_2	Material constant	1/K or 1/°C
m	Reaction order	-
n	Reaction order	-
N_1 , N_2 ,	Node identifier	-
N_3 , N_4 ,		
N_5 , N_6		
p	Hydrostatic pressure	Pa
q	Degree of cure	-
q_0	Initial degree of cure	-
$q_{ m gel}$	Degree of cure at the gel point	-
R	Gas constant, $R = 8.314 \text{ J/(mol K)}$	J/(mol K)
r_1, r_2	Material constants	-
S	Standard distance	m
s_0	Material constant	K/Pa or °C/Pa
t	Time	s
T	Temperature	K or °C
$T_{ m c}$	Cure temperature	K
$T_{ m f}$	Isoconversional temperature	K
$T_{ m g}$	Glass transition temperature	K or °C
$T_{ m gel}$	Temperature at the gel point	K
$T_{\scriptscriptstyle m R}$	Reference temperature	K
$T_{ m trans}$	Transition temperature interval	K
u	Displacement vector	m
u_y	Displacement in <i>y</i> -direction	m
v, v_0, v_4	Specific volume	m ³ /kg
$W_{\rm red}$	= $\omega_{\rm red}$, reduced frequency	1/s
<u>X</u>	Node coordinates in the reference state	m
$x, y, z \text{ or } x_j$	Space coordinates	m

Nomenclature xiii

GREEK LETTERS

α	Coefficient of thermal expansion	1/K
$\alpha(T)$	Temperature-dependent coefficient of thermal ex-	1/K
	pansion	
$lpha_{\scriptscriptstyle \mathrm{g}}$	Coefficient of thermal expansion in the glassy	1/K
	state	
$lpha_{ m r}$	Coefficient of thermal expansion in the rubbery	1/K
	state	
$lpha^{ ext{vol}}$	Volumetric coefficient of thermal expansion	1/K
β	Temperature rate	K/s
β_i, β_{ij}	Main effect and interaction coefficients	m
χ_i	Regression variable	-
δ	Phase lag	-
Δ	Difference	-
δ_{ij}	Kronecker delta	-
ε	One-dimensional strain	-
ε_{ij}	Linear strain tensor	-
$arepsilon^{ m ch},arepsilon_{ij}^{ m ch}$	Chemical strain component	-
$\mathcal{E}_{ ext{tot}}^{ ext{ch}}$	Total chemical strain	-
$ ilde{m{\mathcal{E}}}_{ ext{tot}}^{ ext{ch}}$	Effective chemical shrinkage	-
$arepsilon^{ m me}$, $arepsilon_{ij}^{ m me}$	Mechanical (stress-producing) strain component	-
$arepsilon_{ij}^{ ext{me,dev}}$	Deviatoric part of the mechanical strain compo-	-
• •	nent	
ε^{th} , $\varepsilon^{\text{th}}_{ij}$	Thermal strain component	-
η	Zero-shear-rate viscosity	Pa s
$\eta_{\it m}$	mth viscosity in a generalized Maxwell model	Pa s
$\eta_{m}^{\scriptscriptstyle m R}$	$\it m$ th relaxation time at a reference temperature	s
γ	Response variable in a regression model	m
ν	Possion ratio	-
ω	Radial frequency	1/s
σ	One-dimensional stress	Pa
$\sigma_{ij}^{ ext{ iny dev}}$	Deviatoric part of the Cauchy stress	Pa
$\sigma^{ ext{ iny el}}_{ij}$	Elastic stress component	Pa
σ_{ij}	Cauchy stress tensor	Pa
$\sigma_{ii}^{ ext{vi}}$	Viscoelasic stress component	Pa

xiv Nomenclature

τ_m	<i>m</i> th relaxation time	S
ξ	Material time, reduced time	s

ABBREVIATIONS

Abbreviation	Description
A	Cure cycle identifier
BM1496V	BETAMATE™1496V
Chem.	Chemical strain
CTE	Coefficient of thermal expansion
DIC	Digital Image Correlation
DMA	Dynamic Mechanical Analyser
DSC	Differential Scanning Calorimeter
ech	$=arepsilon_{ m tot}^{ m ch}$
Gg	$=G_{\mathrm{g}}$
Ginf	$=G_{\infty}$
H155, H170	Cure cycle with a high heating rate and a cure tem-
	perature of 170 and 155 °C, respectively
K	Bulk modulus
L155, L170	Cure cycle with a low heating rate and a cure tem-
	perature of 170 and 155 °C, respectively
loga	$=\log a(T)$
M155, M170	Cure cycle with a medium heating rate and a cure
	temperature of 170 and 155 °C, respectively
NP170	Cure cycle with no pre-cure step and a cure tem-
	perature of 170 °C
P170	Cure cycle with pre-cure step and a cure tempera-
	ture of 170 °C
qdot	$=\dot{q}$
qgel	$=q_{ m gel}$
Th.	Thermal strain
TMA	Thermomechanical Analyser
W	With adhesive
WO	Without adhesive

CONTENTS

Sı	ımm	ary		vii
Sa	men	vatting		ix
No	omen	ıclatur	e	хi
1	Intr	oducti	on	1
	1.1	Scope	e of this thesis	. 2
	1.2	Mate	rial	. 3
	Refe	erences	3	. 3
2	Bac	kgroui	nd	5
	2.1	Introd	duction	. 5
	2.2	Panel	distortions due to hot-curing adhesives	. 6
		2.2.1	Types	. 6
		2.2.2	Causes and development	. 8
		2.2.3	Suggested strategies to avoid distortions	. 9
		2.2.4	Visual evaluation of distorted surfaces	. 9
	2.3	Linea	r viscoelasticity	. 10
		2.3.1	Response to sinusoidal strain excitation	. 12
		2.3.2	Three-dimensional stress-strain relation	. 13
		2.3.3	Thermorheologically simple material	. 14
	2.4	The c	ure process	. 16
		2.4.1	Degree of cure	. 16
		2.4.2	Chemical shrinkage	. 17
		2.4.3	Gelation	. 18
		2.4.4	Glass transition	. 19
	2.5	Mode	elling approaches	. 20
		2.5.1	Linear elasticity	. 20
		2.5.2	Linear viscoelasticity	. 20
		2.5.3	Chemical shrinkage	. 20

xvi Contents

		2.5.4	Cure-dependent models
		2.5.5	Temperature cycles
	2.6	Discu	ssion and conclusions
	Refe	erences	23
3	Infl	uence (of the temperature cycle 31
	3.1		luction
		3.1.1	Literature Review
		3.1.2	Research questions of interest
	3.2	Strate	gy
	3.3	Exper	iment and displacement estimate
		3.3.1	Experimental procedure
		3.3.2	Differential Scanning Calorimetry
		3.3.3	Displacement estimate
	3.4	Resul	ts
		3.4.1	Temperature cycles with 170 °C cure temperature
		3.4.2	Temperature cycles with 155 °C cure temperature 44
		3.4.3	Differential Scanning Calorimetry
	3.5	Discu	ssion
	3.6	Concl	usions
	Refe	erences	3
4	Fini	ite-eler	ment model 51
	4.1	Introd	luction
	4.2	Backg	ground
	4.3		nodel
		4.3.1	Stages of the cure cycle
		4.3.2	Abaqus implementation
		4.3.3	Numerical issues
		4.3.4	Simulation of local distortions
	4.4	Resul	ts
		4.4.1	Cure cycle A
		4.4.2	Other cure cycles
		4.4.3	Long-term behaviour
	4.5	Discu	ssion
		4.5.1	Cure cycle A
		4.5.2	Other cure cycles

CONTENTS xvii

	4.6	Concl	usions
	Refe	rences	
5			naracterization and simulation 71
	5.1		luction
	5.2		ial modelling and characterization
			Cure kinetics
			Volume changes
	5.3		ation
		5.3.1	Constitutive equations
		5.3.2	Finite-element model
	5.4	Result	s and discussion
		5.4.1	Cure kinetics
		5.4.2	Volume changes
		5.4.3	Mechanical properties
		5.4.4	Experiment versus simulation
	5.5	Concl	usions
	Refe	rences	92
6	Mod	lel sens	sitivity and surface measurements 97
	6.1		uction
	6.2		neter study
		6.2.1	Parameters and ranges
		6.2.2	Design plan
		6.2.3	Regression models
	6.3	Bimet	al strip
		6.3.1	Specimen
		6.3.2	Sample preparation and experimental procedure 101
		6.3.3	Simulation model
	6.4	Result	s and discussion
			Parameter study
			Measured and predicted strip deformations
	6.5		usions
7		cussion	
	7.1		ation approach
	7.2	Dietor	tions

xviii Contents

8	Conclusions and recommendations	119		
	8.1 Conclusions	. 119		
	8.2 Recommendations for future work	. 120		
A	Material parameters found in literature	121		
	References	. 122		
В	Regression models fitting results	123		
Ac	cknowledgements	127		
Cı	urriculum Vitæ 129			
Li	st of Publications 131			

1

Introduction

Adhesive bonding is a well-established joining technology in many fields of application. Important advantages over other joining methods, such as spot-welding or mechanical fastening, are a higher stiffness due to a more uniform stress distribution by a continuous joint and the ability to join dissimilar materials. It allows the construction of sandwich structures and multi-layered (fibre-metal) laminates with good damping characteristics and excellent crack resistance for aerospace components. Adhesives are used for direct glazing, hem-flange bonding, anti-flutter bonding, the bonding of plastic components and structural bonds in the automobile industry [1]. The tendency towards a larger material diversity driven by the need to limit vehicle weight and consequently reduce CO_2 emissions strengthens the position of adhesive bonding among other joining methods. Hot-curing one-part adhesives are especially beneficial in car body production: the cure process can be integrated in other thermal cycles after e-coating; additional production steps for surface decontamination are not needed because of their good oil absorption [2].

In some cases, however, the bonding process can lead to distortions, *i.e.* unwanted visible deformations of the assembly. Especially bonding processes at high temperatures and bonding of thin-walled structures like car panels are more sensitive to distortions. The residual stresses that occur during the bonding process can lead to cracks in the adhesive layer and consequently to bond failure. But even if the structural integrity is not affected, distortions can be considered defects. A distorted panel surface is perceived as

2 1. Introduction

a visual quality flaw by the customer and, therefore, unacceptable for manufacturers. On highly polished surfaces such as outer car panels even small deformations remain visible to the human eye.

Panel distortions can be divided into local and global ones. Local distortions occur directly at the bond line while global ones affect the entire geometry of the assembly, see figure 1.1. To prevent the occurrence of distortions, a thorough understanding of how they develop during the bonding process is needed. While experimental studies, such as monitoring the panel position in a bonding process or measuring the panel curvature after cure, are essential for that, process simulations can not only help to predict, but also give deeper insight into the development of distortions.

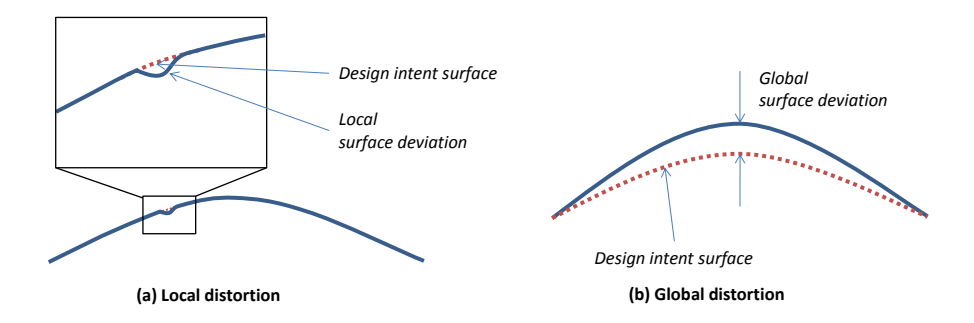


Figure 1.1: Local and global type of panel distortions [3].

1.1. Scope of this thesis

In this work the development of panel distortions due to adhesive bonding is investigated. The research focusses on local distortions that arise during bonding with crosslinking adhesives at elevated temperatures. The objective is to build up a thorough understanding of how local distortions develop over the entire cure cycle. Especially the evolving thermomechanical properties of the adhesive are of interest. One goal is the development of a simulation model that incorporates these properties. By accompanying experimental studies in which panel distortions are monitored, the model provides additional information on how the combination of certain properties, such as chemical shrinkage and a liquid-solid transition, contribute to distortions. Moreover, it allows predictions of distortions for bonding processes in other cure cycles or with other adhesives if the material properties are known.

The knowledge acquired will benefit industrial purposes. Insights into the physical processes and their mathematical description in simulation models will help analysing

1.2. Material 3

and consequently avoiding the occurrence of panel distortions.

Chapter 2 summarizes the state of the art on the panel distortions in literature. Among other things, publications on different distortion types, recommendations for avoidance and mechanisms that cause panel distortions are reviewed. Simulation approaches to predict distortions are discussed. Chapter 3 describes the experimental study on the development of local panel distortions. On a laboratory sample, the displacement of a steel strip is monitored while the sample is exposed to different cycles. A Differential Scanning Calorimeter (DSC) is used to evaluate the cure process in the heating phase. Estimates are given for displacement expected. In chapter 4 a finite-element model is proposed and used to study the development of local distortions. The model takes stress relaxation as well as chemical and thermal deformations into account. Several material characterization tests are performed in chapter 5. The material data is used in the finite-element model to simulate the bonding process from chapter 3. Simulations results and experimental data are compared. Chapter 6 describes a sensitivity analysis of the simulation model to varying material parameters. In addition, the deflection of a steel-aluminium strip after cure in two different cure cycles is investigated. Model predictions and measurements are compared. In chapter 8 final conclusions are drawn and recommendations for future research are given.

1.2. MATERIAL

For all experimental research in this thesis the commercial adhesive BETAMATE 1496V [4] (BM1496V) from Dow Automotive Systems is used. BM1496V is a one-part epoxy-based rubber-toughened system that is used in automotive applications for metal bonds. The producer recommends cure at $170\,^{\circ}$ C (30 minutes) or $155\,^{\circ}$ C (60 minutes).

REFERENCES

- [1] W. Brockmann, P. L. Geiß, J. Klingen, and B. Schröder, *Adhesive Bonding Materials, Applications and Technology* (Wiley-VCH, 2009).
- [2] C. Adderley, Adhesive bonding, Materials & Design 9, 287 (1988).
- [3] H. Fuchs, K. D. Fernholz, and P. Deslauriers, *Predicted and Measured Bond-Line Read-Through Response in Composite Automotive Body Panels Subjected to Elevated Temperature Cure*, Journal of Adhesion **86**, 982 (2010).
- [4] Dow Automotive Systems, BETAMATETM 1496V, data sheet.

1



2

BACKGROUND

In this chapter literature on the panel distortions due the hot-curing adhesives is reviewed. Different types and causes as well as avoidance strategies are discussed. Common simulation models and relevant concepts to describe the cure process are recapitulated. The liquid-solid transition, chemical shrinkage and thermal expansion of the adhesive as well as the temperature field in the oven contribute to panel distortions. For distortions that arise from relative movements of adherends, the temperature field is an important factor that needs accurate measurements or predictions. Studies on actual bonding processes in real industrial applications are needed for that type of distortions. Other types of distortions can be linked to the changing properties of the adhesive during cure. A comprehensive study on development of these distortions over the entire cure cycle by means of a simulation model that takes stress relaxation, thermal and chemical shrinkage into account has not been done yet. Another important field of research is the development of a severity scale for panel distortions. Comparing the severity of distortions helps to improve the robustness of bonding processes. However, a general objective severity scale is not yet applied in industry.

2.1. Introduction

Two advantages of adhesive bonding were already mentioned: joints over large flange areas offer a more uniform stress distribution and ultimately a higher stiffness and strength; different materials such as polymers and metal can be joined without rivet or bolt holes

weakening the structure. A detailed comparison of joining techniques in an automotive application was done by Barnes and Pashby [1, 2]. The authors point out that adhesives offer additional functionality: they act as dampers, isolators or sealants. Adhesives protect hemmed metal sheet edges from corrosion and prevent fluttering of car panels. In addition, adhesive bonding involves less heat input and lower temperature gradients than welding or brazing. That results in less distortions. The bond line behind a highly polished panel of a car door remains usually invisible. In rare cases, however, read-through effects can occur, in which bond lines cause visible markings on the panel, or the entire structure becomes distorted. This chapter reviews the literature on such distortions.

Adhesives can be divided into two groups: those which set in a chemical reaction and those which set by physical change like loss of solvent or water or cooling from a melt [3]. Adhesives that cure by chemical reaction require a curing agent or a catalyst to initiate the cure process. Epoxy, polyurethane, modified acrylic, cyanoacrylate and anaerobic systems belong to this type of adhesives [4]. Metal ions of the substrate or moisture can act as catalysts as well. These adhesives are commonly thermosetting polymers. For some systems, an activation by radiation or heating is necessary. Elevated temperatures usually promote bonding distortions. This review focusses on hot-cure temperature cycles as they are often applied for one-part epoxies.

2.2. PANEL DISTORTIONS DUE TO HOT-CURING ADHESIVES

2.2.1. TYPES

To understand the origin of distortions, it is necessary to differentiate certain types. Eis [5] investigated distortions of car panels that can occur during car body production. He identified four different types of distortions, see figure 2.1. For each of the cases shown, Eis identified the mechanism and gave recommendations (see section 2.2.3) to avoid them. His results are summarized here.

Case 1: Outwards bulge at the bond line. A temperature difference between inner and outer panel increases the bonding gap. The adhesive, still in the liquid state, follows that movement. After that, the adhesive solidifies in the widened gap. During cooling down, the assembly returns to the position before the heating. The bonding gap, however, cannot shrink due to the solidified adhesive.

Case 2: Deformations directly next to the bond line. The adhesive is squeezed out from the bonding area during heating. The adhesive layer is thicker outside the intended

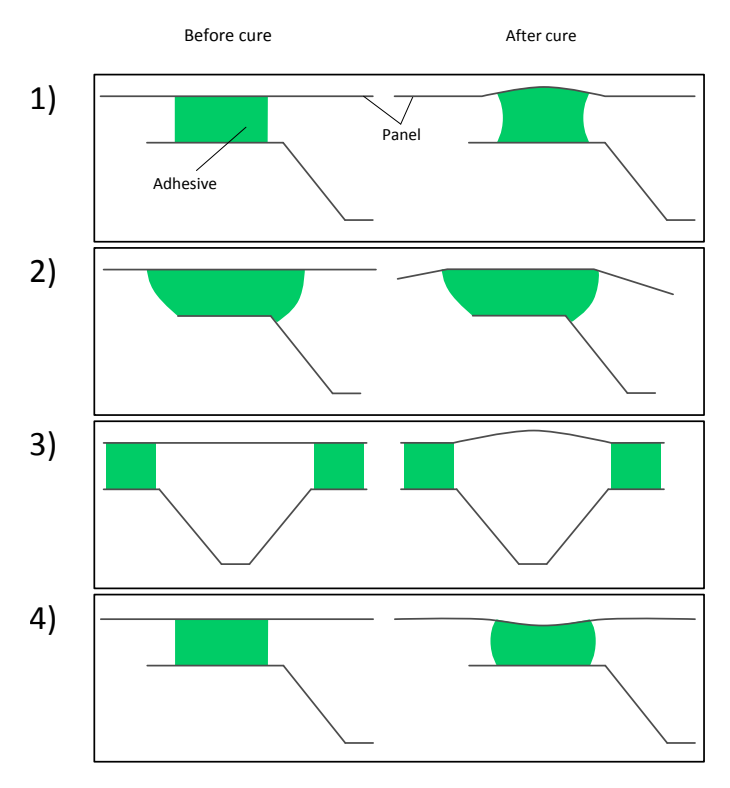


Figure 2.1: Deformation cases defined by Eis [5].

bonding flange area. The thermal shrinkage is proportional to the layer thickness. In the border zone the squeezed out adhesive pulls in the outer panel to a greater extent than the adhesive in the middle of the bonding area.

Case 3: Bulged panel between two bond lines. A temperature difference between inner and outer panel arises during cooling down. The faster cooling adherend contracts faster than the other. Still in the liquid state, the adhesive allows the relative movement between the adherends. During further cooling the adhesive solidifies. The adherends are fixed in their shifted position. One of the adherends forms a bulge between the bond lines.

Case 4: Inwards bulge at the bond line. The expansion of the adhesive in the heating phase is constrained; the bonding gap size does not change. Some of the adhesive is squeezed out from the bonding area. Therefore, there is less adhesive mass in the bonding area. The outer panel is pulled in by the thermally shrinking adhesive during cooling.

8 2. Background

To apply the classification shown in figure 1.1, cases 1, 2 and 4 may be considered local distortions while case 3 describes the global type. Combinations of types are also imaginable. Local distortions are also referred to as bond-line read-through [6–8] or bond-line read-out [9, 10]. In case of outer car panels, visible distortions, even though they may not affect the structural integrity, are considered defects unacceptable to customers [8]. Even with displacements of less than 10 micrometres, the local type can remain visible to the human eye [11].

Global distortions may reach displacements of several millimetres [5]. It is noteworthy that they can also occur in cases where additional joining methods seemingly prevent the relative movement of the adherends. Meschut *et al.* [12–14] compared adhesive bonds with rivet and hybrid joints. The high thermal stresses resulting from an " α -mismatch" of the materials involved can permanently damage the joint area and cause distortions even if rivets support the adhesive bond.

Blunk and Wilkes conducted research into another type of panel distortions [15–17]. The bond line creates a temperature sink during the coating process of bonded panels. That temperature sink affects the surface tension of the coat and, therefore, its flow on the substrate surface. After cure of the coat, a visible surface defect can remain along the bond line. That type of distortions differs from the previous ones since the defect is not caused by a panel deformation during the bonding process, but occurs during coating.

2.2.2. CAUSES AND DEVELOPMENT

Hahn and Orth [6] named thermal and chemical deformation of the adhesive as well as relative movement of the adherends as contributing factors to distortions. The latter is caused by the expansion of the whole structure in the oven when the adhesive cannot sustain any load yet. The adherends will freeze in their current state at the moment the adhesive begins to transfer forces; they cannot return to their state before the cure cycle. Relative movements depend on the fixture and the mechanical properties of the assembly. Some researchers regard the temperature field in the oven as the most important factor for relative movements [5, 18].

Chudaska and his co-workers [19–22] investigated the displacement of composite panels during cure cycles with different cure temperatures, heating and cooling rates. They found that the temperature profile influences not only the development of displacements, but also the final displacement after the cure cycle. The displacement of the panel appears in two distinct steps. They conclude that the first step is caused by the chemical shrinkage and the second one by thermal shrinkage during cooling. Eis [5]

2

2

identified flow-out of the adhesive as an additional factor.

2.2.3. SUGGESTED STRATEGIES TO AVOID DISTORTIONS

Eis [5] provides strategies for each of the cases in figure 2.1. Those include: homogenizing the temperature during cure by lowering the heating rate or by improving the air flow in the oven (cases 1 and 3), modifying adhesive properties such as reducing thermal and chemical shrinkage or a lowering glass transition temperature (cases 1, 3 and 4), better dosing of the adhesive to avoid squeeze-out (case 2) and better design of the bonding area to prevent varying adhesive layer thickness (case 2). A lower cure temperature is also considered beneficial [23]. Lee [9] recommends to reduce the mismatch in thermal expansion coefficients (CTE) between panel and adhesive and to increase the Young's modulus ratio of panel to adhesive. A typical remedy for distortions is to increase the thickness of the panel [8], which has been proven in laboratory tests to reduce distortions [21, 24]. However, that contradicts lightweight design guidelines which are of great importance to the aerospace and automotive industry.

2.2.4. VISUAL EVALUATION OF DISTORTED SURFACES

An evaluation of the visual surface quality involves the identification of visual defects. For panel distortions that originate from the bonding process, identifying a defect is not always easy. Hahn and Orth [6] point out that broadening the bond line may decrease the deformation of a panel. They assume, however, that the reduced deformation is perceived as more severe. Fuchs *et al.* [8] state that relatively large displacements of the global type might not be viewed as defects. A curved panel that has a slightly different radius of curvature than intended might still be accepted since customers do not make comparisons to a reference shape. Large changes in curvature along a short path on the panel surface can become visible through unsteadiness in light reflections.

Car panels are usually evaluated by personnel. That involves subjectivity to some extent [11] and, therefore, the risk of unnecessary part rejections. It is desirable to assign values to distortions, which would allow to compare their severity. By that, a defect threshold could be specified and bonding processes could be evaluated more easily with regard to their robustness to bonding distortions.

Eis gives an estimate for a defect threshold from which on deformations become visible [5, p. 37 ff.]. Research has been conducted into a severity scale for distortions in car panels and into correlating the scale to human perception [11, 25–29]. Fernholz [30] proposes the variation in surface curvature as a measure for distortions. Her procedure to measure severity correlates well to human perception for panels intended to be flat.

curvature that includes unwanted panel distortions remains an open question.

2.3. LINEAR VISCOELASTICITY

The stress-strain relation of polymeric systems such as adhesives can often, when subjected to small strain and small strain rates, accurately be described by the theory of linear viscoelasticity. Many prediction models for panel distortions describe the adhesive with viscoelastic relations. Here, a short extract is given based on the various textbooks on that topic [31–35].

A linear viscoelastic material is described by the convolution integral

$$\sigma(t) = \int_{-\infty}^{t} E(t - \hat{t}) \dot{\varepsilon}(\hat{t}) d\hat{t}, \qquad (2.1)$$

2. Background

where (\cdot) denotes the derivative with respect to time t; σ and ε are the one-dimensional stress and strain function, respectively. The role of relaxation function E(t) becomes apparent when equation 2.1 is solved for a strain function which jumps from zero to ε_0 at t=0. In that case, the stress response follows the relaxation function: $\sigma(t)=E(t)\varepsilon_0$, see figure 2.2.

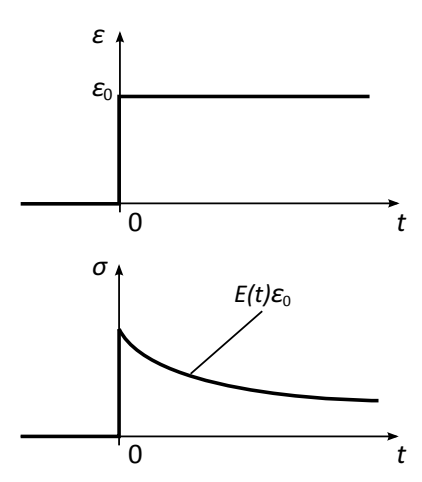


Figure 2.2: Stress response of a linear viscoelastic material to a sudden strain step ε_0 at t = 0.

The relaxation function is often written as a Prony series

$$E(t) = E_{\infty} + \sum_{m=1}^{M} E_m \exp\left(-\frac{t}{\tau_m}\right)$$

2

10

2

with the long-term or equilibrium modulus E_{∞} . (E_m, τ_m) is the discrete relaxation spectrum.

The resulting stress-strain relation

$$\sigma(t) = E_{\infty}\varepsilon(t) + \sum_{m=1}^{M} E_{m} \int_{-\infty}^{t} \exp\left(-\frac{t-\hat{t}}{\tau_{m}}\right) \dot{\varepsilon}(\hat{t}) d\hat{t}$$
 (2.2)

coincides with the so-called generalized Maxwell model which describes the stress-strain relation with a system of springs and dash pots, see figure 2.3. Spring elements have an

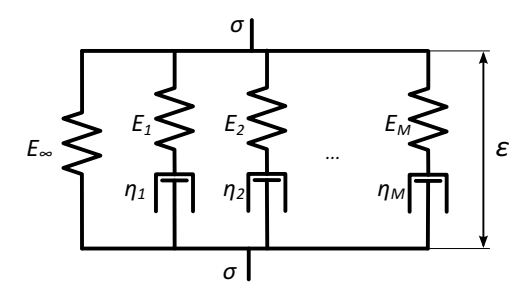


Figure 2.3: The generalized Maxwell model represents the stress response to strain analogue to a force response to relative displacement in depicted system of dash pots and springs.

elastic modulus E_m while dash pots have a viscosity η_m . Force applied in that model is analogue to σ , the displacement is analogue to ε and the displacement rate is analogue to $\dot{\varepsilon}$. The equation

$$\sigma(t) = E_{\infty}\varepsilon(t) + \sum_{m=1}^{M} E_m u^m(t)$$
 (2.3)

together with the differential equation

$$\dot{u}^{m}(t) + \frac{1}{\tau_{m}} u^{m}(t) = \dot{\varepsilon}(t), \quad m = 1, 2, ...M,$$
(2.4)

and

$$\tau_m = \eta_m / E_m$$

describes such a model. The solution is equation 2.2.

There are other ways to describe the stress relaxation than with the discrete spectrum (E_m, τ_m) ; with continuously varying relaxation times for instance. The Prony series has the advantage that it can represent experimental relaxation curves spread over several

12

time decades at sufficient accuracy if the relaxation times τ_m are chosen adequately. In addition, it is computationally cheap because equation 2.4 can be discretized in a one-step numerical scheme requiring to store information about the previous step only.

2.3.1. RESPONSE TO SINUSOIDAL STRAIN EXCITATION

A common approach to determine viscoelastic functions is to apply a sinusoidal strain load $\varepsilon(t) = \varepsilon_0 \sin(\omega t)$ of an amplitude ε_0 and a radial frequency ω . With the substitution $s = t - \hat{t}$ and the relation $\cos(x - y) = \sin(x)\sin(y) + \cos(x)\cos(y)$, equation 2.1 becomes

$$\sigma(t) = \varepsilon_0 \left[\omega \int_0^\infty E(s) \sin(\omega s) ds \right] \sin(\omega t) + \varepsilon_0 \left[\omega \int_0^\infty E(s) \cos(\omega s) ds \right] \cos(\omega t)$$
 (2.5)

with the storage modulus

$$E'(\omega) = \omega \int_{0}^{\infty} E(s) \sin(\omega s) ds$$
 (2.6)

2. Background

representing the stress part in-phase with the strain and the loss modulus

$$E''(\omega) = \omega \int_{0}^{\infty} E(s) \cos(\omega s) ds$$
 (2.7)

representing the stress part in-phase with the strain rate. Interpreting the measured stress response as a shifted sine curve $\sigma(t) = \sigma_0 \sin(\omega t - \delta)$ with a phase lag δ allows to determine E' and E'' through

$$E'(\omega) = \frac{\sigma_0}{\varepsilon_0} \cos \delta, \ E''(\omega) = \frac{\sigma_0}{\varepsilon_0} \sin \delta$$

and

$$\frac{E''}{E'} = \tan \delta,$$

which, in turn, allow to calculate E(t) through inverse Fourier transformation:

$$E(t) = E(\infty) + \frac{2}{\pi} \int_{0}^{\infty} \frac{E'(\omega) - E(\infty)}{\omega} \sin(\omega t) d\omega$$

or

$$E(t) = E(\infty) + \frac{2}{\pi} \int_{0}^{\infty} \frac{E''(\omega)}{\omega} \cos(\omega t) d\omega.$$

2.3.2. THREE-DIMENSIONAL STRESS-STRAIN RELATION

The integral 2.1 can be generalized to three dimensions

$$\sigma_{ij}(t) = \int_{-\infty}^{t} C_{ijkl}(t - \hat{t}) \dot{\varepsilon}_{kl}(\hat{t}) d\hat{t},$$

where σ_{ij} is the Cauchy stress tensor, ε_{kl} the linear strain tensor and $C_{ijkl}(t)$ a fourth order relaxation tensor. In case of an isotropic material, C_{ijkl} contains two independent relaxation functions, e.g. the bulk relaxation modulus K(t) and the shear relaxation modulus G(t):

$$\sigma_{ij}(t) = \int_{-\infty}^{t} K(t - \hat{t}) \dot{\varepsilon}_{kk}(\hat{t}) \delta_{ij} d\hat{t} - \frac{2}{3} \int_{-\infty}^{t} G(t - \hat{t}) \dot{\varepsilon}_{kk}(\hat{t}) \delta_{ij} d\hat{t}$$
$$+2 \int_{-\infty}^{t} G(t - \hat{t}) \dot{\varepsilon}_{ij}(\hat{t}) d\hat{t}, \tag{2.8}$$

where δ_{ij} is the Kronecker delta. Definitions for loss and storage moduli and the relaxation function can be applied accordingly to the tensile, shear or bulk modulus by replacing the designated strain and stress components.

In case of a viscoelastic fluid, the shear modulus G(t) approaches zero for $t \to \infty$. Moreover, a Newtonian fluid reaches steady-state flow, in case of a simple shear deformation with the constant shear rate $\dot{\varepsilon}_{12}$:

$$\sigma_{12}=2\eta\dot{\varepsilon}_{12}.$$

Equation 2.8 yields

$$\eta = \int_{0}^{\infty} G(\hat{t}) d\hat{t}, \tag{2.9}$$

where η is the zero-shear-rate viscosity [31]. For a solid, G(t) approaches a value G_{∞} different from zero for $t \to \infty$.

2.3.3. THERMORHEOLOGICALLY SIMPLE MATERIAL

This section summarizes the relationship between a thermorheologically simple material and the time-temperature superposition principle as described in [34].

For a thermorheologically simple material, η_m are the only material constants shown in figure 2.3 that vary with temperature. Moreover, all η_m depend on temperature in the same manner, so that the dependence of all η_m can be described by a single function a(T):

$$\eta_m = a(T)\eta_m^R, \ \tau_m = a(T)\tau_m^R, \ m = 1, 2, ..., M,$$
(2.10)

where T is the temperature and $\eta_m^{\rm R}$ and $\tau_m^{\rm R}$ denote the mth viscosity and relaxation time at a reference temperature $T_{\rm R}$, respectively. Now, the so-called reduced time (or material time) ξ can be introduced:

$$\xi(t) = \int_{-\infty}^{t} \frac{\mathrm{d}\hat{t}}{a(T(\hat{t}))}, \ \dot{\xi}(t) = \frac{1}{a(T)}.$$

At a temperature T =const. other than T_R , equation 2.4 transforms to

$$\dot{u}^{m}(t) + \frac{1}{a(T)\tau_{m}} u^{m}(t) = \dot{\varepsilon}(t). \tag{2.11}$$

With the substitute functions

$$\tilde{\sigma}(\xi(t)) = \sigma(t), \ \tilde{\varepsilon}(\xi(t)) = \varepsilon(t), \ \tilde{u}^m(\xi(t)) = u^m(t),$$

and application of the chain rule follows

$$\tilde{\sigma}(\xi) = E_{\infty}\tilde{\varepsilon}(\xi) + \sum_{m=1}^{M} E_{m}\tilde{u}^{m}(\xi), \tag{2.12}$$

$$(\tilde{u}^m)'(\xi) + \frac{1}{\tau_m} \tilde{u}^m(\xi) = \tilde{\varepsilon}'(\xi), \tag{2.13}$$

where $(\cdot)'$ denotes the derivative with respect to ξ .

Equation 2.12 and 2.13 coincide with equation 2.3 and 2.4 except that the time variable is replaced by ξ and τ_m by $\tau_m^{\rm R}$. Accordingly, the solution coincides with equation

2

2.2:

$$\tilde{\sigma}(\xi) = E_{\infty}\tilde{\varepsilon}(\xi) + \sum_{m=1}^{M} E_{m} \int_{-\infty}^{\xi} \exp\left(-\frac{\xi - \hat{\xi}}{\tau_{m}^{\text{R}}}\right) \tilde{\varepsilon}'(\hat{\xi}) d\hat{\xi}.$$

Reverse transformation leads to

$$\sigma(t) = E_{\infty}\varepsilon(t) + \sum_{m=1}^{M} E_{m} \int_{-\infty}^{t} \exp\left(-\frac{t - \hat{t}}{a(T)\tau_{m}^{R}}\right) \dot{\varepsilon}(\hat{t}) d\hat{t}.$$
 (2.14)

Comparing equation 2.2 and 2.14 results in

$$E(t,T) = E\left(\frac{t}{a(T)}, T_{R}\right).$$

In other words, the relaxation function at a temperature T equals the one at the reference temperature T_R if the time variable is scaled with a factor 1/a(T) or, on a logarithmic time scale, if the curve is shifted by $\log a(T)$. Accordingly,

$$E'(\omega, T) = E'(\omega a(T), T_{R}),$$

$$E''(\omega, T) = E''(\omega a(T), T_{R})$$
(2.15)

hold for the dynamic moduli in equation 2.6 and 2.7.

The assumption of thermorheologically simple behaviour entails a tremendous reduction of time and effort needed for the experimental determination of relaxation curves. Instead of measuring relaxation curves at different temperatures over the entire time scale, measurements at different temperatures over a smaller time interval can be made. The curves obtained are shifted and reassembled to a master curve, see figure 2.4.

The relaxation curves at different temperatures for a thermorheologically simple material are all identical if plotted over ξ instead of t. The temperature dependence lies within ξ entirely. Therefore, ξ is often referred to as material time or material clock as it describes how fast or slowly relaxation processes in the material take place at a designated temperature.

For polymers, a(T) can be interpreted as the ratio of the monomeric friction coefficient at the current temperature T to the one at the reference temperature $T_{\mathbb{R}}$ [32]. Instead of temperature, the material time can also describe dependence on other parameters such as moisture or degree of cure [36] with analogue superposition principles.

16 2. Background

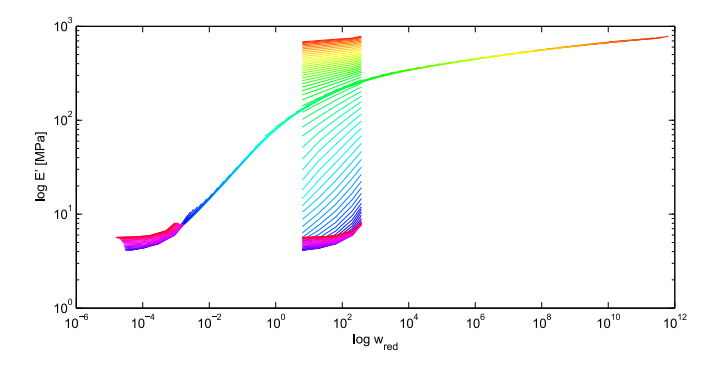


Figure 2.4: Curves measured over a small window of frequencies at different temperatures are assembled to a master curve

2.4. THE CURE PROCESS

2.4.1. DEGREE OF CURE

During cure, the adhesive transforms from a viscous fluid to a viscoelastic solid. The exothermic cross-linking reaction causes heat release and a volume shrinkage of the adhesive. In addition, the glass transition temperature increases.

As a simplification of the chemical process, the reaction can be described by a single variable, the degree of cure q. q can be defined as

$$q(t) = \frac{H(t)}{H_{\infty}},\tag{2.16}$$

where H(t) is the accumulated released heat and H_{∞} is the ultimate heat after completion of the chemical reaction. Equation 2.16 suggests that the cure rate can be determined directly by monitoring the heat flow to and from a material sample. A DSC is often used for that purpose [18, 24, 37, 38].

Equations for the cure rate often have the form

$$\frac{\mathrm{d}q}{\mathrm{d}t} = f(q, T, \dots),\tag{2.17}$$

where T is the absolute temperature. A list of different evolution equations for the degree of cure can be found in [39]. Wenzel [38] points out that the general equation for autocatalytic reactions

$$\dot{q}(t) = (r_1 + r_2 q^m)(1 - q)^n$$

from Horie *et al.* [40] has been used to describe epoxy cure in many cases. It was applied in the empirical sense, that is reaction orders m and n may not be integers. A modified version has also been used successfully to describe automotive adhesives [18, 24]. the special case for $r_1 = 0$ is investigated in [41].

2.4.2. CHEMICAL SHRINKAGE

The cure process also leads to volume changes of the adhesive. Next to temperature-induced expansion and shrinkage over a non-isothermal cure cycle, the cross-linking of polymer chains reduces the specific volume of the adhesive. This phenomenon is often referred to as cure shrinkage or chemical shrinkage. The relative volume shrinkage due to curing can vary for different types of adhesives. Table 2.1 lists values for common adhesive types [42].

Table 2.1: Relative cure-induced volume shrinkage of common adhesives [42].

Adhesive type	Relative volume shrinkage (%)
Acrylic	5-10
Epoxy	4-5
Polyurethane	3-5
Polyamide	1-2
Silicone	< 1

The volume shrinkage can be determined by measuring the specific volume before and after cure. This can be done by weighing or by buoyancy measurements and has already been applied for automotive adhesives [18, 43]. But also continuous measurements over time are possible [38, 44–46].

De Vreugd [47, p. 70] points out that the measurements before and after the cure cycle are usually done at ambient temperature. In non-isothermal cure cycles, that temperature is far below the cure temperature at which the shrinkage presumably takes place. These measurements are therefore not accurate for hot-curing adhesives. Consequently, he measures the volume change over the entire cycle. His reasoning implies that the thermal expansion of the adhesive in the heating phase is different from the thermal volume reduction in the cooling phase. This is true provided that the fully cured adhesive passes the glass transition temperature during cooling down at which its CTE changes significantly.

2.4.3. GELATION

The transition from a viscous liquid to viscoelastic solid can also be seen as a sol-gel transition. The moment the polymer turns into a solid is the gel point. Before the gel point, the polymer consists of finite clusters and is called a sol as it is soluble in a solvent. From the gel point on, it is called a gel and is not soluble anymore since it consists of a macromolecule of infinite molecular weight [48]. Discussions on different gelation theories can be found in [38, 48, 49].

To describe the development of distortions in a bonding process, the changing macroscopic mechanical properties of the adhesive are of interest. Te Nijenhuis [50], even though pointing out difficulties in defining a gel, describes the gelation process and the gel point as follows: "The system is liquid-like before crosslinking starts and remains a liquid till the viscosity becomes infinite. At that moment, which is called the gel point, there is at least one molecule with an infinite molecular weight. After the gel point, an equilibrium shear modulus develops[...]." Figure 2.5 illustrates that. Indeed, a nonzero

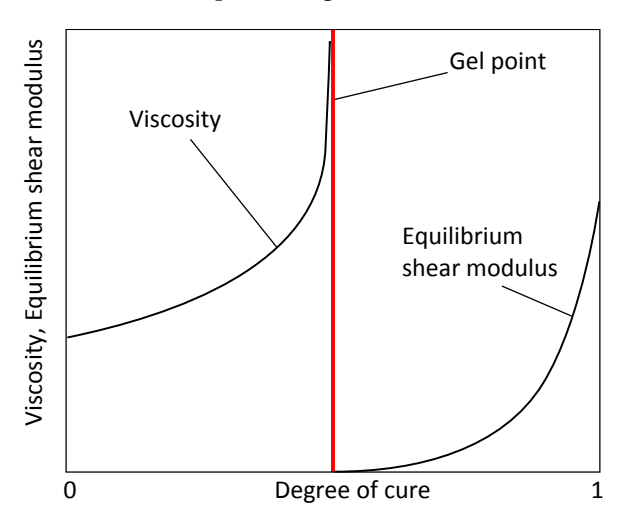


Figure 2.5: Schematic representation of changing material properties during cure [50].

equilibrium shear modulus causes the viscosity to be infinite as the integral in equation 2.9 has no finite solution; steady-state flow cannot be achieved anymore.

Different approaches to determine the gel point can be found in [50]. Rheological methods rely on the change of mechanical properties at the gel point. The storage modulus, for instance, rises in measurements during cure from an immeasurably low value. That jump can be identified as the gel point [43]. It is often assumed that the point where storage and loss modulus are equal is the gel point. In a viscous liquid, most of the energy supplied dissipates (G' < G'') while in an elastic solid, more energy is stored

(G' > G''). Hence, the transition point with G' = G'' is assigned to the gel point. The empirical method of Winter and Chambon assumes

$$\frac{G''}{G'} = \tan\left(\frac{n\pi}{2}\right)$$

to hold at the gel point [50]. For stoichiometric balanced systems, n is 0.5.

2.4.4. GLASS TRANSITION

Non-crystalline polymers can show a rubbery behaviour with low stiffness at high temperatures and a glassy behaviour with high stiffness at lower temperatures. The temperature at which the polymer transfers between these two states is called glass transition temperature $T_{\rm g}$. Glass transition affects not only mechanical properties. The heat capacity shows a peak at $T_{\rm g}$ and the slope of the CTE has a discontinuity at $T_{\rm g}$. Therefore, it is common to determine $T_{\rm g}$ by measuring the specific volume as a function of temperature [49] or via a DSC [18, 51].

The glass transition temperature increases during cure and reaches a final value when all cross links are formed. Models for the development of $T_{\rm g}$ can be found in [52, 53]. An increasing glass transition temperature during cure implies that the polymer can go over into the glassy state (vitrification) during isothermal cure if the glass transition temperature surpasses the cure temperature or even during heating if $T_{\rm g}$ raises faster than the temperature. Lange et~al.~ [54–56] and Wenzel [38] investigated cure progress and residual stresses for cross-linking polymers above and below the glass transition temperature.

The glass transition temperature can affect the cure rate. When the temperature falls below the glass transition temperature, the mobility of polymer chains becomes severely restricted. The reaction becomes diffusion-controlled [52]. The cure process slows down significantly, even to a point where complete cure is not reached anymore [57]. To avoid incomplete cure in bonding processes, adhesive producers usually recommend a cure temperature well above the final glass transition temperature. Structural adhesives require moduli in the order of magnitude of 10^9 Pa [58]. To meet these requirements, they cannot operate in a rubbery state, but need to be cooled down below their glass transition temperature after cure.

2.5. MODELLING APPROACHES

2.5.1. LINEAR ELASTICITY

In an early work, Gent [59] used simple linear stress-strain relations to estimate stresses in an adhesive layer between two rigid plates during cooling. He assumes the adhesive to be stress-free at elevated temperature. Stresses that might originate from the cross-linking of the adhesive before cooling are not accounted for. Hahn and Pagano [60] examined the manufacturing process of composite laminates. They argue that the modulus of the polymer is low during cross-linking and assume a stress-free state when the material is fully cured and cooling sets in. They calculate cooling stresses by means of a linear elastic model. It has been common to calculate cooling-down stresses rather than cure stresses in composite materials [61–63]. The same approach is used for panel distortions due to hot-curing adhesives [64].

Kim and Hahn [65] investigated a two-step cure cycle where a composite structure dwells at elevated temperature first before it is heated up further to the final cure temperature. They found that warpage begins to develop from the gel point on, at both dwell and cure temperature before the cooling phase. White and Hahn [66] worked on the cure cycle optimization. They found that warpage for a specific composite material can be reduced when another dwelling step before the cure temperature is integrated in the cure cycle. Evidently, these effects cannot be reproduced by prediction models that focus on the cooling phase only.

2.5.2. LINEAR VISCOELASTICITY

Weitsman [67] found that thermal stresses in epoxy composites are overestimated when calculated with a linear elastic model. His linear viscoelastic model yields better results. Jendrny [18] investigated panel distortions in automotive structures due to adhesive bonding. He looked into different kinds of adhesives. In his research, a linear elastic model based on the equilibrium modulus of the adhesive showed satisfactory results only for adhesive types that have a glass transition temperature at or below room temperature. A structural adhesive with a $T_{\rm g}$ close to 100 °C requires a linear viscoelastic description. Similar conclusions are drawn by Fuchs *et al.* [8]. Several viscoelastic models for the prediction of local panel distortions focus on the cooling phase only [8, 10, 24].

2.5.3. CHEMICAL SHRINKAGE

In some models, the chemical shrinkage during cure is neglected [24, 64]. It is reasoned that the contribution of chemical strain to residual stresses compared to that of thermal

deformation is small [6, 68]. Genidy *et al.* [69], however, point out that the influence of chemical strain in [68] was later proven to be underestimated [66]. Experimental work on curing adhesives indicate that a significant portion of panel distortions that develop before the cooling phase is caused by chemical shrinkage [20].

2.5.4. CURE-DEPENDENT MODELS

Adolf and Martin [36, 70] developed a constitutive model that accounts for the developing viscoelastic properties during cross-linking. Analogue to thermorheological simplicity (section 2.3.3), they propose chemorheological simplicity with a degree-of-cure-dependent shift factor and equilibrium shear modulus. Their model shows good agreement with experimental data for stresses in curing epoxies [71] and has also been implemented in finite-element code to predict stresses in electronic components [51]. Others applied their model successfully to coating processes [72] or electronic packaging [73]. Also, cure-dependent models which include plasticity [74, 75] can be found in literature as well as models for large strain and non-linear behaviour [39, 76–79].

2.5.5. TEMPERATURE CYCLES

The highly automated production of car bodies is a complex and time-sensitive process. The cure process of adhesives does usually not happen in a separate step, but is integrated in the thermal cycles after electrophoretic coating [80]. The temperature distribution of car bodies within the dryer ovens depends on the complex air flow around the structures. Jendrny [18] names the temperature field in the oven as the main factor for global distortions. He recommends a heat flux analysis prior to stress calculations. Blanke [80] investigated the temperature distribution in dryer ovens of an automotive plant by means of computational fluid dynamics. She concludes that the accuracy of these simulations needs to be increased in order to facilitate accurate predictions of the cure process of adhesives. It is noteworthy, however, that simulations of the temperature development in dryer ovens in combination with a cure-dependent material model have been used recently to predict relative movements of adherends in car body production [81].

2.6. DISCUSSION AND CONCLUSIONS

Panel distortions due to adhesive bonding has been subject to research for many years. Most of the studies were aimed at the automotive industry where adhesive bonding is an established joining technology for car panels.

22 2. Background

While the structural integrity of an adhesive bond can be evaluated objectively, the assessment of the surface quality of a bonded panel bears the challenge of accounting for human perception. That makes the evaluation and improvement of bonding processes difficult. A severity scale as an objective measure to characterize distortions would allow an optimization of bonding processes by providing comparability. Therefore, the research and the progress in that area benefits the reduction and avoidance of distortions. It should be noted, however, that such a scale – in a general sense – may not exist. Manufacturers usually define their own measure of quality and what standard of quality to offer. While insights in human perception are certainly welcome, the dictation of a quality scale might be dismissed.

2

Once distortions occur, they can be easily assigned to the local or global type. For research purposes, another classification might be more favourable: 1) those which are caused mainly by the relative movement of adherends and 2) those which are caused mainly by the changing properties of the adhesive such as thermal and chemical shrinkage. Type 1 includes global distortions in which bulges are formed between two bond lines. But also local ones where the shrinking or growing size of the bonding gap causes distortions belong to this group. A clear distinction between these types requires a preceding examination and may not be possible in some cases. However, these types have different origins and should be handled differently.

The relative movement of adherends is caused by the thermal expansion of the entire structure in the oven. That means the temperature field, the fixture and the geometry of the assembly, and the materials involved affect this type. The materials affect the heat conduction which, in turn, affects the temperature field. The geometry affects the air flow in the oven which, in turn, again, affects the temperature field. While these processes are well understood, they can be quite complex in real applications. The author believes that research on this type of distortions cannot be limited to laboratory studies. Actual bonding processes of real parts need to be investigated.

For type 2, the research on the cooling phase suggests viscoelastic models for the adhesive to describe the development of distortions especially if glass transition takes place during cooling. Temperature- and cure-dependent models have been proven to accurately reproduce the relevant effects such as thermal and chemical shrinkage and are applied to cross-linking polymers in many other fields. A comprehensive study on the development of panel distortions over an entire cure cycle by means of these models is unknown to the author.

REFERENCES

- [1] T. Barnes and I. Pashby, *Joining techniques for aluminum spaceframes used in automobiles. Part I solid and liquid phase welding*, Journal of Materials Processing Technology **99**, 62 (2000).
- [2] T. Barnes and I. Pashby, *Joining techniques for aluminium spaceframes used in automobiles: Part II adhesive bonding and mechanical fasteners*, Journal of Materials Processing Technology **99**, 72 (2000).
- [3] C. Adderley, Adhesive bonding, Materials & Design 9, 287 (1988).
- [4] E. M. Petrie, Handbook of Adhesives and Sealants, 2nd ed. (McGraw-Hill, 2007).
- [5] M. Eis, Fertigungsbedingte Bauteildeformationen beim Kleben dünnwandiger Stahlbauteile: Analyse der Entstehungsmechanismen und Hinweise zur Minimierung, Ph.D. thesis, Universität Paderborn (2000).
- [6] O. Hahn and T. Orth, Avoiding bondline readthrough on thin steel elements by modification and optimization of processes, adhesives and sample shape, in International Body Engineering Conference (1997) pp. 111 115.
- [7] S. R. Durso, S. E. Howe, and M. W. Pressley, *Adhesive Bond-line Read-through: The-oretical and Experimental Investigations*, Tech. Rep. (SAE Transactions, 1999).
- [8] H. Fuchs, K. D. Fernholz, and P. Deslauriers, *Predicted and Measured Bond-Line Read-Through Response in Composite Automotive Body Panels Subjected to Elevated Temperature Cure*, Journal of Adhesion **86**, 982 (2010).
- [9] C.-C. Lee, *A finite element study of bond-line-read-out,* Journal of Reinforced Plastics and Composites **14**, 1226 (1995).
- [10] K. A. Patankar, D. A. Dillard, and K. D. Fernholz, *Characterizing the constitutive properties and developing a stress model for adhesive bond-line readout,* International Journal of Adhesion and Adhesives **40**, 149 (2013).
- [11] A. Andersson, *Evaluation and visualisation of surface defects on auto-body panels*, Journal of Materials Processing Technology **209**, 821 (2009).
- [12] G. Meschut, O. Kläger, and H. Wetter, *Multi-Material Design (Part 1): Thermal stress in lacquer drying processes [Multi-material-design (Teil 1): Thermische Beanspruchung in Lacktrocknungsprozessen]*, Adhäsion Kleben und Dichten **4**, 30 (2003).

24 REFERENCES

[13] G. Meschut, O. Kläger, and H. Wetter, *Multi-Material-Design (Part 2): Simulation of thermal strain [Multi-Material-Design (Teil 2): Simulation der Thermischen Beanspruchung]*, Adhäsion Kleben und Dichten **5**, 31 (2003).

- [14] G. Meschut and T. Gänsicke, Experimental and computational analysis of the stresses on adhesive-bonded layers in joints between thermally incompatible materials, Welding and Cutting 55, 322 (2003).
- [15] R. H. J. Blunk and J. O. Wilkes, *Computational analysis of surface-tension-driven coating-defect flow,* AIChE Journal **47**, 779 (2001).
- [16] R. H. J. Blunk and J. O. Wilkes, *Surface-tension-driven flows of coatings: Bondline readout formation*, Journal of Coatings Technology **73**, 63 (2001).
- [17] R. H. J. Blunk and J. O. Wilkes, *Numerical analysis of surface-tension-driven coating flow*, Polymer Engineering and Science **42**, 258 (2002).
- [18] J. Jendrny, Entwicklung von Berechnungsmodellen zur Abschätzung der Verformung geklebter dünnwandiger Stahlbauteile in Leichtbaukonstruktionen der Warmaushärtung, Ph.D. thesis, Universität Paderborn (2004).
- [19] A. Chudaska and O. Hahn, Untersuchungen zum temperatur- und reaktionsbedingten Klebstoffschrumpf - Maßnahmen zur Reduzierung schrumpfbedingter Bauteilschädigungen, in Wärmearme Fügetechniken - Kleben - Durchsetzfügen - Nieten (1993) pp. 121 – 130.
- [20] A. Chudaska and O. Hahn, Damages of bonded parts caused by the thermal and reactionary contraction of adhesives during the curing process, in Vide-Science Technique Et Applications (1994) pp. 223–227.
- [21] A. Chudaska and O. Hahn, *Influence of constructive factors and the process conditions during the curing of hot setting adhesives on the properties of bonded joints*, in *Special Joining Technologies International Symposium* (1994) pp. 12 24.
- [22] O. Hahn and A. Chudaska, Einfluß von Schwindungsmechanismen auf das Eigenschaftsprofil geklebter Bauteile, Schweißen und Schneiden 47, 467 (1995).
- [23] S. K. Basu and H. G. Kia, *Strategies to reduce bond-line read-out in adhesive joined smc automotive body panels*, Journal of Composite Materials **42**, 1801 (2008).
- [24] O. Hahn and J. Jendrny, Evaluation of simulation models for the estimation of deformation of adhesively bonded steel sheets during curing, Welding in the World 47, 31 (2003).

- [25] K. Fernholz, R. Hsakou, K. Lazarz, C. S. Wang, B. Emerson, D. Biernat, and D. Case, Development of a tool to measure bond-line read-through, in SPE Automotive and Composites Divisions - 7th Annual Automotive Composites Conference and Exhibition, ACCE 2007 - Driving Performance and Productivity, Vol. 1 (2007) pp. 90–106.
- [26] K. D. Fernholz, The influence of bond dam design and hard hits on bond-line readthrough severity, in Society of Plastics Engineers - 10th Annual Automotive Composites Conference and Exhibition 2010, ACCE 2010 (2010) pp. 858–875.
- [27] K. D. Fernholz and K. Lazarz, Effect of bond fixture temperature on the severity of bond-line read-through induced surface distortion, in The 33rd Annual Meeting of the Adhesion Society (2010) pp. 211 213.
- [28] K. D. Fernholz, C. S. Wang, and K. Lazarz, *The influence of smc formulation, inner panel thickness, and bond stand-offs on bond-line read-through severity,* in 9th Annual Automotive Composites Conference and Exhibition, ACCE 2009 (2009) pp. 345–361.
- [29] H. Fuchs and P. Deslauriers, Effect of adhesive joint cross-section parameters on the bond-line read-through severity in composite automotive body panels bonded at elevated temperature, in Society of Plastics Engineers 10th Annual Automotive Composites Conference and Exhibition 2010, ACCE 2010 (2010) pp. 843–857.
- [30] K. Fernholz, *Quantifying the visibility of surface distortions in class a automotive exterior body panels*, Journal of Manufacturing Science and Engineering, Transactions of the ASME **135** (2013).
- [31] R. Christensen, *Theory of Viscoelasticity* (Academic Press, 1971).
- [32] J. Ferry, Viscoelastic properties of polymers (Wiley, 1980).
- [33] N. W. Tschoegl, *The Phenomenological Theory of Linear Viscoelastic Behavior*, 2nd ed. (Springer, Berlin, 1989).
- [34] A. Lion, *Einführung in die Lineare Viskoelastizität*, Vol. 4 (Universität der Bundeswehr München, 2007).
- [35] K. Jansen, *Thermomechanical modelling and characterisation of polymers* (TU Delft, 2007).
- [36] D. Adolf and J. E. Martin, *Time Cure Superposition during Cross-Linking*, Macromolecules **23**, 3700 (1990).

- [37] S. Sourour and M. R. Kamal, *Differential scanning calorimetry of epoxy cure: isother-mal cure kinetics*, Thermochimica Acta **14**, 41 (1976).
- [38] M. Wenzel, *Spannungsbildung und Relaxationsverhalten bei der Aushärtung von Epoxidharzen*, Ph.D. thesis, Technical University of Darmstadt (2005).
- [39] A. Lion and P. Höfer, *On the phenomenological representation of curing phenomena in continuum mechanics*, Archives of Mechanics **59**, 59 (2007).
- [40] K. Horie, H. Hiura, M. Sawada, I. Mita, and H. Kambe, *Calorimetric investigation of polymerization reactions. iii. curing reaction of epoxides with amines*, Journal of Polymer Science Part A-1: Polymer Chemistry **8**, 1357 (1970).
- [41] M. Kamal and S. Sourour, *Kinetics and thermal characterization of thermoset cure*, Polymer Engineering and Science **13**, 59 (1973).
- [42] G. Habenicht, *Kleben Grundlagen, Technologie, Anwendungen*, 3rd ed. (Springer, Berlin, 1997).
- [43] S. Menzel, Zur Berechnung von Klebverbindungen hybrider Karosseriestrukturen beim Lacktrocknungsprozess, Ph.D. thesis, Technische Universität Dresden (2011).
- [44] M. S. Kiasat, *Curing shrinkage and residual stresses in viscoelastic thermosetting resins and composites*, Ph.D. thesis, Delft University of Technology (2000).
- [45] C. Li, K. Potter, M. R. Wisnom, and G. Stringer, *In-situ measurement of chemical shrinkage of MY750 epoxy resin by a novel gravimetric method*, Composites Science and Technology **64**, 55 (2004).
- [46] L. Khoun and P. Hubert, *Cure shrinkage characterization of an epoxy resin system by two in situ measurement methods*, Polymer Composites **31**, 1603 (2010).
- [47] J. de Vreugd, *The effect of aging on molding compound properties*, Ph.D. thesis, Technische Universiteit Delft (2011).
- [48] H. Winter and M. Mours, *Rheology of polymers near liquid-solid transitions*, Advances in Polymer Science **134**, 164 (1997).
- [49] R. J. Young and P. A. Lovell, *Introduction to polymers*, 3rd ed. (Taylor and Francis, 2011).
- [50] K. te Nijenhuis, *Thermoreversible networks. Viscoelastic properties and structure of gels* (Springer, Berlin, 1997).

- [51] D. B. Adolf, J. E. Martin, R. S. Chambers, S. N. Burchett, and T. R. Guess, *Stresses during thermoset cure*, Journal of Materials Research **13**, 530 (1998).
- [52] A. T. DiBenedetto, *Prediction of the glass transition temperature of polymers: A model based on the principle of corresponding states*, Journal of Polymer Science, Part B: Polymer Physics **25**, 1949 (1987).
- [53] A. Hale, C. W. Macosko, and H. E. Bair, *Glass transition temperature as a function of conversion in thermosetting polymers*, Macromolecules **24**, 2610 (1991).
- [54] J. Lange, S. Toll, J.-A. E. Manson, and A. Hult, *Residual stress build-up in thermoset films cured above their ultimate glass transition temperature*, Polymer **36**, 3135 (1995).
- [55] J. Lange, J.-A. E. Manson, and A. Hult, *Build-up of structure and viscoelastic properties in epoxy and acrylate resins cured below their ultimate glass transition temperature*, Polymer **37**, 5859 (1996).
- [56] J. Lange, S. Toll, J.-A. E. Manson, and A. Hult, *Residual stress build-up in thermoset films cured below their ultimate glass transition temperature*, Polymer **38**, 809 (1997).
- [57] J. De Vreugd, K. M. B. Jansen, L. J. Ernst, and J. A. C. M. Pijnenburg, *Modelling of viscoelastic properties of a curing adhesive*, in *WIT Transactions on Engineering Sciences*, Vol. 57 (2007) pp. 241–251.
- [58] W. Brockmann, P. L. Geiß, J. Klingen, and B. Schröder, *Adhesive Bonding Materials, Applications and Technology* (Wiley-VCH, 2009).
- [59] A. N. Gent, *Fracture mechanics of adhesive bonds*. Rubber Chemistry and Technology **47**, 202 (1974).
- [60] H. Hahn and N. Pagano, *Curing stresses in composite laminates*, Journal of Composite Materials **9**, 91 (1975).
- [61] M. L. Dano and M. W. Hyer, *Thermally-induced deformation behavior of unsymmetric laminates*, International Journal of Solids and Structures **35**, 2101 (1998).
- [62] C. S. Lopes, P. P. Camanho, Z. Gürdal, and B. F. Tatting, Progressive failure analysis of tow-placed, variable-stiffness composite panels, International Journal of Solids and Structures 44, 8493 (2007).

[63] F. S. Jumbo, I. A. Ashcroft, A. D. Crocombe, and M. M. Abdel Wahab, *Thermal residual stress analysis of epoxy bi-material laminates and bonded joints*, International Journal of Adhesion and Adhesives **30**, 523 (2010).

- [64] S. K. Basu and H. G. Kia, *Theoretical modeling of bond-line read-out in adhesive joined smc automotive body panels*, Journal of Composite Materials **42**, 539 (2008).
- [65] K. S. Kim and H. T. Hahn, *Residual stress development during processing of graphite/epoxy composites*, Composites Science and Technology **36**, 121 (1989).
- [66] S. R. White and H. T. Hahn, Cure cycle optimization for the reduction of processinginduced residual stresses in composite materials, Journal of Composite Materials 27, 1352 (1993).
- [67] Y. Weitsman, *Residual thermal stresses due to cool-down of epoxy-resin composites*, Journal of Applied Mechanics, Transactions ASME **46**, 563 (1979).
- [68] S. R. White and H. T. Hahn, *Process modeling of composite materials: Residual stress development during cure. part i. model formulation*, Journal of Composite Materials **26**, 2402 (1992).
- [69] M. S. Genidy, M. S. Madhukar, and J. D. Russell, *New method to reduce cure-induced stresses in thermoset polymer composites, part ii: closed loop feedback control system,* Journal of Composite Materials **34**, 1905 (2000).
- [70] D. Adolf and J. E. Martin, Calculation of Stresses in Crosslinking Polymers, Journal of Composite Materials 30, 13 (1996).
- [71] D. Adolf and R. Chambers, *Verification of the capability for quantitative stress pre- diction during epoxy cure*, Polymer **38**, 5481 (1997).
- [72] K. M. B. Jansen, J. De Vreugd, and L. J. Ernst, *Analytical estimate for curing-induced stress and warpage in coating layers*, Journal of Applied Polymer Science **126**, 1623 (2012).
- [73] J. De Vreugd, K. M. B. Jansen, L. J. Ernst, and C. Bohm, *Prediction of cure induced warpage of micro-electronic products*, Microelectronics Reliability **50**, 910 (2010).
- [74] C. Liebl, M. Johlitz, B. Yagimli, and A. Lion, *Three-dimensional chemo-thermomechanically coupled simulation of curing adhesives including viscoplasticity and chemical shrinkage*, Computational Mechanics **49**, 603 (2012).

[75] C. Liebl, M. Johlitz, B. Yagimli, and A. Lion, *Simulation of curing-induced viscoplastic deformation: A new approach considering chemo-thermomechanical coupling*, Archive of Applied Mechanics **82**, 1133 (2012).

- [76] D. B. Adolf and R. S. Chambers, *A thermodynamically consistent, nonlinear vis-coelastic approach for modeling thermosets during cure,* Journal of Rheology **51**, 23 (2007).
- [77] M. Hossain, G. Possart, and P. Steinmann, *A small-strain model to simulate the curing of thermosets*, Computational Mechanics **43**, 769 (2009).
- [78] M. Hossain, G. Possart, and P. Steinmann, *A finite strain framework for the simulation of polymer curing. part i: Elasticity,* Computational Mechanics **44**, 621 (2009).
- [79] M. Hossain, G. Possart, and P. Steinmann, *A finite strain framework for the simulation of polymer curing. part ii. viscoelasticity and shrinkage,* Computational Mechanics **46**, 363 (2010).
- [80] C. Blanke, Modellierung und numerische Simulation des Aufheizverhaltens von PKW-Bauteilen und -Karossen in Trocknern, Ph.D. thesis, Technische Universität Darmstadt (2009).
- [81] S. Paulke, Challenges in developing tools for the digital factory, in MAGNA-Conference: Enhanced Dip Painting Process by Simulation Tools (2013).



3

INFLUENCE OF THE TEMPERATURE CYCLE

Adhesive bonding is becoming a more and more important joining technology in automotive industry. Hot-curing epoxy adhesives are often used for structural bonds of car body shells. The cure process of the adhesive, however, can cause panel distortions. These distortions can occur close to the bond line (local distortions) or concern the whole geometry of a part (global distortions). In order to avoid these defects, a fundamental understanding of how distortions develop is needed. This chapter summarizes the experimental work in which the development of distortions is monitored over entire temperature cycles by means of a displacement measurement. The focus is on how different cure temperatures and heating rates affect the development and the final state of local distortions. It was found that distortions can already develop in the heating phase before the cure temperature is reached. Changes in the heating rate influence the development of distortions.

3.1. Introduction

Hot curing one-part epoxy adhesives are often used in automotive industry. They provide excellent chemical resistance, high strength and a good oil absorption needed in the manufacturing process of car bodies. Furthermore, the elevated temperature needed for

A modified version of this chapter has been published in International Journal of Adhesion and Adhesives **50**, 216 (2014) [1].

the cure process of the adhesive is reached during the thermal cycles for the baking process of the coatings. Thus, apart from a pre-cure treatment, additional time-consuming steps do not need to be integrated in the manufacturing process.

One of the main challenges of adhesively bonded car body shells is the prevention of surface defects. These defects develop during coating [2] or, in an earlier stage, during bonding: the cure process of the adhesive can cause distortions, *i.e.* unwanted, visible deformations of the adherends. Distortions can not only occur close to the adhesive bond lines (local distortions), they can also affect the overall geometry of a structure through bulging effects (global distortions).

In order to prevent these distortions by means of proper control of the bonding process and a adequate selection of adherends and adhesives, a fundamental understanding of how the distortions develop over time is essential.

3.1.1. LITERATURE REVIEW

The goal of the experimental study in this chapter is to monitor how local distortions caused by the changing properties of the one-part epoxy adhesive BM1496V [3] develop during cure over different temperature cycles.

Eis [4] investigated the mechanisms that cause surface distortions during the adhesive bonding process of car body shells. He names the squeeze-out of the adhesive from the bonding area (where the squeezed out adhesive shrinks and bends the upper panel over an edge of the lower one), the chemical shrinkage of the adhesive, the thermal shrinkage of the adhesive during cooling down and an in-homogeneous temperature distribution of the assembly, which leads to relative movements of the adherends, as the main causes for the 4 distortion types he identified (see section 2.2.1 and section 2.2.2). He provides strategies for different deformation cases to reduce distortions, including measures as lowering the cure temperature, reducing the adhesive squeeze-out or reducing temperature gradients in the structure.

Experimental investigations on bonding defects [5] or panel distortions [6–8] mainly focus on a state after manufacture. In that state the development of distortions is already completed. Only in a few works distortions are monitored over time when the adhesive material is chemically reacting under temperature changes.

Eis [4] monitored distortions caused by foaming polyurethanes for different heating rates. These adhesives expand during the setting process in order to bridge larger bonding gaps. He concludes that, for specific adhesives, the rate can affect the foaming (expansion) process and, therefore, distortions that remain after the cure cycle. One-part epoxies that shrink during cure are not investigated.

33

Chudaska and Hahn [9, 10] measured the displacement of a composite panel during different cure cycles. A significant amount of displacement occurs before the cooling phase and is influenced by the heating rate or the cure temperature. The authors explained that displacement by the chemical shrinkage of the adhesive. The displacement in the cooling phase is caused by thermal contraction.

Hahn and Jendrny [11] monitored distortions by means of a displacement measurement over time for one specific temperature profile. Their viscoelastic simulation model shows good agreement with the experiment, even though displacements before the cooling phase are neglected.

There have also been several other approaches to predict deformations due to curing epoxies. Some prediction models are based on linear elastic material behaviour [12–16]. In other approaches viscoelastic properties are assumed [11, 17, 18], in which the stress development during the heating phase was neglected.

In other publications, temperature- and cure-dependent viscoelastic material laws are proposed [19, 20]. With these models the stress build-up during the entire temperature cycle, *i.e.* also in the heating and the isothermal dwell period, can be taken into account. However, to apply this approach to a specific adhesive many characterization tests are necessary since material parameters need to be determined as functions of temperature, time and degree of cure.

With regard to car panel distortions, the question arises if the newer approaches offer better predictions and if they describe the process more realistically. The lack of experimental data for the entire development process of distortions limits an analysis of this topic.

3.1.2. RESEARCH QUESTIONS OF INTEREST

The cure process is accompanied by a number parallel processes: On a molecular level, the polymer chains cross-link to a dense network. Macroscopically, this leads to an increase in the mass density, *i.e.* chemical shrinking occurs. The mechanical properties of the adhesive change as well. An increasing temperature leads to a decrease in viscosity. The progress in cure increases the viscosity. In addition, the adhesive transforms from a viscous fluid to a viscoelastic solid. It develops the ability to sustain static load other than hydrostatic, *i.e.* an equilibrium shear modulus develops. Moreover, geometrical changes of the entire structure occur due to temperature changes. The adhesive and the adherends expand and shrink thermally.

The combination of these processes leads to stresses in the materials and between the adhesive and the adherends. If these stresses are big enough, they will force the steel sheet to visually deform, i.e. panel distortions occur.

The cure process is temperature dependent. Therefore, changes in the temperature cycle, *e.g.* a different temperature rate during heating or a different (maximum) cure temperature, are expected to affect the development and the final state of distortions. Hence, the following questions arise:

- How do local distortions develop during a temperature cycle?
 - Are current models able to describe this development?
 - When do distortions start to occur? Does the temperature rate affect this point?
- How does the temperature cycle affect the final distortion?
 - How does the maximum temperature (isothermal dwell period) influence the remaining distortion?
 - How does the temperature rate in the heating phase influence the final distortion?

3.2. STRATEGY

In order to answer the research questions, the development of local distortions in a steel strip will be monitored over time for different temperature cycles.

Car panel distortions result from a three-dimensional displacement field in a complex structure. Capturing the displacement function for each material point of a body over the entire cure process would lead to both experimental difficulties and challenges in data analysis. The approach chosen here is to perform displacement measurements on a test specimen that is a simplified representation of a bond line in a situation in which local distortions occur.

Figure 3.1 shows a drawing of such a scenario. It correlates with case 4 depicted in figure 2.1. While in a liquid state, the adhesive is squeezed out at the edges of the bond line. Subsequent shrinkage due to cross-linking or cooling pulls down the upper panel and causes distortions [4].

The displacement curve of a single point of a steel strip right above a bond line is monitored. This out-of-plane displacement is caused by the changing properties of the adhesive. Assuming the adhesive causes distortions by displacing the strip locally at the bond line, the displacement curve obtained indicates how distortions in the entire panel develop over time. The test is performed for different temperature cycles.

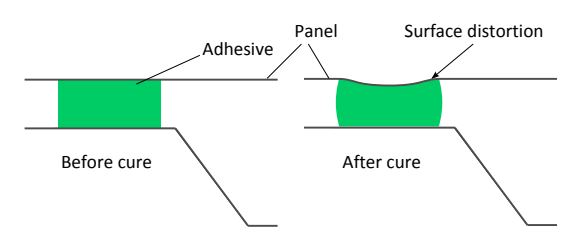


Figure 3.1: Local panel distortion resulting from adhesive cure [4].

3.3. EXPERIMENT AND DISPLACEMENT ESTIMATE

3.3.1. EXPERIMENTAL PROCEDURE

SPECIMEN

The test specimen is an assembly of an aluminium substructure (see figure 3.2) with a steel strip. The steel strip with the dimensions $20 \text{ mm} \times 85 \text{ mm} \times 0.70 \text{ mm}$ is placed

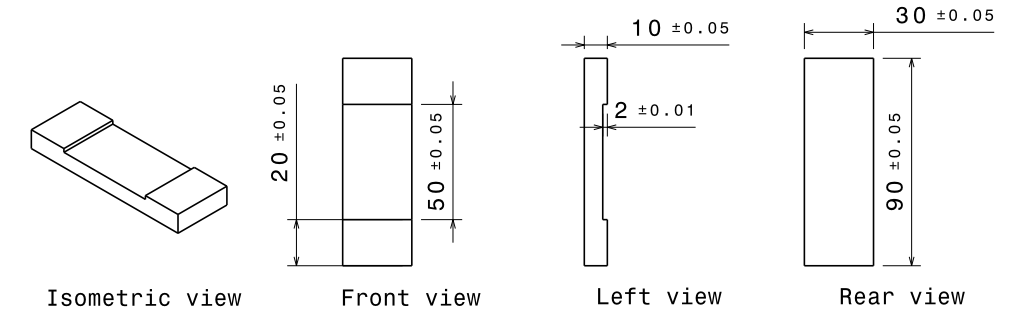


Figure 3.2: Dimensions of the substructure of the specimen in millimeters.

on top of the substructure above the 2-mm-deep bonding gap. Two aluminium blocks, screwed to the substructure, prevent the steel strip from lifting upwards but allow an inplane movement (no clamping) of the steel strip in the longitudinal direction (see photograph in figure 3.3). A 10-mm-broad line of adhesive is applied between steel strip and substructure. The out-of-plane (y-direction) displacement d of the central point of the steel strip above the adhesive bond line is recorded (see figure 3.3). Similar specimens have been used before by others [4, 10, 11].

MATERIALS

The substructure with the two blocks are made of aluminium 6082. Steel DX54D+Z from Tata is used for the strip. The adhesive system investigated is the epoxy-based BetamateTM 1496V. A Thermomechanical Analyser (TMA) is used to determine the CTEs α for the adhesive and the aluminium in different temperature ranges. Material properties

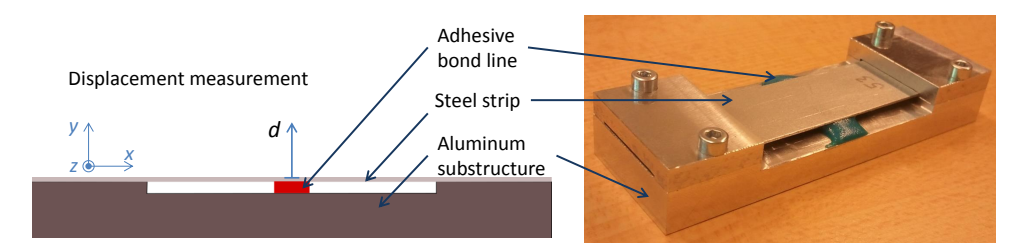


Figure 3.3: Drawing (left) and photograph (right) of the specimen. The displacement of the steel strip right above the adhesive layer is measured in *y*-direction.

are listed in table 3.1. The degree of cure at the gel point ($q_{\rm gel}$ = 0.455) and the final glass transition temperature ($T_{\rm g}$ = 85 °C) of the adhesive were measured in [21].

Table 3.1: Young's moduli E and CTE for the materials used.

Material	E (GPa)	$\alpha (10^{-6}/\text{K})$	
		40 to 60 ° C	120 to 140 °C
Steel DX54D+Z	210	12.4	12.8
Aluminium 6082	69	23.2	23.8
BM1496V	1.6	118.8	188.5

SET-UP

To measure the displacement, a laser sensor of the type KEYENCE LK-G152 is used. The specimen is put in an oven consisting of a box container and four heating elements. In order to allow for a good heat transfer and to minimize temperature differences inside the oven, the box container is made out of aluminium and the heating elements are integrated in the top and the bottom wall of the container (see figure 3.4). The container has an opening slot on top which allows the laser sensor to perform measurements on the specimen from outside the heated box where the laser stays within its operating temperature range from zero to 50 °C. A thermocouple on the inner side of the container wall allows to control the temperature inside the box. A second thermocouple monitors the temperature on one of the aluminium blocks of the specimen. An aluminium fixture holds the laser in its position above the aluminium box container. Thermocouples, the laser and the heating elements are connected to a computer for data handling and temperature control.

Preliminary tests indicated an influence of the environmental temperature on the test results. Therefore, the set-up is placed in a temperature-controlled chamber to maintain constant environmental temperature (see figure 3.4).

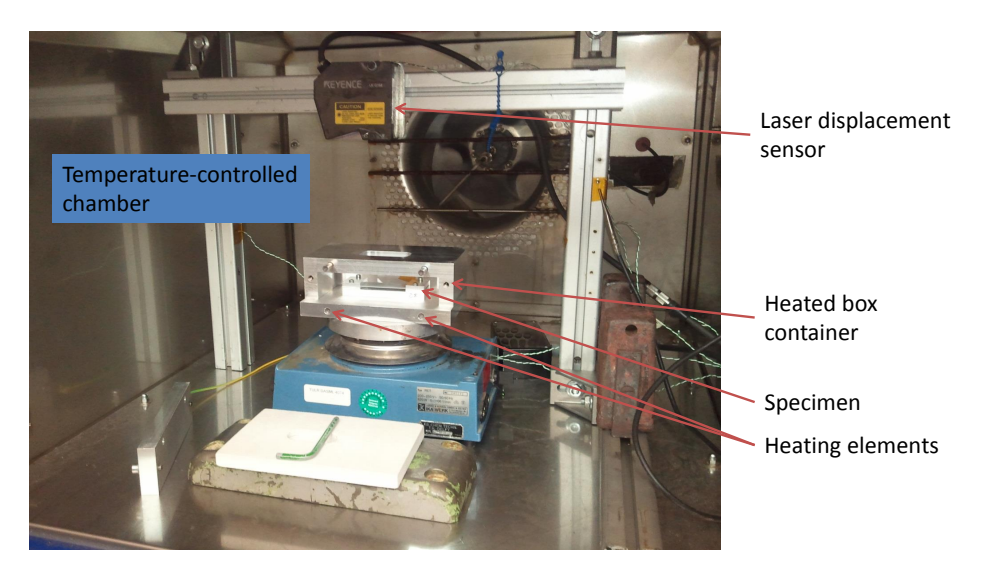


Figure 3.4: The set-up is placed in a temperature-controlled chamber. A laser sensor measures displacements on a specimen in a heated aluminium box container.

PROCEDURES

The adhesive producer recommends two different cure cycles: 30 minutes at 170 °C or 60 minutes at 155 °C. Taking these recommendations into account, several temperature profiles have been defined. Table 3.2 shows the investigated temperature curves. After the isothermal dwell period, the specimen cools down to 50 °C. The average cooling rate of all cycles is -3 K/min (see figures 3.5 and 3.6).

Table 3.2: Temperature cycles.

Name	Temperature rate	Dwell temp.	Dwell time
L170	Low (1 K/min)	170 °C	33 min
M170	Medium (7 K/min)	170 °C	33 min
H170	High (35 K/min)	170 °C	33 min
L155	Low (1 K/min)	155 °C	63 min
M155	Medium (7 K/min)	155 °C	63 min
H155	High (35 K/min)	155 °C	63 min

The idea is to heat the specimen to the recommended cure temperatures applying a low, medium and high (highest possible with this set-up) temperature rate.

Before the specimen is heated at the selected temperature rate, the temperature in the aluminium box is set to 50 $^{\circ}$ C for one hour to make sure all tests start from the same temperature distribution in the set-up. The final cooling down temperature is 50 $^{\circ}$ C as well. DSC tests indicated that significant chemical reactions in this specific adhesive

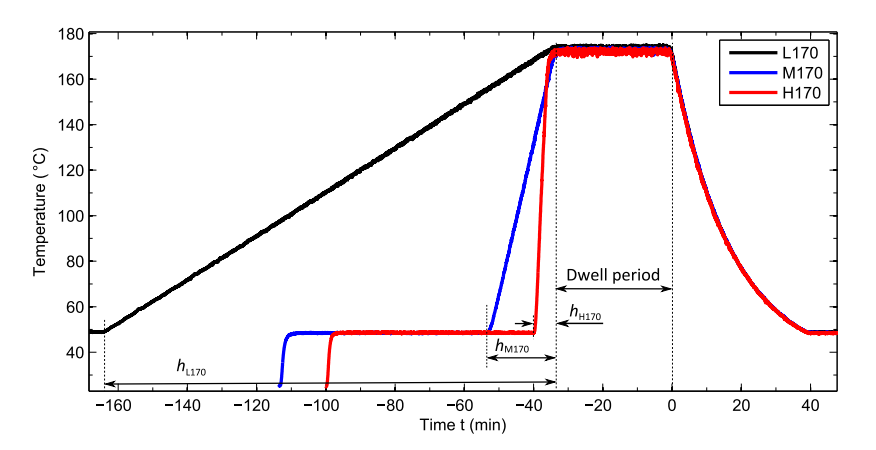


Figure 3.5: Specimen temperature profiles for a cure temperature of 170 °C with the different heating time intervals $h_{\rm L170}$, $h_{\rm M170}$ and $h_{\rm H170}$.

take place only at temperatures above 100 °C (see sections 3.3.2 and 3.4.3). Therefore, it is assumed that a starting and final temperature of 50 °C instead of room temperature in the temperature cycle does not affect the cure process. Figure 3.5 shows the temperature curves for the 3 different cycles with a cure temperature of 170 °C. Profiles with 155 °C cure temperature are shown in figure 3.6.

The cycle of one test is as follows: The specimen is placed in the oven with a thermocouple taped to one of the aluminium blocks. The climate chamber is set to 25 $^{\circ}$ C. The temperature inside the oven is computer controlled and follows a predefined cycle. At the same time the displacement as well as the specimen temperature is monitored with a sample rate of 1 Hz.

For each specimen, this procedure is performed twice: once without (WO) and once with (W) the adhesive. In both tests the specimen is exposed to the same temperature profile. An average curve for the WO-curves as well as for the W-curves is calculated. Each curve is based on at least two replicates. The WO-curves provide reference displacement curves allowing to determine the displacement that is caused by the adhesive.

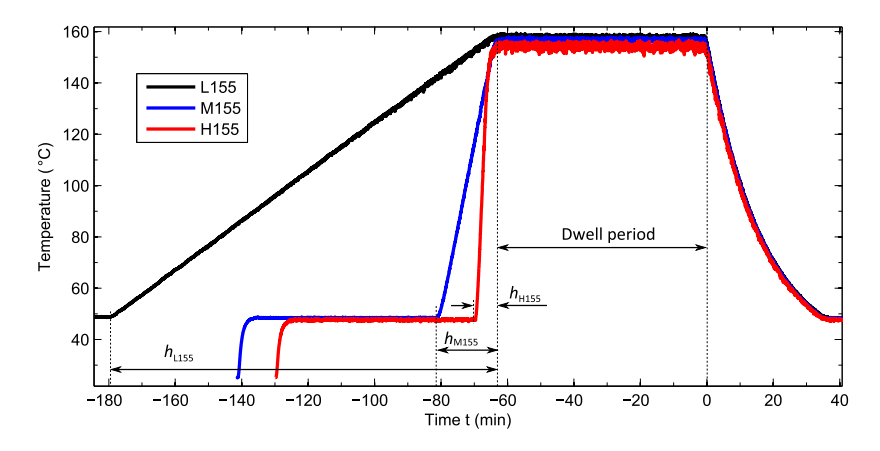


Figure 3.6: Specimen temperature profiles for a cure temperature of 155 °C with the different heating time intervals h_{L155} , h_{M155} and h_{H155} .

3.3.2. DIFFERENTIAL SCANNING CALORIMETRY

The progress in cure can be described by a single variable q, the degree of cure. Since the cross-linking process is an exothermic reaction, it is common to assume that the cure rate is proportional to a measured heat flow $\mathrm{d}H/\mathrm{d}t$:

$$\frac{\mathrm{d}q(t)}{\mathrm{d}t} = \frac{1}{H_{\infty}} \frac{\mathrm{d}H(t)}{\mathrm{d}t},\tag{3.1}$$

where H_{∞} is the (total) heat of reaction [22]. A DSC allows to measure the released heat for different temperature rates. DSC tests were performed for the low, medium and high heating rates, *i.e.* 1, 7 and 35 K/min.

3.3.3. DISPLACEMENT ESTIMATE

In order to get an idea of how much displacement to expect, a rough estimate on the displacement Δa of a a-thick adhesive layer is made (figure 3.7). The strain in the adhesive can be described by

$$\varepsilon_{ij} = \varepsilon^{\text{th}} \delta_{ij} + \varepsilon^{\text{ch}} \delta_{ij} + \varepsilon_{ij}^{\text{me}}, \tag{3.2}$$

where δ_{ij} is the Kronecker delta; ε^{th} , ε^{ch} and $\varepsilon^{\text{me}}_{ij}$ are the thermal, chemical and mechanical strains, respectively. Equation 3.2 implies an isotropic behaviour regarding thermal

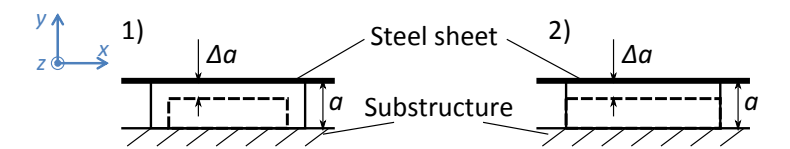


Figure 3.7: Models for the vertical displacement Δa of a adhesive layer with a thickness of a: 1) The adhesive can shrink freely, 2) the in-plane (x-z-plane) shrinkage is constrained.

and chemical strains. In addition, a constant CTE α is assumed:

$$\varepsilon^{\text{th}} = \alpha \Delta T$$

with ΔT being the difference between the actual and the cure temperature, at which the adhesive is presumably strain-free.

In a first approach, it is assumed that the adhesive can shrink freely without being constrained by the adherends (figure 3.7, case 1). The mechanical part in equation 3.2 is zero and it can easily be written:

$$\Delta a = \varepsilon_{yy} a \tag{3.3}$$

$$\Delta a = (\varepsilon^{\text{th}} + \varepsilon^{\text{ch}}) a.$$

With a=2 mm, $\Delta T=-120$ K, $\alpha=150\cdot 10^{-6}$ /K and a linear chemical shrinkage of $\varepsilon^{\rm ch}=-1$ % we receive $\Delta a=-56$ μ m.

In a second approach the shrinkage of the adhesive in the x-z-plane is considered to be constrained by the adherends. To keep things simple, normal strains in that plane are neglected:

$$\varepsilon_{xx} = \varepsilon_{zz} = 0.$$

This leads to the mechanical components:

$$\varepsilon_{xx}^{\text{me}} = \varepsilon_{zz}^{\text{me}} = -(\varepsilon^{\text{th}} + \varepsilon^{\text{ch}}),$$
 (3.4)

If the adhesive is assumed to be linear elastic during the cooling down and no force is

¹These material constants are rough estimates only. To account for the glass transition during the cooling down, the chosen CTE lies between the rubbery and glassy one listed in table 3.1. 1 % chemical strain results in a volume shrinkage (factor 3) slightly below the 4 to 5 % for epoxies (table 2.1), which can be easily achieved with inert filler material.

exerted on it in y-direction, it can be written

$$\sigma_{yy} = \frac{E}{(1+\nu)(1-2\nu)} \left(\nu(\varepsilon_{xx}^{\text{me}} + \varepsilon_{zz}^{\text{me}}) + (1-\nu)\varepsilon_{yy}^{\text{me}} \right) = 0, \tag{3.5}$$

with σ_{yy} being the normal stress in *y*-direction. *E* and *v* are the elastic constants of the adhesive. With equation 3.2, 3.4 and 3.5 follows

$$\varepsilon_{yy} = \frac{1+\nu}{1-\nu} (\varepsilon^{\text{ch}} + \varepsilon^{\text{th}})$$

and with equation 3.3 follows

$$\Delta a = \frac{1+\nu}{1-\nu} \left(\varepsilon^{\text{ch}} + \varepsilon^{\text{th}} \right) a.$$

With the values from the previous estimate and v = 0.4, $\Delta a = -131 \,\mu\text{m}$ is received.

3.4. RESULTS

In order to compare displacement curves, a horizontal and a vertical reference point need to be defined. Therefore, the displacement value is set to 0 μ m at the point where the specimen reaches 55 °C for the first time. All curves are shifted on the time scale, so that t=0 indicates the beginning of the cooling down.

Displacement curves for the tests with adhesive at the medium temperature rate and a cure temperature of $170\,^{\circ}\text{C}$ can be seen in figure 3.8. These plots show the raw data. In a next step, the curves are filtered with a moving-average filter over an 11-seconds-interval for noise reduction. Two mean curves per temperature cycle were calculated, one for the tests with and one for the tests without adhesive layer (see figure 3.9). The WO-curves, as the one in figure 3.9, are reference curves. They capture the expansion of the entire structure of the setup below the measurement point, *i.e.* the specimen, the bottom plate of the heated box and the heating plate the box is mounted on, see figure 3.4. The difference between the W-curves and the WO-curves are shown in figures 3.10 and 3.11, respectively. They show the displacement that is caused by the adhesive. Note that the size of the bonding gap (in *y*-direction) changes with the expansion of the substructure (figure 3.3). Thus, differences in the W- and WO-curves only occur if the adhesive fills less or more space in *y*-direction than the actual size of the gap. Only then, the steel strip is bent.

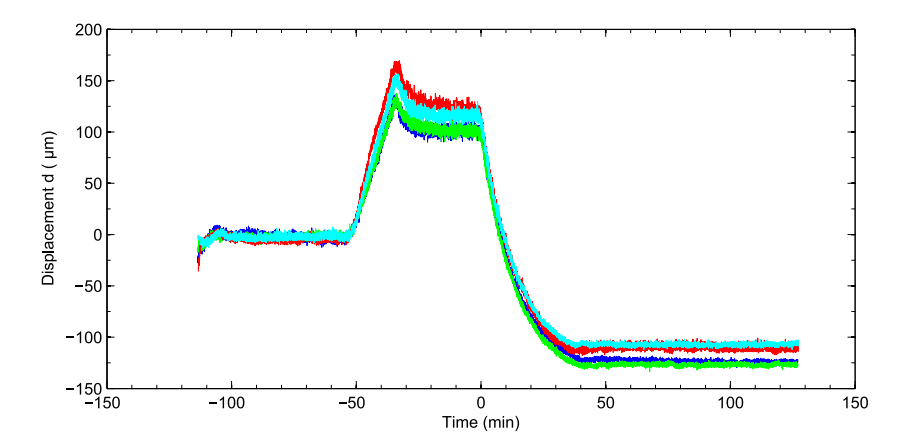


Figure 3.8: Unfiltered displacement curves for the tests with adhesive layer at the medium temperature rate and a cure temperature of 170 $^{\circ}$ C.

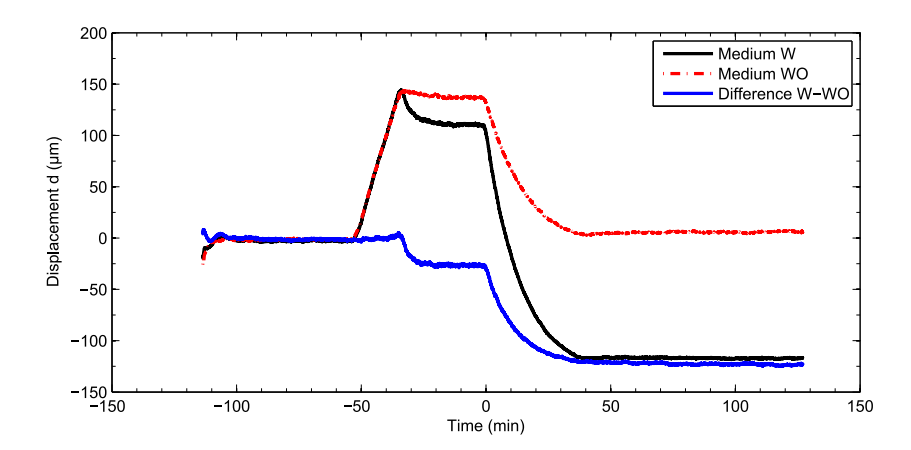


Figure 3.9: Averaged displacement curves for tests with and without adhesive layer in the 170 $^{\circ}$ C cure cycles at medium temperature rate and the difference between both.

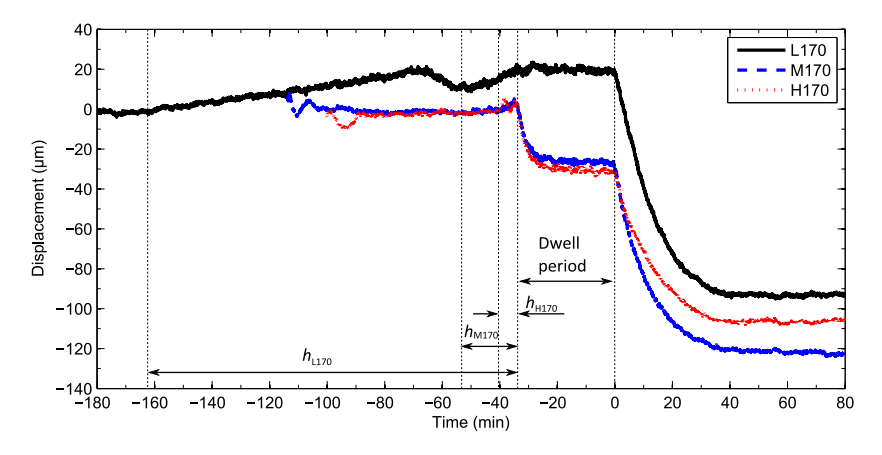


Figure 3.10: Displacement caused by the adhesive at temperature cycles with 170 $^{\circ}$ C cure temperature and low, medium and high temperature rate.

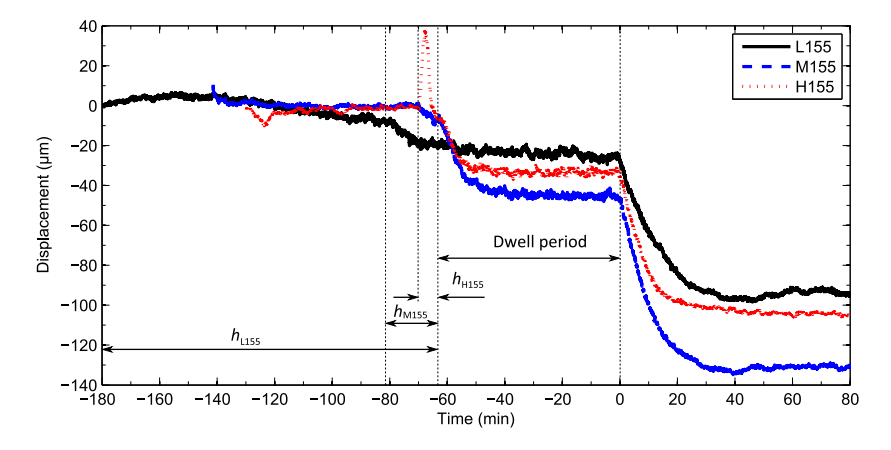


Figure 3.11: Displacement caused by the adhesive at temperature cycles with 155 $^{\circ}$ C cure temperature and low, medium and high temperature rate.

3.4.1. Temperature cycles with 170 °C cure temperature

The curves in figure 3.10 show that the displacement caused by the adhesive does not start with heating. For the medium and the high temperature rates, the displacement starts at about t=-35 min, a time when the specimen's temperature is close to the maximum temperature. At that time, the curve drops rather rapidly to about -27 μ m in case of the medium temperature rate and to -30 μ m for the high heating rate, respectively. The curves stay constant at that value for the rest of the isothermal dwell period and start to drop further when the cooling phase sets in. The final displacement for the medium rate is about -122 μ m; the curve for the high temperature rates reaches -107 μ m.

In the test with the low temperature rate, the behaviour is different (figure 3.10). The displacement starts at t=-160 min. The displacement curve rises and reaches a local maximum at around t=-68 min. After that, a decrease and another increase in the displacement takes place until the maximum temperature is reached and the displacement stays at +19 μ m. During the dwell period, no further displacement takes place. During cooling down, another downwards movement sets in until a final displacement of about -93 μ m is reached.

3.4.2. Temperature cycles with 155 °C cure temperature

Tests with a cure temperature of 155 °C show a similar behaviour for the medium and the high temperature rates. The blue curve for the M155 rate in figure 3.11 shows a first drop beginning at t=-70 min. At that time the specimen has a temperature of about 110 °C (see figure 3.6). It stays at a plateau of about $-44~\mu m$ and drops then further in the cooling down phase to about $-131~\mu m$. The curve for the H155 rate shows the same tendency except for a peak at t=-68 min. It reaches a plateau of $-35~\mu m$ and a final displacement of about $-100~\mu m$.

Tests for the L155 rate show a slow but steady drop to about $-27 \,\mu m$ at t=0; the final displacement is $-92 \,\mu m$.

3.4.3. DIFFERENTIAL SCANNING CALORIMETRY

Figure 3.12 shows the exothermic peaks in the heat flow for the different heating rates obtained with a DSC. The degree of cure at a certain temperature in the temperature ramp can be estimated by integrating the heat flow curve over time up to the point in time at which that temperature is reached and dividing the result by H_{∞} , *i.e.* the integral over the full curve, see equation 3.1. Table 3.3 shows H_{∞} and the degree of cure at the point when the cure temperature is reached.

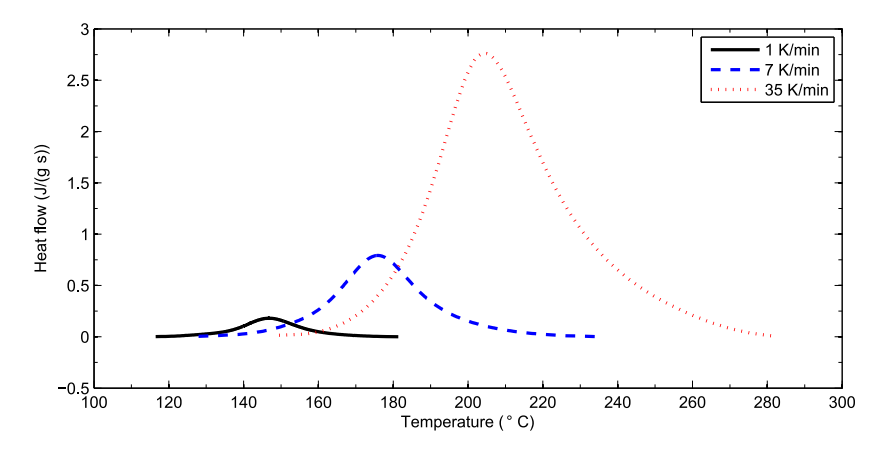


Figure 3.12: DSC curves for different heating rates.

Table 3.3: H_{∞} and the degree of cure when the cure temperature is reached.

	1 K/min	7 K/min	35 K/min
q(155 °C) (-)	0.813	0.061	0.002
q(170 °C) (-)	0.985	0.290	0.013
H_{∞} (J/g)	224.2	207.0	202.0

3.5. DISCUSSION

After the curves in figure 3.8 are filtered, they have a scatter band of 23 μ m in the state after cooling down. Therefore, results presented here provide an insight into general behaviour rather than quantitative information.

The final displacements measured correspond approximately with the second estimate in section 3.3.3, which takes in-plane constraints into account. The first estimate, a simple one-dimensional calculation, predicts significantly lower displacements. Both models are not capable of predicting differences in displacements due to different heating rates.

The curves for the medium and high temperature rates (with 155 as well as 170 $^{\circ}$ C cure temperature, see figure 3.10 and 3.11) show a split in three distinct parts: A first part where the displacement stays zero, a second where it drops rapidly to a plateau value and a third one with a second drop to the final displacement. The last part starts with the cooling down.

The second part starts close to the point when the maximum temperature, *i.e.* the dwell phase, is reached; the main drop takes place in the dwell period. The point in time when the first displacement occurs must be beyond the time when the adhesive reaches

the gel point. The gel point is the point where the cross-linking of the polymer reaches a level at which the adhesive is able to build up residual stresses and deform the steel strip (cf. [23]). From the displacement curves of the medium and high temperature rates, it is difficult to establish with certainty whether the gel point is passed before the maximum temperature is reached. The DSC results (figure 3.12) indicate a shift of the cure process to higher temperatures in case the heating rate is increased. For a rate of 35 K/min, 0.2 % of cure is reached at 155 °C and 1.3 % is reached 170 °C. These values are too low for complete gelation. Thus, the gel point is passed during isothermal phase at 155 and 170 °C, respectively. With the medium heating rate, 6.1 % of conversion is reached at 155 °C and 29.0 % is reached at 170 °C. Both values are below $q_{\rm gel} = 0.455$ measured in [21].

The cause of the upwards displacement for the L170 rate starting at t=-160 min is unclear. The specimen reaches 100 °C at t=-110 min (see figure 3.5). Below that temperature, there are no significant chemical reactions according to the DSC results (see figure 3.12). Therefore, the adhesive remains in the liquid state; a deflection of the steel strip caused by the adhesive is not possible. An upwards movement (above 100 °C, i.e. after t=-110 min) is possible if the thermal expansion exceeds the chemical shrinkage. In that case, the curve for the L155 profile should show the same tendency, which it does not. Therefore, it seems likely that the tendency of an upwards displacement is caused by measurement errors.

The first downwards drop in all graphs can be explained by the chemical shrinkage that takes place until the adhesive is fully cured. In case of medium and high temperature rates (M170, H170, M155, H155), this happens rather fast and stops early in the dwell period. The last 20 min of the dwell period in the 170 °C cure cycles and the last 40 min of the dwell period in the 155 °C cure cycles show no change in the displacement. This indicates that chemical shrinking ended. As the different calculations in section 3.3.3 indicate, in-plane strain can affect the out-of-plane displacement. In case the thermal expansion of the adherends exceeds the chemical and thermal deformations of the adhesive, the adhesive layer is stretched in in-plane direction. That leads to a contraction in y-direction. Displacements due to such a Poisson effect stop with temperature changes. Since the first downwards displacement stops soon after the dwell period is reached, the Poisson effect can be an explanation for it.

In case of the low temperature rates (L170 and L155), the first development of displacement happens slowly. For these rates, the adhesive reaches 81.3 % and 98.5 % of conversion at the end of the heating phase (table 3.3). Assuming the chemical shrinkage is proportional to the degree of cure, very little chemical shrinkage would be expected in the dwell phase for L155 and L170. Since there is no thermal deformation in the dwell

period, displacements should be close to zero in that phase for the low heating rate. This agrees with the L155 and L170 curves in figures 3.10 and 3.11.

The peak in the displacement curve for the H155 temperature rate (see figure 3.11) is possibly due to measurement errors. The W- and WO- displacements change rapidly in the heating phase so that small deviations can lead to big differences between these curves.

The displacement curves for the low temperature rates (L155 and L170) show no significant difference in the final value they reach after the cure cycle. This means that, in this specific case, a lower cure temperature does not lower distortions significantly. Although it cannot be ruled out that small deviations might have occurred but stayed undetected in this experiment, the case that the lower cure temperature does not lower the distortion for the low temperature rate, is not unexpected. Due to the low temperature rate, the adhesive reaches the gel point in the heating phase before the maximum temperature is reached. Therefore, stress build-up after that point due to an increasing temperature will be reversed as soon as the specimen is cooled down, again, to the temperature it had at that point. Accordingly, a higher maximum temperature does not affect the displacement after cooling down. For the medium and the high temperature rates, the differences between the two cure temperatures in the final displacement are less than $10 \, \mu m$. With regard to the accuracy of the set-up, these differences can be due to measurement deviations. To clarify this, further investigations are needed.

The low rates show less absolute final displacement than the other rates for both cure temperatures. Due to the low heating rate the adhesive reaches the gel point at a lower temperature. This leads to less thermal deformation and less absolute final displacement, respectively.

Surprising is that the absolute final displacements for the high rates are lower than those for the medium rates. A fast heating should push the gel point to a higher temperature and cause more thermal deformation in the final state. It is possible that the high temperature rate leads to big temperature gradients in the adhesive layer. That may affect the cure process and lead to different mechanical behaviour of the adhesive. This matter needs further investigation.

3.6. CONCLUSIONS

Local distortions develop in two main parts: the first part is mainly caused by the chemical shrinkage. This part starts already in the heating phase, when the cure temperature is not reached yet. The temperature rate can affect this point: At low temperature rates, this point shifts to a lower temperature. The first part ends before the cooling down starts.

The second part is caused by thermal shrinkage of the adhesive during the cooling down phase. Models which cover only the cooling down phase neglect the first part.

An effect of the cure temperature on the final distortions was not observed. Due to gelation in the heating phase, the maximum temperature does not affect the final position of the strip after the cure cycle. The temperature rate in the heating phase can affect local distortions. A low rate can reduce the distortion given that this rate is low enough so that the adhesive can reach the gel point at a lower temperature.

REFERENCES

- [1] K. Priesnitz, J. Sinke, and R. Benedictus, *Influence of the temperature cycle on lo*cal distortions in car panels caused by hot curing epoxies, International Journal of Adhesion and Adhesives **50**, 216 (2014).
- [2] R. H. J. Blunk and J. O. Wilkes, *Numerical analysis of surface-tension-driven coating flow,* Polymer Engineering and Science **42**, 258 (2002).
- [3] Dow Automotive Systems, *BETAMATE*TM 1496V, data sheet.
- [4] M. Eis, Fertigungsbedingte Bauteildeformationen beim Kleben dünnwandiger Stahlbauteile: Analyse der Entstehungsmechanismen und Hinweise zur Minimierung, Ph.D. thesis, Universität Paderborn (2000).
- [5] R. L. Vijaya Kumar, M. R. Bhat, and C. R. L. Murthy, *Evaluation of kissing bond in composite adhesive lap joints using digital image correlation: Preliminary studies,* International Journal of Adhesion and Adhesives **42**, 60 (2013).
- [6] A. Andersson, *Evaluation and visualisation of surface defects on auto-body panels*, Journal of Materials Processing Technology **209**, 821 (2009).
- [7] P. C. P. Bouten, On the stability of the adhesive layer thickness, in 4th International Adhesion Conference, Cambridge University, England (1990).
- [8] K. Fernholz, R. Hsakou, K. Lazarz, C. S. Wang, B. Emerson, D. Biernat, and D. Case, Development of a tool to measure bond-line read-through, in SPE Automotive and Composites Divisions - 7th Annual Automotive Composites Conference and Exhibition, ACCE 2007 - Driving Performance and Productivity, Vol. 1 (2007) pp. 90–106.
- [9] A. Chudaska and O. Hahn, *Untersuchungen zum temperatur- und reaktions*bedingten Klebstoffschrumpf - Maßnahmen zur Reduzierung schrumpfbedingter

- Bauteilschädigungen, in Wärmearme Fügetechniken Kleben Durchsetzfügen Nieten (1993) pp. 121 130.
- [10] A. Chudaska and O. Hahn, Damages of bonded parts caused by the thermal and reactionary contraction of adhesives during the curing process, in Vide-Science Technique Et Applications (1994) pp. 223–227.
- [11] O. Hahn and J. Jendrny, Evaluation of simulation models for the estimation of deformation of adhesively bonded steel sheets during curing, Welding in the World **47**, 31 (2003).
- [12] H. Hahn and N. Pagano, *Curing stresses in composite laminates*, Journal of Composite Materials **9**, 91 (1975).
- [13] A. Plepys, M. S. Vratsanos, and R. J. Farris, *Determination of residual stresses using incremental linear elasticity*, Composite Structures **27**, 51 (1994).
- [14] Y. Yu, I. A. Ashcroft, and G. Swallowe, *An experimental investigation of residual stresses in an epoxy-steel laminate*, International Journal of Adhesion and Adhesives **26**, 511 (2006).
- [15] S. K. Basu and H. G. Kia, *Theoretical modeling of bond-line read-out in adhesive joined smc automotive body panels*, Journal of Composite Materials **42**, 539 (2008).
- [16] F. S. Jumbo, I. A. Ashcroft, A. D. Crocombe, and M. M. Abdel Wahab, *Thermal residual stress analysis of epoxy bi-material laminates and bonded joints*, International Journal of Adhesion and Adhesives **30**, 523 (2010).
- [17] H. Fuchs, K. D. Fernholz, and P. Deslauriers, *Predicted and Measured Bond-Line Read-Through Response in Composite Automotive Body Panels Subjected to Elevated Temperature Cure*, Journal of Adhesion **86**, 982 (2010).
- [18] K. A. Patankar, D. A. Dillard, and K. D. Fernholz, *Characterizing the constitutive properties and developing a stress model for adhesive bond-line readout,* International Journal of Adhesion and Adhesives **40**, 149 (2013).
- [19] J. De Vreugd, K. M. B. Jansen, L. J. Ernst, and C. Bohm, *Prediction of cure induced warpage of micro-electronic products*, Microelectronics Reliability **50**, 910 (2010).
- [20] D. Adolf and J. E. Martin, *Calculation of Stresses in Crosslinking Polymers*, Journal of Composite Materials **30**, 13 (1996).

[21] S. Menzel, Zur Berechnung von Klebverbindungen hybrider Karosseriestrukturen beim Lacktrocknungsprozess, Ph.D. thesis, Technische Universität Dresden (2011).

- [22] B. Prime, *Thermosets*, in *Thermal characterization of polymeric materials*, Vol. 2, edited by E. A. Turi (Academic Press, 1997) pp. 1380 1766.
- [23] K. te Nijenhuis, *Thermoreversible networks. Viscoelastic properties and structure of gels* (Springer, Berlin, 1997).

J

4

FINITE-ELEMENT MODEL

Hot-curing one-part adhesives are often used to bond car body shells. The cure process of the adhesive, however, can lead to distortions, i.e. unwanted, visible deformations of the adherends. In case of outer car panels, these distortions are considered visual defects, even though the structural integrity might not be affected. In order to avoid distortions by a proper control of the bonding process, a thorough understanding of the development of distortions is necessary. Finite-element simulations can help to gain insight into this development. In this chapter a simulation model is proposed and used to study the appearance of distortions in a steel strip over different temperature cycles. The model takes chemical shrinkage and thermal deformation as well as gelation and stress relaxation into account. It was found that the heating rate can affect distortions. Lowering the cure temperature only lowers distortions for high heating rates. Low heating rates can reduce distortions.

4.1. Introduction

Adhesive bonding is a widely-used joining technology in automotive industry. Hot-curing one-part adhesives are well suited for car body manufacturing because of their good oil absorption and flexible applicability. Bonding processes with this type of adhesive are not restricted by pot life or assurance of a correct mixture ratio. Moreover, the baking

A modified version of this chapter has been published in International Journal of Solids and Structures **51**, 2470 (2014) [1].

process after electrophoretic coating can serve as a cure cycle for the adhesive eliminating the need for another stopover in the oven. The cure process of the adhesive at elevated temperatures, however, can lead to distortions, i.e. unwanted, visible deformations of the structure, especially when thin-walled structures as outer car panels are involved. These distortions can occur along the bond line (local distortions) or affect the entire geometry (global distortions). Adapting the production process or repair work can be costly and time-consuming, once these defects occur. Therefore, it is desirable to predict distortions before they arise and modify manufacturing accordingly to prevent them. Several constitutive models of curing polymers have been successfully used to predict residual stresses in composite manufacturing and other processes [2-4]. With regard to car panel distortion, however, models mainly focused on the cooling down phase [5, 6]. These models do not allow for following the development of distortions over the entire cure cycle. They assume a stress-free state when the cooling down sets in. But investigations on residual stresses in laminates show that the structure is not warpagefree if heated up, again, to cure temperature after manufacturing [7]. The objective in this chapter is to build up a simulation model for local panel distortions, which is capable of predicting the development of distortions over different cure cycles. It should take known phenomena of curing polymers into account. By that, it will be a basis for analyzing bonding processes with regard to panel distortions.

4.2. BACKGROUND

A main cause for panel distortions is the combination of changing properties of the adhesive. During the bonding process, the adhesive develops from a viscous liquid to a viscoelastic solid [8, 9]. At the same time, the adhesive's specific volume changes. Due to the cross-linking of polymer chains, the density of the adhesive increases. This process is referred to as chemical or reactive shrinkage. The changing temperature leads to additional thermal deformation of the adhesive. The evolving properties of the adhesive can cause local panel distortions, *i.e.* deformations close to the bond line. Therefore, they are the main focus of this work. But it should be emphasized that further phenomena play a role in panel distortions. The temperature cycle can cause relative movements of the adherends during the bonding process [5, 10]. These displacements depend on boundary conditions of the bonding process such as geometry and fixture of the structure, temperature field in the oven [11] and the thermal expansion and conductivity of the adherend materials. Especially in multi-material design, different CTEs can lead to thermally induced relative movements during the bonding process which remain after the cure cycle. This " α -mismatch" problem has been subject to numerous research ac-

4

53

tivities [12-16].

While several experimental investigations focus on a final state of distortions after the cure process [17–20], in some works their development over the temperature cycle is examined (see chapter 3 or [21–24]). These publications show that significant deformation develops during the cooling phase. But even in the heating and isothermal dwell phase of a temperature cycle, deformations can arise. Changes to the temperature cycle (such as cure temperature, dwelling periods at elevated temperature before the final cure step, heating and cooling rates) affect significantly residual stresses and the properties of the adhesive bond [13, 25, 26]. This knowledge is already applied in cure cycle optimization. White and Hahn [26] found that dwelling at elevated temperatures before the final cure temperature is reached can reduce residual stresses in composites.

Besides experimental research, there have also been several different numerical approaches to predict residual stresses in composites [27–29] or adhesive bonds [5, 6, 20]. Prediction models based on elastic material behaviour [30–34] are available as well as models based on viscoelasticity [5, 6, 20]. These approaches take only the cooling down phase into account. Stresses in the heating and dwell phase are neglected. Other constitutive models of curing polymers [2–4, 35–38] allow to capture the full cure cycle. They indicate that stresses can occur before the cooling down sets in. These models have been successfully applied to coating processes [4], electronic packaging [3] and composites manufacturing [2]. An application to local panel distortions due to adhesive bonding is missing.

In some prediction models, the chemical shrinkage is not accounted for [5, 33]. Some authors argue that the contribution of chemical shrinkage to residual stresses is small [39, 40]. Genidy *et al.* [41] state that the low influence of chemical shrinkage on residual stresses in composites predicted in [40] is due to an underestimation as further experimental work by the same authors show [26]. Other investigations on the development of panel distortions (chapter 3,[22]) indicate a significant deformation before the cooling down sets in. Chudaska and Hahn [22] reason that this displacement is caused by chemical shrinkage of the adhesive. De Vreugd [42, p. 70] points out that standard tests for measuring chemical shrinkage are performed by measuring volumes at ambient temperature before and after curing. But the shrinking process takes place at elevated temperatures. Therefore, he measures changes in the specific volume over a full temperature cycle. A three-dimensional simulation model on distortion development would give insight in how chemical shrinkage and other changing material properties mentioned above contribute to the development of local panel distortions.

4.3. THE MODEL

In this chapter, a simulation model for developing local distortions due to hot curing adhesives is proposed. The cure process is assumed to be quasi-static. In that case, the balance of linear momentum can be expressed by the equation

$$\frac{\partial \sigma_{ij}}{\partial x_i} = 0, (4.1)$$

where σ_{ij} is the Cauchy stress tensor. In addition, it is assumed that the state of cure can be described by a single variable q, the degree of cure. The cure evolution is described by the Kamal-Sourour equation for auto-catalytic reactions [43, 44]

$$\dot{q} = k_0 \exp\left[-\frac{E_a}{RT}\right] q^m (1-q)^n,$$
 (4.2)

where $R=8.314\,\mathrm{J/(mol\,K)}$ is the ideal gas constant; the material parameters k_0 , $E_{\rm a}$, m and n need to be determined by fitting the equation to experimental data. To avoid q=0 for all times, $q_0=0.01$ is chosen as an initial value for q.

An important part of a simulation model are the material equations for the adhesive. The adhesive is assumed to be isotropic. As in other works [37, 45], this model is based on an additive decomposition of the strain tensor. Here, ε_{ij} is split in a mechanical, a thermal and a chemical part:

$$\varepsilon_{ij} = \varepsilon_{ij}^{\text{me}} + \varepsilon_{ij}^{\text{th}} + \varepsilon_{ij}^{\text{ch}}. \tag{4.3}$$

Since the mechanical properties of the adhesive change significantly over a cure cycle, the process is divided into three stages. In each of these stages, the mechanical behaviour is described by different constitutive equations. The gel point and the glass transition represent the transition points between the stages (see figure 4.1).

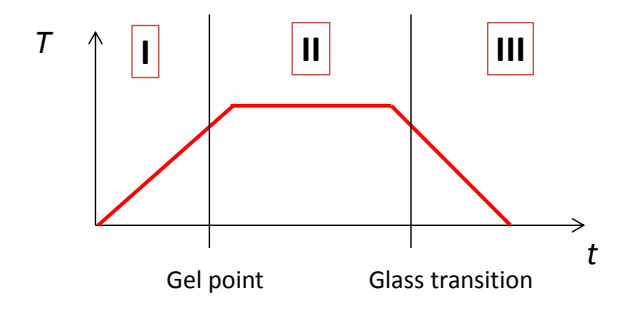


Figure 4.1: Three different stages of the temperature cycle.

4.3. The model 55

4.3.1. STAGES OF THE CURE CYCLE

STAGE I

Te Nijenhuis [9] describes the gel point as the moment where the material develops an equilibrium shear modulus. With the equilibrium shear modulus being zero, *i.e.* before the gel point is reached, the adhesive is a viscoelastic liquid [8]. In that state, the polymer cannot sustain static stresses other than hydrostatic ones. Therefore, thermal and chemical strains cannot contribute to residual stresses. They are not calculated in stage I.

STAGE II

In stage II, residual stresses can start to build up. The constitutive equations used here to describe the behaviour of the adhesive are based on [3, 4, 35, 42]. Typical cure cycles for automotive adhesives have high cure temperatures to minimize the curing time. These cure temperatures are usually well above the final glass transition temperature of the adhesive. Under these conditions, the rubbery (fully relaxed) modulus dominates the mechanical behaviour of the adhesive [4, 35], and relaxation phenomena are negligible. Thus, the material can be described with temperature (T) and T-dependent elastic stress-strain relations. For that, the stress tensor T-displayed in its deviatoric part T-displayed in T-displayed and the hydrostatic pressure T-displayed and T

$$\sigma_{ij} = \sigma_{ij}^{\text{dev}} - p\delta_{ij}, \tag{4.4}$$

where δ_{ij} is the Kronecker delta. The volume deformation is described by

$$-\dot{p} = K(T)\dot{\varepsilon}_{kk}^{\text{me}} \tag{4.5}$$

with $\dot{\varepsilon}_{kk}^{\text{\tiny me}}$ being the time derivative of the trace of the mechanical strain tensor. Changes in shape are described by

$$\dot{\sigma}_{ij}^{\text{dev}} = 2 G(q) \, \dot{\varepsilon}_{ij}^{\text{me,dev}}, \tag{4.6}$$

where G(q) is the cure dependent rubbery shear modulus. Equations 4.5 and 4.6 describe a hypo-elastic material. Similar rate equations have been used before to describe evolving properties of polymers [46–48]. Hossain *et al.* [47] point out, that these equations reflect a physical observation of cure: the stress state will remain unaltered if the applied deformation does not change, even though the elastic properties of the material evolve.

As in [42], the bulk modulus K is conveniently approximated based on a modified Tait equation:

$$K(T) = \frac{1}{\beta(T)},\tag{4.7}$$

$$\beta(T) = k_1 s_0 + \frac{1}{2} k_2 s_0 (1 + \tanh(C_0 (T - T_g))) + \frac{C}{B(T)}, \tag{4.8}$$

$$B(T) = b_1 \exp(-b_2 T),$$
 (4.9)

where s_0 , k_1 , k_2 , b_1 , b_2 and C_0 are material constants and C = 0.0894 [49]. T_g is the glass transition temperature of the fully cured adhesive. A plot of the bulk modulus versus the temperature with the material parameters used here (appendix A) can be found in [3] and [42].

A function for a degree-of-cure-dependent shear modulus is proposed by Adolf and Martin [35] and used in [4] among others. This function is used to describe the elastic shear modulus of stage II:

$$G(q) = G^{\text{final}} \left(\frac{q^2 - q_{\text{gel}}^2}{1 - q_{\text{gel}}^2} \right)^{\frac{8}{3}},$$

where G^{final} is the shear modulus of the fully cured adhesive and q_{gel} is the degree of cure at the gel point.

Besides elastic properties, functions for the thermal and chemical strains need to be determined. The CTE α is obtained in a similar way as the bulk modulus [3, 42] resulting in:

$$\alpha(T) = \frac{1}{3} \left[k_1 + \frac{1}{2} k_2 (1 + \tanh(C_0 (T - T_g))) \right]. \tag{4.10}$$

The parameter C_0 in equations 4.8 and 4.10 was introduced by De Vreugd *et al.* [3] to smoothen the transition between a constant CTE below and above $T_{\rm g}$. Here, we only take thermal strain into account that occurs beyond the gel point:

$$\varepsilon_{ij}^{\text{th}}(T) = \varepsilon^{\text{th}} \delta_{ij}, \qquad \varepsilon^{\text{th}}(T) = \int_{T_{\text{gel}}}^{T} \alpha(\tilde{T}) d\tilde{T}, \qquad (4.11)$$

with $T_{\rm gel}$ being the temperature at which the adhesive reaches the gel point in the cure cycle. De Vreugd [3] found a linear correlation between chemical shrinkage and the degree

4.3. The model 57

of cure. In this model, only strain beyond the gel point is considered:

$$\varepsilon_{ij}^{\text{ch}}(q) = \varepsilon^{\text{ch}} \delta_{ij}, \qquad \varepsilon^{\text{ch}}(q) = (q - q_{\text{gel}}) \varepsilon_{\text{tot}}^{\text{ch}},$$
 (4.12)

where $\varepsilon_{\text{tot}}^{\text{ch}}$ is the total linear chemical strain at the cure temperature ($\sim 1/3$ of the volumetric chemical strain) after full cure.

STAGE III

In stage III, chemical and thermal strain are calculated as before by equations 4.10, 4.11 and 4.12.

Also, as in stage II, volume changes are assumed to be elastic with a temperature-dependent bulk modulus (equations 4.5, 4.7, 4.8 and 4.9).

The deviatoric part is defined by a linear viscoelastic relation. Analogue to equation 2.4, the stress rate reads

$$\dot{\sigma}_{ij}^{\text{dev}} = 2G_{\infty} \dot{\varepsilon}_{ij}^{\text{me, dev}} + 2\sum_{m=1}^{M} G_{m} \dot{u}_{ij}^{m}, \tag{4.13}$$

$$\dot{u}_{ij}^{m} + \frac{1}{\tau_{m}} u_{ij}^{m} = \dot{\varepsilon}_{ij}^{\text{me,dev}}, \quad m = 1, 2, ...M,$$
(4.14)

where G_{∞} is the equilibrium (or rubbery) shear modulus and G_m are moduli of the Prony series of the shear relaxation modulus

$$G(t) = G_{\infty} + \sum_{m=1}^{M} G_m \exp(-t/\tau_m)$$
 (4.15)

with the according relaxation times τ_m (cf. [50]).

In general, a viscoelastic model with temperature and degree-of-cure-dependent relaxation times can be used to describe all three stages of the cure cycle. However, for cure at temperatures high above the final glass transition temperature, such a model would not improve the prediction of distortions. Relaxation effects at different degrees of cure are small and difficult to measure in that temperature range. They hardly affect stress calculations. Cure cycles with these high temperatures are common for bonding car body shells. Therefore, switching the constitutive model does not come with any drawbacks for that specific application.

4.3.2. ABAQUS IMPLEMENTATION

The equations mentioned above were implemented in Abaqus subroutines. This allows to apply the material law to arbitrary geometries. Abaqus solves equation 4.1. The de-

gree of cure is treated as an additional field variable and calculated in the subroutine USDFLD. An explicit Euler scheme is used to calculate q increments from equation 4.2. Thermal and chemical strains are calculated in the subroutine UEXPAN. Equation 4.11 is approximated with the trapezoidal integration scheme.

In Abaqus, it is not possible to switch between the elastic and viscoelastic material model. Therefore, both were implemented as subroutines and the switch is done in Abaqus' UMAT subroutine. To obtain an incremental scheme, the time derivative of equation 4.4, and equation 4.5 and 4.6 are approximated by applying the simple but stable increment scheme

$$\dot{f}_{t+\frac{\Delta t}{2}} = \frac{\Delta f}{\Delta t}, \quad f_{t+\frac{\Delta t}{2}} = f_t + \frac{\Delta f}{2},$$

where f is replaced by the corresponding stress or strain component. The same scheme is applied to the equations 4.13 and 4.14. The tangent moduli $\frac{\partial \Delta \sigma_{ij}}{\partial \Delta \varepsilon_{kl}^{\rm me}}$ needed for the solving algorithm of Abaqus are calculated in the same manner.

4.3.3. Numerical issues

The adhesive is a liquid in stage I. Strain that occurs in that stage is assumed to cause no static stresses other than hydrostatic ones; neither in this stage, nor in later stages. Therefore, in this approach, the simulation of stage I is done without the adhesive. At the transition to stage II, the adhesive is inserted in the model with the *MODEL CHANGE statement in Abaqus. This function allows to insert the adhesive elements at the gel point in a strain-free state.

A sudden switch between the material models of stages II and III can cause oscillations in the stress and strain functions. Therefore, the stress tensor is calculated by linear interpolation between both models in a transition region between $T_{\rm g}$ and $T_{\rm g} + T_{\rm trans}$:

$$\sigma_{ij} = (1 - w)\sigma_{ij}^{\text{el}} + w\sigma_{ij}^{\text{vi}}$$

where $\sigma^{\rm el}_{ij}$ is the elastic stress tensor, calculated with the equations 4.4, 4.5 and 4.6, and $\sigma^{\rm wi}_{ij}$ the viscoelastic one, using equation 4.13 and 4.14 instead of 4.6. w is defined as

$$w = \begin{cases} 1 + \frac{T_{\rm g} - T}{T_{\rm trans}} & \text{for} \quad T_{\rm g} \le T \le T_{\rm g} + T_{\rm trans} \\ 0 & \text{for} \quad T > T_{\rm g} + T_{\rm trans} \\ 1 & \text{else.} \end{cases}$$

The tangent moduli are calculated accordingly:

4.3. The model **59**

$$\frac{\partial \Delta \sigma_{ij}}{\partial \Delta \varepsilon_{kl}^{\text{me}}} = (1 - w) \frac{\partial \Delta \sigma_{ij}^{\text{el}}}{\partial \Delta \varepsilon_{kl}^{\text{me}}} + w \frac{\partial \Delta \sigma_{ij}^{\text{vi}}}{\partial \Delta \varepsilon_{kl}^{\text{me}}}.$$

4.3.4. SIMULATION OF LOCAL DISTORTIONS

The bonding between a $0.7 \times 50 \times 20$ mm steel strip and a $8 \times 50 \times 20$ mm steel bulk part with a 10 mm broad and 2 mm thick bond line is simulated (see figure 4.2). The

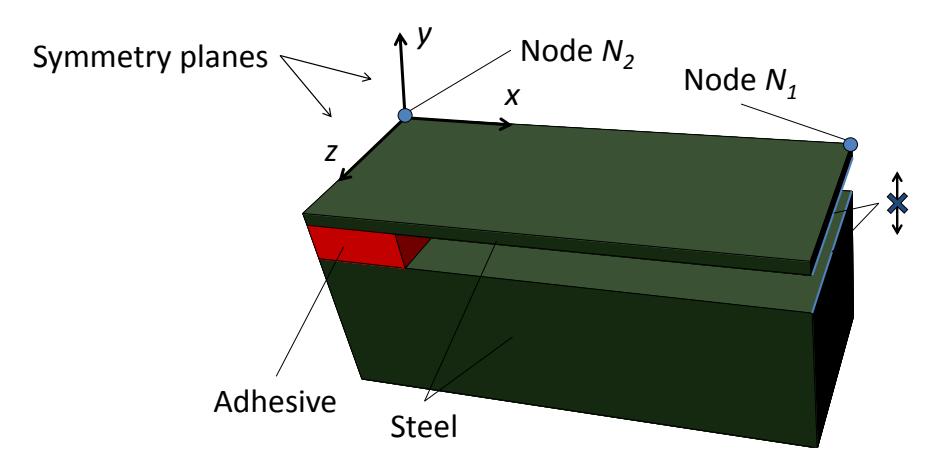


Figure 4.2: Structure for simulating local distortions. The y-displacement is inhibited at the edges marked in blue. The symmetry allows to reduce the simulation model to the depicted quarter piece.

material parameters for the steel are $E = 210\,\mathrm{GPa}$, v = 0.3, $\alpha = 1.3 \cdot 10^{-5}/\mathrm{K}$. Parameters for the adhesive are taken from [3] (material C) and can be found in appendix A. The material used there is an epoxy moulding compound for electronic packaging.

Different cure processes are investigated, in which the structure is exposed to the temperature cycles listed in table 4.1. The cycles share the same cooling rate of 5 K/min.

Table 4.1: Temperature cycles.

Name	Heating rate	Cure temp.	Dwell time
A	5 K/min	170 °C	30 min
L170	1 K/min	170 °C	30 min
M170	7 K/min	170 °C	30 min
H170	45 K/min	170 °C	30 min
L155	1 K/min	155 °C	60 min
M155	7 K/min	155 °C	60 min
H155	21 K/min	155 °C	60 min

The cycles start and end at 20 °C.

4.4. RESULTS

For better comparison, all curves are shifted on the time scale so that the cooling down phase starts at t = 0.

4.4.1. CURE CYCLE A

Figure 4.3 shows the temperature curve and the evolution of cure in cycle A. In this cycle,

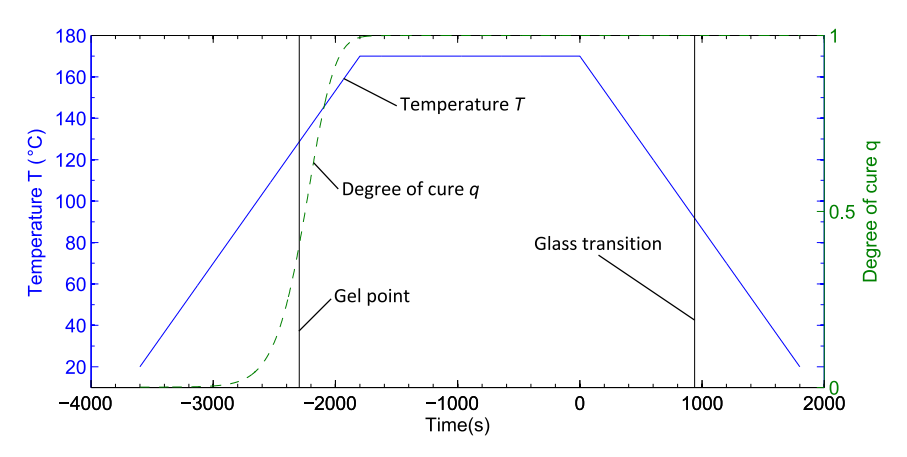


Figure 4.3: Temperature profile applied and degree of cure calculated for cycle A.

the chemical and thermal strains "compete" in the heating phase (figure 4.4). When

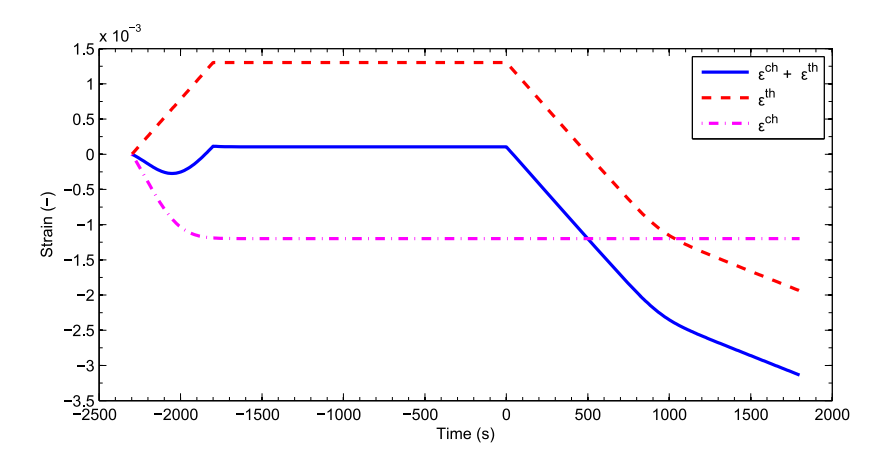


Figure 4.4: The development of chemical and thermal strains in in cycle A.

4.4. Results 61

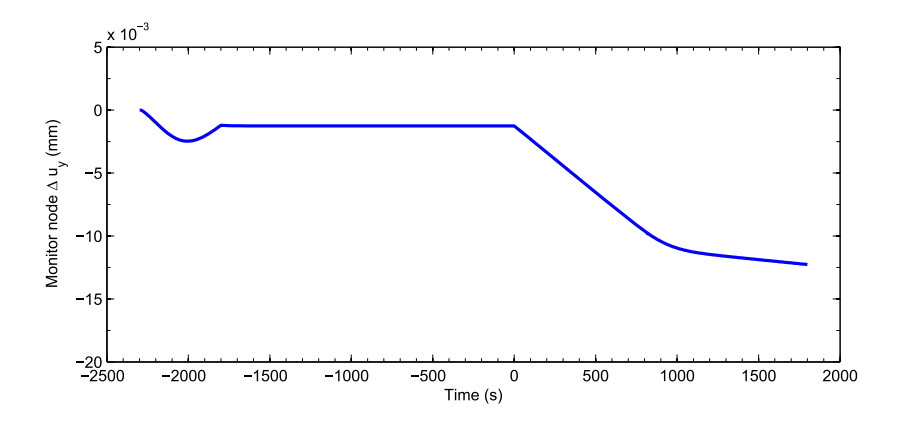


Figure 4.5: Out-of-plane displacement of the steel strip right above the adhesive layer for cure cycle A.

the cure temperature is reached, the sum of both components is above zero, *i.e.* the sum of chemical and thermal deformations leads to an increased volume of the adhesive (mechanical strain neglected, see equation 4.3). The difference in *y*-displacement of nodes N_1 and N_2 , $\Delta u_y = u_y(N_2) - u_y(N_1)$, is monitored over time (see figure 4.2). As can be seen in figure 4.5, the steel strip shows a first downwards and then upwards movement in the heating phase. At cure temperature, however, the steel strip stays in a downwards bent state before it gets pulled down further in the cooling phase.

Figure 4.6 illustrates the stress and strain development in the adhesive layer over cycle A. The curves show σ_{xy} and ε_{xy} at an arbitrarily chosen integration point positioned at X = (2.211, -1.542, 5.789) mm in the reference configuration (see figure 4.2).

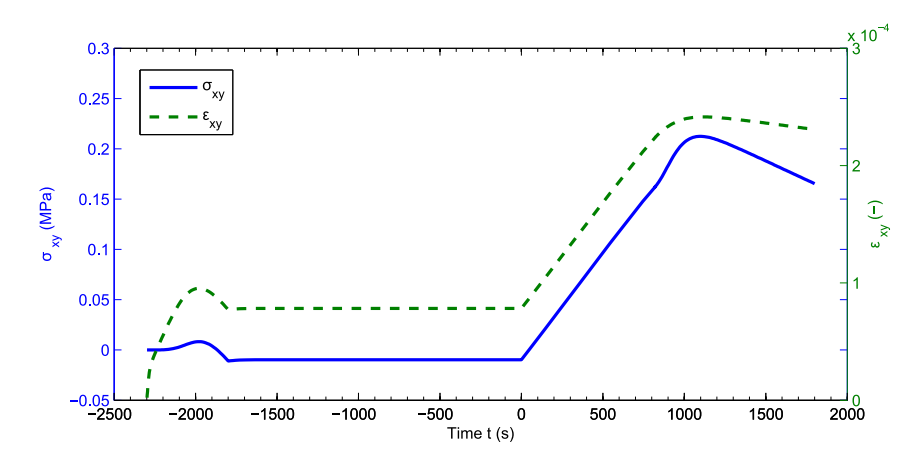


Figure 4.6: Shear stress and strain inside the adhesive layer over cure cycle A.

4.4.2. OTHER CURE CYCLES

Figures 4.7 and 4.8 show the displacement of the steel strip for the different cure cycles. The temperature at which the gel point is reached in the temperature cycle, $T_{\rm gel}$, changes with the temperature rate in the heating phase, see figure 4.9. For the cycles H155 and H170, $T_{\rm gel}$ is equal to the cure temperature and would not increase with higher temperature rates.

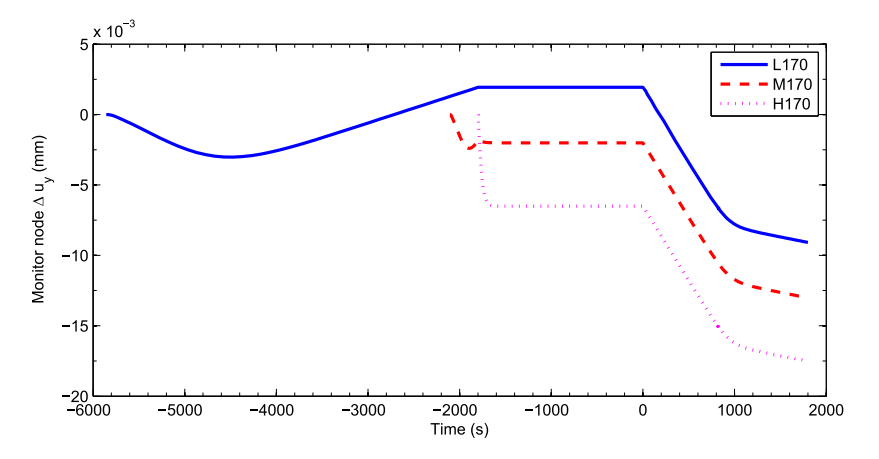


Figure 4.7: Displacement curves of the steel strip for the cycles with a cure temperature of 170 °C.

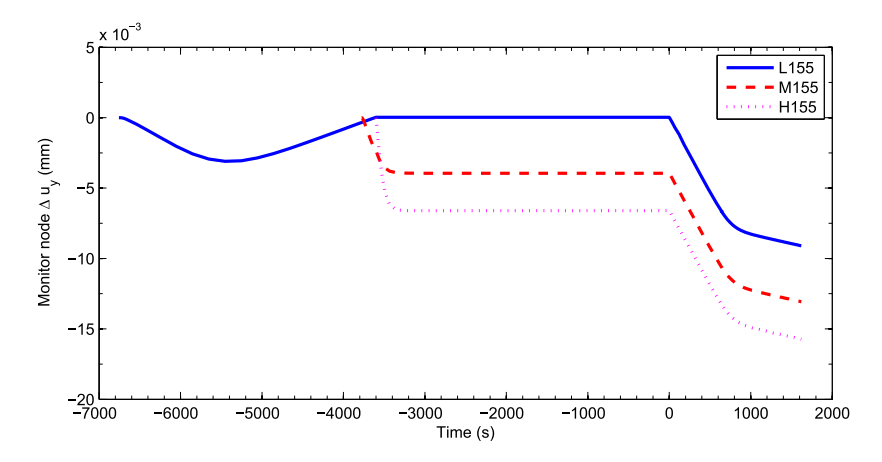


Figure 4.8: Displacement curves of the steel strip for the cycles with a cure temperature of 155 °C.

The low rates show first a downwards movement followed by an upwards movement of the steel strip before the cure temperature is reached. This behaviour can also be seen in the curves for the cycles A and M170. In all other cycles, the strip moves downwards

63

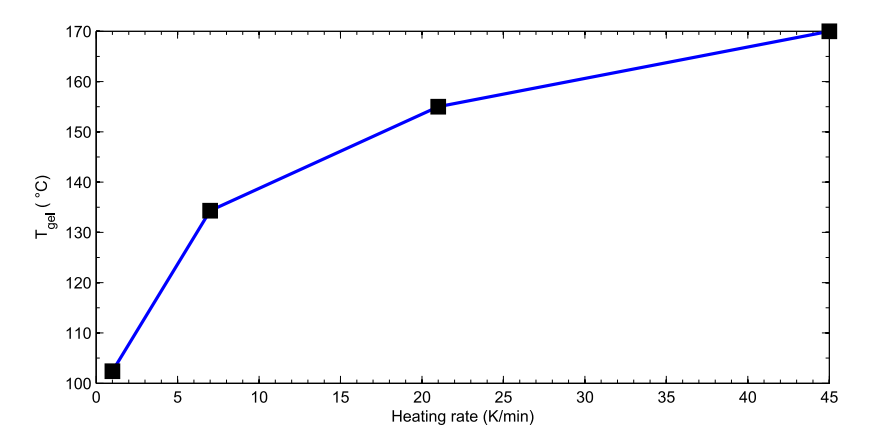


Figure 4.9: Increasing heating rate shifts the gel point to higher temperatures in the cure cycle.

only.

Figure 4.10 shows the displacement after different cycles. The model predicts the

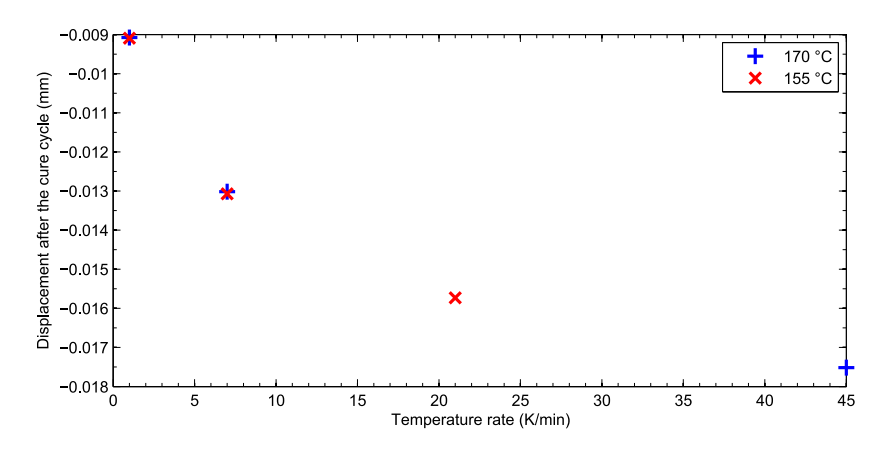


Figure 4.10: Displacement of the steel strip after the cure cycle for the different heating rates.

same displacement for both cure temperatures with low and medium heating rates.

The subroutine switched to the transition region between stage II and III at t=820 s for cure at 170 °C and at t=620 s for cure at 155 °C, respectively. The displacement curves in figures 4.5, 4.7 and 4.8 start to gradually flatten from that point on.

4.4.3. LONG-TERM BEHAVIOUR

The Prony series for the shear modulus of the material contains large relaxation times. This allows to investigate the long-term behaviour of the material. For that reason, another time step after the cure cycle was calculated, where the material stays at 20 °C and has time to reduce distortions by relaxation. The step time is two years. For all cure cycles, the displacement changes less than 0.13 % in these two years after the cure cycle.

4.5. DISCUSSION

4.5.1. CURE CYCLE A

Figure 4.4 shows that chemical and thermal strains are in the same order of magnitude for the material combination and temperature cycle investigated. Therefore, neglecting chemical deformation is not justifiable. The downwards and upwards movements of the steel strip in the heating phase can be explained by thermal and chemical strains in that phase, which leads first to a decrease and later to an increase in the volume of the adhesive (mechanical strain neglected). In the isothermal dwell phase, the strip remains in a downwards bent state. Experimental investigations on similar geometries (chapter 3, [21-24]) show the same behaviour. In the case at hand, however, the displacement cannot be explained by a volume reduction that is caused by reactive shrinkage, since the volume increases (mechanical strain neglected), see figure 4.4. Hence, the mechanical part of the strain tensor must cause the downwards displacement. Further study revealed that in this specific material combination the adherends expand even more than the adhesive. This leads to a Poisson effect. The adhesive is stretched in in-plane direction (the x-z-plane, see figure 4.2) and contracts in out-of-plane direction. The Poisson effect is caused by a low CTE of the polymer. A high CTE of the adhesive would cause an inverse effect and an upwards displacement. Due to the temperature-dependent CTE of the adhesive, both effects can occur in one temperature cycle. In the cooling phase, these effects are partly reversed since the thermal deformation of the adherends decreases.

The increase of ε_{xy} from the gel point on (see figure 4.6) does not immediately lead to shear stress σ_{xy} . This is because the shear modulus is still zero at the gel point. With the shear modulus increasing, changes in strain lead to changes in stress. When the strain stays constant in the dwell phase, the stress does not alter, either. At the transition to stage III, the stress curve raises slightly steeper. This is due to the increased instantaneous stiffness in the viscoelastic model.

4.6. Conclusions 65

4.5.2. OTHER CURE CYCLES

The low heating rates show the same downwards-upwards movement as in cycle A. The development of the chemical and thermal strains explains this behaviour. For the medium and high rates, the gel point is at higher temperatures. Therefore, the thermal strain causing displacements in the heating phase is less dominant. The curves in figures 4.7 and 4.8 show already significant differences at the end of the dwell period (t=0). These differences do not change much in the cooling phase. Models focusing on the cooling down only would not be able to show these differences.

The model predicts the same displacement for both cure temperatures with low and medium heating rates. That implies that lowering the cure temperature from 170 to 155 °C would not decrease the distortions for these rates. Increasing the temperature rate in the heating phase leads to more absolute final displacement. However, if the gel point is shifted to the dwell phase, the final displacement would not change further with an increasing heating rate. For the cure temperature of 155 °C, this point is reached at a rate of 21 K/min and for 170 °C at a rate of 45 K/min, respectively. Therefore, only between these two rates, lowering the cure temperature would affect the final displacement and, therefore, distortions in the strip.

The steepening of the displacement curves during the transition to stage III in figures 4.5, 4.7 and 4.8 can be explained by the increase in the stiffness due to the switch to the viscoelastic material law. The gradually decreasing CTE (see figure 4.4) at T_g leads to a flattening of the displacement curves afterwards.

4.6. CONCLUSIONS

A model for local panel distortions due to hot-curing adhesives is proposed and used to study the development of local panel distortions. Displacements occurring during the cure process can not only be caused by chemical shrinkage but also by a Poisson effect where the adhesive is stretched in in-plane direction of the steel strip. The temperature curve, especially the heating rate, affects final distortions. Lowering the cure temperature reduces distortions only for high temperature rates. Lower temperature rates in the heating phase lead to a gelation at lower temperature and to less distortions.

In chapter 5, the material constant for the adhesive system BM1496V are determined and a comparison between distortion predictions based on the model presented in this chapter and the experimental studies from chapter 3 is done.

66 References

REFERENCES

[1] K. Priesnitz, J. Sinke, and R. Benedictus, *On the simulation of panel distortions due to hot curing adhesives*, International Journal of Solids and Structures **51**, 2470 (2014).

- [2] M. S. Kiasat, *Curing shrinkage and residual stresses in viscoelastic thermosetting resins and composites*, Ph.D. thesis, Delft University of Technology (2000).
- [3] J. De Vreugd, K. M. B. Jansen, L. J. Ernst, and C. Bohm, *Prediction of cure induced warpage of micro-electronic products*, Microelectronics Reliability **50**, 910 (2010).
- [4] K. M. B. Jansen, J. De Vreugd, and L. J. Ernst, *Analytical estimate for curing-induced stress and warpage in coating layers*, Journal of Applied Polymer Science **126**, 1623 (2012).
- [5] O. Hahn and J. Jendrny, *Evaluation of simulation models for the estimation of deformation of adhesively bonded steel sheets during curing*, Welding in the World **47**, 31 (2003).
- [6] H. Fuchs, K. D. Fernholz, and P. Deslauriers, *Predicted and Measured Bond-Line Read-Through Response in Composite Automotive Body Panels Subjected to Elevated Temperature Cure*, Journal of Adhesion **86**, 982 (2010).
- [7] M. Gigliotti, M. R. Wisnom, and K. D. Potter, *Development of curvature during the cure of as4/8552 [0/90] unsymmetric composite plates*, Composites Science and Technology **63**, 187 (2003).
- [8] J. Ferry, Viscoelastic properties of polymers (Wiley, 1980).
- [9] K. te Nijenhuis, *Thermoreversible networks. Viscoelastic properties and structure of gels* (Springer, Berlin, 1997).
- [10] M. Eis, Fertigungsbedingte Bauteildeformationen beim Kleben dünnwandiger Stahlbauteile: Analyse der Entstehungsmechanismen und Hinweise zur Minimierung, Ph.D. thesis, Universität Paderborn (2000).
- [11] C. Blanke, Modellierung und numerische Simulation des Aufheizverhaltens von PKW-Bauteilen und -Karossen in Trocknern, Ph.D. thesis, Technische Universität Darmstadt (2009).

67

- [12] O. Hahn and B. Hüsgen, Erarbeitung von technologischen Grundlagen für das Kleben von Fügeteilen mit unterschiedlichen Ausdehnungskoeffizienten, in Forschungsbericht des Laboratoriums füer Werkstoff- und Fügetechnik der Univerität-GH Paderborn (1991).
- [13] O. Hahn, A. Chudaska, and B. Hüsgen, *Influence of the process parameters on the quality of thermosetting adhesive joints*, Welding in the World, Le Soudage Dans Le Monde **31**, 277 (1993).
- [14] G. Meschut, O. Kläger, and H. Wetter, *Multi-Material Design (Part 1): Thermal stress in lacquer drying processes [Multi-material-design (Teil 1): Thermische Beanspruchung in Lacktrocknungsprozessen]*, Adhäsion Kleben und Dichten **4**, 30 (2003).
- [15] G. Meschut, O. Kläger, and H. Wetter, *Multi-Material-Design (Part 2): Simulation of thermal strain [Multi-Material-Design (Teil 2): Simulation der Thermischen Beanspruchung]*, Adhäsion Kleben und Dichten **5**, 31 (2003).
- [16] G. Meschut and T. Gänsicke, *Experimental and computational analysis of the stresses on adhesive-bonded layers in joints between thermally incompatible materials*, Welding and Cutting **55**, 322 (2003).
- [17] A. Andersson, *Evaluation and visualisation of surface defects on auto-body panels*, Journal of Materials Processing Technology **209**, 821 (2009).
- [18] P. C. P. Bouten, On the stability of the adhesive layer thickness, in 4th International Adhesion Conference, Cambridge University, England (1990).
- [19] K. Fernholz, R. Hsakou, K. Lazarz, C. S. Wang, B. Emerson, D. Biernat, and D. Case, Development of a tool to measure bond-line read-through, in SPE Automotive and Composites Divisions - 7th Annual Automotive Composites Conference and Exhibition, ACCE 2007 - Driving Performance and Productivity, Vol. 1 (2007) pp. 90–106.
- [20] K. A. Patankar, D. A. Dillard, and K. D. Fernholz, *Characterizing the constitutive properties and developing a stress model for adhesive bond-line readout,* International Journal of Adhesion and Adhesives **40**, 149 (2013).
- [21] A. Chudaska and O. Hahn, Untersuchungen zum temperatur- und reaktionsbedingten Klebstoffschrumpf - Maßnahmen zur Reduzierung schrumpfbedingter Bauteilschädigungen, in Wärmearme Fügetechniken - Kleben - Durchsetzfügen - Nieten (1993) pp. 121 – 130.

68 References

[22] A. Chudaska and O. Hahn, Damages of bonded parts caused by the thermal and reactionary contraction of adhesives during the curing process, in Vide-Science Technique Et Applications (1994) pp. 223–227.

- [23] A. Chudaska and O. Hahn, *Influence of constructive factors and the process conditions during the curing of hot setting adhesives on the properties of bonded joints*, in *Special Joining Technologies International Symposium* (1994) pp. 12 24.
- [24] O. Hahn, M. Eis, and G. Meschut, *Curing caused tensions on adhesive bonding of steel sheets*, Welding in the World **43**, 47 (1999).
- [25] A. Mathias, Einfluß der Abbindebedingungen auf die Struktur und das beanspruchungsabhängige Eigenschaftsprofil der Bindeschicht von Klebverbindungen, Ph.D. thesis, Universität-GH-Paderborn (1989).
- [26] S. R. White and H. T. Hahn, Cure cycle optimization for the reduction of processinginduced residual stresses in composite materials, Journal of Composite Materials 27, 1352 (1993).
- [27] M. L. Dano and M. W. Hyer, *Thermally-induced deformation behavior of unsymmetric laminates*, International Journal of Solids and Structures **35**, 2101 (1998).
- [28] M. L. Dano and M. W. Hyer, *Snap-through of unsymmetric fiber-reinforced composite laminates*, International Journal of Solids and Structures **39**, 175 (2002).
- [29] C. S. Lopes, P. P. Camanho, Z. Gürdal, and B. F. Tatting, *Progressive failure analysis of tow-placed, variable-stiffness composite panels*, International Journal of Solids and Structures **44**, 8493 (2007).
- [30] H. Hahn and N. Pagano, *Curing stresses in composite laminates*, Journal of Composite Materials **9**, 91 (1975).
- [31] A. Plepys, M. S. Vratsanos, and R. J. Farris, *Determination of residual stresses using incremental linear elasticity*, Composite Structures **27**, 51 (1994).
- [32] Y. Yu, I. A. Ashcroft, and G. Swallowe, *An experimental investigation of residual stresses in an epoxy-steel laminate*, International Journal of Adhesion and Adhesives **26**, 511 (2006).
- [33] S. K. Basu and H. G. Kia, *Theoretical modeling of bond-line read-out in adhesive joined smc automotive body panels*, Journal of Composite Materials **42**, 539 (2008).

REFERENCES 69

[34] F. S. Jumbo, I. A. Ashcroft, A. D. Crocombe, and M. M. Abdel Wahab, *Thermal residual stress analysis of epoxy bi-material laminates and bonded joints*, International Journal of Adhesion and Adhesives **30**, 523 (2010).

- [35] D. Adolf and J. E. Martin, *Calculation of Stresses in Crosslinking Polymers*, Journal of Composite Materials **30**, 13 (1996).
- [36] D. B. Adolf and R. S. Chambers, *A thermodynamically consistent, nonlinear vis-coelastic approach for modeling thermosets during cure,* Journal of Rheology **51**, 23 (2007).
- [37] C. Liebl, M. Johlitz, B. Yagimli, and A. Lion, *Three-dimensional chemo-thermomechanically coupled simulation of curing adhesives including viscoplasticity and chemical shrinkage*, Computational Mechanics **49**, 603 (2012).
- [38] C. Liebl, M. Johlitz, B. Yagimli, and A. Lion, *Simulation of curing-induced viscoplastic deformation: A new approach considering chemo-thermomechanical coupling*, Archive of Applied Mechanics **82**, 1133 (2012).
- [39] O. Hahn and T. Orth, Avoiding bondline readthrough on thin steel elements by modification and optimization of processes, adhesives and sample shape, in International Body Engineering Conference (1997) pp. 111 115.
- [40] S. R. White and H. T. Hahn, *Process modeling of composite materials: Residual stress development during cure. part i. model formulation*, Journal of Composite Materials **26**, 2402 (1992).
- [41] M. S. Genidy, M. S. Madhukar, and J. D. Russell, *New method to reduce cure-induced stresses in thermoset polymer composites, part ii: closed loop feedback control system,* Journal of Composite Materials **34**, 1905 (2000).
- [42] J. de Vreugd, *The effect of aging on molding compound properties*, Ph.D. thesis, Technische Universiteit Delft (2011).
- [43] M. Kamal and S. Sourour, *Kinetics and thermal characterization of thermoset cure*, Polymer Engineering and Science **13**, 59 (1973).
- [44] S. Sourour and M. R. Kamal, *Differential scanning calorimetry of epoxy cure: isother-mal cure kinetics*, Thermochimica Acta **14**, 41 (1976).
- [45] B. Yagimli and A. Lion, *Experimental investigations and material modelling of curing processes under small deformations*, ZAMM Zeitschrift für Angewandte Mathematik und Mechanik **91**, 342 (2011).

4

70 References

[46] J. E. Martin and D. Adolf, *Constitutive equation for cure-induced stresses in a vis-coelastic material*, Macromolecules **23**, 5014 (1990).

- [47] M. Hossain, G. Possart, and P. Steinmann, *A small-strain model to simulate the curing of thermosets*, Computational Mechanics **43**, 769 (2009).
- [48] A. Lion and M. Johlitz, *On the representation of chemical ageing of rubber in contin- uum mechanics*, International Journal of Solids and Structures **49**, 1227 (2012).
- [49] P. Zoller and Y. A. Fakhreddine, *Pressure-volume-temperature studies of semi-crystalline polymers*, Thermochimica Acta **238**, 397 (1994).
- [50] O. C. Zienkiewicz and R. L. Taylor, *The Finite Element Method Volume 2: Solid Mechanics*, 5th ed. (Butterworth-Heinemann, 2000).

4

5

MATERIAL CHARACTERIZATION AND SIMULATION

Hot-curing one-part epoxy adhesives are often chosen for structural bonds requiring high strength. The changing properties of the adhesive during the bonding process, however, can lead to distortions of the structure, especially if thin adherends like car panels are involved. Computer simulations can help to reduce these undesired deformations. In this chapter, the hot-curing epoxy system BM1496V is characterized and incorporated in the model from the previous chapter. Predictions for the different temperature cycles are compared with experimental data from chapter 3. The model predicts well the deformations that occur over the entire cure cycle including the heating and isothermal phases.

5.1. Introduction

Structural bonds, as they occur in car bodies for instance [2, 3], require adhesives with a high shear strength. Hot-curing one-part epoxies are often chosen candidates for these applications [4]. The cure at elevated temperature, however, can cause distortions, especially if thin-walled structures like *e.g.* car body shells are involved. Panel distortions can roughly be divided into local and global ones [5]. While global ones describe the overall deformation of the bonded structure, local distortions appear along the bond line close

A modified version of this chapter has been published in Journal of Materials Processing Technology **225**, 405 (2015) [1].

to the adhesive (see chapter 2).

These distortions can be caused by the evolving properties of the adhesive over a cure cycle: the adhesive transforms from a viscous liquid to a viscoelastic solid. At the same time, the cross-linking process causes a volume reduction of the polymer, often referred to as chemical shrinkage. In addition, both the adhesive and the adherends expand and shrink due to a changing temperature. These simultaneous processes can lead to residual stresses and subsequently to panel distortions.

In some studies, the development of panel distortions is monitored over a cure cycle [6–9]. These publications as well as the study in chapter 3 show that distortions can occur early in the cure cycle when the structure is still heating up. Prediction models, however, focus only on stresses that occur during cooling down [5, 10, 11]. Models capable of describing the above mentioned evolving properties of the adhesive over an entire cure cycle [12–15] have not been applied to local panel distortions yet.

In this work, the development of local panel distortions is simulated and compared with experiments. To that end, the material constants of the commercial epoxy-based hot-curing adhesive system BM1496V [16] are determined. The simulation model is based on the model presented in chapter 4 and allows for chemically and thermally induced property changes of the adhesive. Experimental data on distortion development in different cure cycles is presented in chapter 3.

5.2. MATERIAL MODELLING AND CHARACTERIZATION

5.2.1. CURE KINETICS

The cross-linking process of polymer chains in the adhesive can be characterized with a single variable q, the degree of cure. In the uncured state before any cross-links are formed, q has the value 0. During a cure cycle, q increases steadily until no reactive groups are left over. In that fully cured state, q has the value 1.

A well-known equation for describing thermoset cure can be found in [17]:

$$\dot{q} = k_0 \exp\left[-\frac{E_a}{RT}\right] q^m (1-q)^n, \tag{5.1}$$

where R = 8.314 J/(mol K) is the ideal gas constant. Fitting the equation to experimental data determines the material parameters k_0 , E_a , m and n. Kinetic parameters can be obtained with a DSC. A DSC monitors the heat flow $\mathrm{d}H/\mathrm{d}t$ over time for a given temperature profile. Since each epoxy group reacts exothermically and, therefore, releases a

specific amount of heat, the degree of cure can be linked to the heat flow:

$$\frac{\mathrm{d}q(t)}{\mathrm{d}t} = \frac{1}{H_{\infty}} \frac{\mathrm{d}H(t)}{\mathrm{d}t} \tag{5.2}$$

with H_{∞} being the (total) heat of reaction [18]. Here, uncured samples were exposed to different heating rates while the heat flows were monitored over time. Similar to [19], the kinetic parameters were obtained as follows: the activation energy $E_{\rm a}$ was determined with the type B-1.92 method described in [20], which is based on the linear relation

$$\ln \frac{\beta}{T_{\rm f}^{1.92}} = -1.0008 \frac{E_{\rm a}}{RT_{\rm f}} + C, \tag{5.3}$$

where ln is the natural logarithm, β is the temperature rate, $T_{\rm f}$ is the isoconversional temperature and C is a constant independent of β and $T_{\rm f}$. Thus, the slope of the plot determines $E_{\rm a}$. The procedure is as follows: A set of constant temperature rates β is chosen and a DSC run is performed for each β providing H_{∞} and H(t) for the respective temperature rate. The DSC data and equation 5.2 are used to determine the temperatures $T_{\rm f}$, at which the degree of cure has the values q=0.1,0.2,...,0.9. After that, $\ln(\beta/T_{\rm f}^{1.92})$ versus $1/T_{\rm f}$ is plotted for all β and the mean slope is used to determine $E_{\rm a}$ according to equation 5.3. Equation 5.1 is modified to

$$\frac{\dot{q}}{\exp\left[-\frac{E_{a}}{RT}\right]} = k_0 q^m (1 - q)^n$$

and fitted to the DSC data to determine the remaining parameters k_0 , m and n.

5.2.2. VOLUME CHANGES

The change in the specific volume ν of a material point in a continuum is described by

$$v = v_0 J, \tag{5.4}$$

where v_0 is the specific volume in a reference state and J is the Jacobi determinant of the deformation gradient (*cf.* [21]). For small deformations, that is when second-order and higher-order terms of the displacement gradient $\nabla \mathbf{u}$ can be neglected, J can be written as

$$J = 1 + \varepsilon_{kk} \tag{5.5}$$

with ε_{kk} being the trace of the linear strain tensor [22].

An isotropic material is assumed. As in other works [23, 24], the strain is decomposed in several parts. Here, a distinction is drawn between mechanical, thermal and chemical contributions:

$$\varepsilon_{ij} = \varepsilon_{ij}^{\text{me}} + \varepsilon_{ij}^{\text{th}} + \varepsilon_{ij}^{\text{ch}} = \varepsilon_{ij}^{\text{me}} + \varepsilon^{\text{th}} \delta_{ij} + \varepsilon^{\text{ch}} \delta_{ij}, \tag{5.6}$$

where δ_{ij} is the Kronecker Delta. In case an isotropic material undergoes no other volume changes than thermal expansion or contraction (*i.e.* no pressure or other stresses are applied, nor are volume changes chemically induced), then, from equations 5.4 and 5.5 follows:

$$v = v_0 (1 + 3\varepsilon^{\text{th}})$$
$$\varepsilon^{\text{th}} = \int_{T_0}^{T} \alpha(\tilde{T}) d\tilde{T}$$

 ε^{th} is the thermal strain, T_0 is the reference temperature at which the material has the volume v_0 , T is the current temperature and α is the linear coefficient of thermal expansion (CTE). A volumetric CTE can be defined as

$$\alpha^{\text{vol}}(T) := \frac{1}{\nu_0} \frac{\mathrm{d} \nu(T)}{\mathrm{d} T} = 3\alpha(T).$$

If only thermal and chemical deformations occur,

$$\nu = \nu_0 (1 + 3\varepsilon^{\text{th}} + 3\varepsilon^{\text{ch}}) \tag{5.7}$$

holds.

The volume changes in an idealized cure cycle, in which the adhesive is heated up, held at a cure temperature T_c and cooled back down to ambient temperature T_0 , is shown in figure 5.1 [25]. The epoxy expands thermally while heated up (0-1), shrinks chemically at cure temperature (1-2), then shrinks due to temperature decrease, first with a high, rubbery CTE α_r (2-3), then, below the glass transition temperature T_g , with a lower, glassy CTE α_g (3-4). It is noteworthy that in this cycle, a glassy state trajectory in the heating phase, as described by others [26], is not accounted for. It was pointed out by others [25, 27] that standard procedures to measure cure shrinkage are performed at ambient

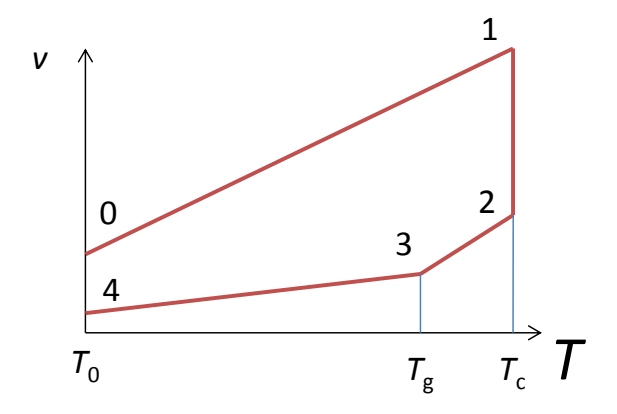


Figure 5.1: Volume changes over an idealized cure cycle [25].

temperature, i.e. these methods measure an effective shrinkage

$$\tilde{\varepsilon}_{\text{tot}}^{\text{ch}} = \frac{1}{3} \frac{\nu_4 - \nu_0}{\nu_0} \tag{5.8}$$

(from point 0 to 4 in figure 5.1) rather than the real chemical shrinkage $\varepsilon_{\mbox{\tiny tot}}^{\mbox{\tiny ch}}$ (1-2).

As an approximation, the thermal expansion of the adhesive during heating up is assumed to occur with the same CTE α_r as in the rubbery state during cooling down. Therefore, the total chemical shrinkage can be estimated in case α_r , α_g and $\tilde{\varepsilon}_{tot}^{ch}$ are known (*cf.* [25]):

$$\varepsilon_{\text{tot}}^{\text{ch}} = \tilde{\varepsilon}_{\text{tot}}^{\text{ch}} + (\alpha_{g} - \alpha_{r})(T_{g} - T_{0}). \tag{5.9}$$

In many cases, the chemical shrinkage is found to increase linearly with the degree of cure [26, 28]:

$$\varepsilon^{\text{ch}}(q) = q \, \varepsilon_{\text{tot}}^{\text{ch}}. \tag{5.10}$$

The function

$$\alpha(T) = \frac{1}{3} \left[k_1 + \frac{1}{2} k_2 (1 + \tanh(C_0 (T - T_g))) \right]$$
 (5.11)

with the material constants k_1 , k_2 and C_0 , proposed in [15, 27, 29], describes the transi-

tion from a rubbery CTE,

$$\alpha_{\rm r} = \frac{1}{3}(k_1 + k_2),\tag{5.12}$$

to a glassy one,

$$\alpha_{\rm g} = \frac{1}{3}k_1,\tag{5.13}$$

based on the Tait equation of state [30]. C_0 determines the sharpness of the transition from the glassy to the rubbery state. The constants are determined with a TMA: a 4.7 \times 5.1 \times 4.2 mm-sized block of fully cured material is exposed to three temperature cycles in which the polymer is heated up slowly to about 200 °C and cooled down back to room temperature. The third heating phase is used to determine the CTE. While the curve of the second and third heat-up show hardly any difference, the first heating phase seemingly shows a negative CTE when approaching T_g . This observation, however, is attributed to a rearrangement of the contact area of the probe and the specimen during the first heating cycle. Therefore, the first heat-up phase is ignored.

The viscoelastic properties of the fully cured material are determined with a Dynamic Mechanical Analyser (DMA). In a tensile set-up, the elongation of a strip of the epoxy $(23.0 \times 7.58 \times 0.34 \text{ mm})$ is monitored under dynamic loading. A frequency sweep from 1 to 60 Hz is performed repeatedly during continuous heating from 20 to 180 °C at 1 K/min.

A thermorheologically simple material behaviour is assumed such that a master curve for the tensile storage modulus E' can be obtained by shifting the isothermal curves according to

$$E'(\omega, T) = E'(\omega a(T), T_{\rm g}),$$

where ω is the frequency and $T_{\rm g}$ is chosen as the reference temperature (see equation 2.15).

The shift factors $\log a(T)$ are fitted to the Williams-Landel-Ferry equation [31] above $T_{\rm g}$ and to an Arrhenius model below:

$$\log a(T) = \begin{cases} -\frac{C_1(T - T_g)}{C_2 + T - T_g} & \text{for } T \ge T_g \\ \frac{A}{2.303R} \left[\frac{1}{T} - \frac{1}{T_g} \right] & \text{for } T < T_g, \end{cases}$$
 (5.14)

where C_1 , C_2 and A are fitting constants.

5.3. SIMULATION 77

5.3. SIMULATION

The constitutive equations used here for the adhesive coincide with the ones from chapter 4 with minor modifications. For completeness reasons, those are summarized here. The material data obtained in section 5.2 is implemented in that model and allows the comparison of simulation and experiment (from chapter 3).

5.3.1. CONSTITUTIVE EQUATIONS

An isotropic material is assumed whose deformation can be described by equation 5.6. Increments of thermal strain are calculated by

$$\Delta \varepsilon^{\text{th}} = \frac{1}{2} (\alpha_i + \alpha_{i+1}) \Delta T.$$

The CTE at the start (α_i) and the end (α_{i+1}) of the increment are calculated with equation 5.11 in case full cure is reached and with equation 5.12 otherwise. Equation 5.10 is used for the chemical strain contribution. Equation 5.1 is used to calculate the cure evolution; in order to ensure a non-zero starting cure rate, $q_0 = 0.01$ is chosen as an initial value.

To derive the constitutive equations, the stress tensor σ_{ij} is split in its deviatoric part $\sigma_{ij}^{\text{dev}} = \sigma_{ij} - \frac{1}{3}\sigma_{kk}\delta_{ij}$ and the hydrostatic pressure p:

$$\sigma_{ij} = \sigma_{ij}^{\text{dev}} - p\delta_{ij}.$$

In this model, volume changes are described by the hypo-elastic equation:

$$-\dot{p} = K\dot{\varepsilon}_{kk}^{\text{me}}$$

with a constant bulk modulus K. Experimental determination of K can be a difficult task and is not done in this work because of lack of proper equipment. Instead, it is assumed that the bulk modulus has less influence on stresses than the tensile or shear modulus in cases where the adhesive occupies an unconfined open geometry. That is the case for the bond line in the experimental set-up investigated in chapter 3 and modelled here. The bulk modulus changes by a factor of about 2 to 3 during the glass-to-rubber transition, which is much less than the 100- to 1000-fold changes of the shear and elongation moduli during that transition. Therefore, to come up with a value for K, a quasi-static approximation is used:

$$K=\frac{E_g}{3(1-2\nu)},$$

where E_g is the instantaneous glassy tensile modulus obtained by DMA. Assuming incompressibility often yields sufficiently accurate stress predictions for polymers in the rubbery state. Here a slightly smaller Poisson ratio of $\nu=0.45$ is chosen. This, however, is a rough estimate only. The impact of the bulk modulus on predicted deformations is discussed in chapter 6.

In order to model the shear behaviour, the cure cycle is divided into three different stages (see figure 4.1). In stage I, the adhesive is liquid and cannot exert permanent stresses on the steel strip. Here, this behaviour is realized by a small but non-zero shear modulus.

In stage II, a rubbery shear modulus develops. A hypo-elastic approach for the deviatoric stress-strain relation is chosen:

$$\dot{\sigma}_{ij}^{\text{dev}} = 2 \ G(q) \ \dot{\varepsilon}_{ij}^{\text{me,dev}},$$

where the shear modulus *G* is defined by the equation from Adolf and Martin [12]:

$$G(q) = G^{\text{final}} \left(\frac{q^2 - q_{\text{gel}}^2}{1 - q_{\text{gel}}^2} \right)^{\frac{8}{3}},$$

with $q_{\rm gel}$ being the degree of cure at the gel point and $G^{\rm final}$ the rubbery shear modulus in the fully cured state. $q_{\rm gel}$ depends on details of the chemical formulation and varies from adhesive to adhesive. Values from 0.3 to 0.6 are common for epoxy-based systems [32]. The value $q_{\rm gel} = 0.455$, measured in [33] for BM1496V, is used in this model.

During transition to stage III, relaxation behaviour becomes important. Therefore, in stage III, a linear viscoelastic material law is chosen:

$$\begin{split} \dot{\sigma}_{ij}^{\text{\tiny dev}} &= 2G_{\infty}\dot{\varepsilon}_{ij}^{\text{\tiny me, dev}} + 2\sum_{m=1}^{M}G_{m}\dot{u}_{ij}^{m},\\ \dot{u}_{ij}^{m} &+ \frac{1}{a(T)\tau_{m}}u_{ij}^{m} = \dot{\varepsilon}_{ij}^{\text{\tiny me, dev}}, \quad m=1,2,...M. \end{split}$$

These equations characterize a thermorheologically simple material [34] with a shift factor log a(T) (*cf.* equation 2.11). The shear relaxation modulus at the reference temperature is given by

$$G(t) = G_{\infty} + \sum_{m=1}^{M} G_m \exp(-t/\tau_m)$$

with the rubbery modulus G_{∞} . A quasi-static approach is used to obtain G(t) from a

5.3. SIMULATION 79

master curve of the tensile and bulk moduli:

$$G(t) = \frac{3KE(t)}{9K - E(t)}.$$

E is determined by the previously described DMA.

All mentioned constitutive equations are implemented as Abaqus user subroutines by applying the simple but stable increment scheme

$$\dot{f}_{t+\frac{\Delta t}{2}} = \frac{\Delta f}{\Delta t}, \ f_{t+\frac{\Delta t}{2}} = f_t + \frac{\Delta f}{2},$$

where f is replaced by the corresponding stress or strain component. The same scheme is used for the tangent moduli $\partial \Delta \sigma_{ij}/\partial \Delta \varepsilon_{kl}^{\text{me}}$.

5.3.2. FINITE-ELEMENT MODEL

Geometry, material and process parameters of this finite-element simulation are chosen to coincide with the experimental set-up from chapter 3. Figure 5.2 shows the geometry of the finite-element model and a photo of the specimen used in the experiment. Symmetry allows to reduce the model to a quarter piece of the real part. The marked edges of the strip and the substructure are not connected; they cannot move in y-direction but slide in x- and z-direction. The metals are assumed to behave linear elastically with the

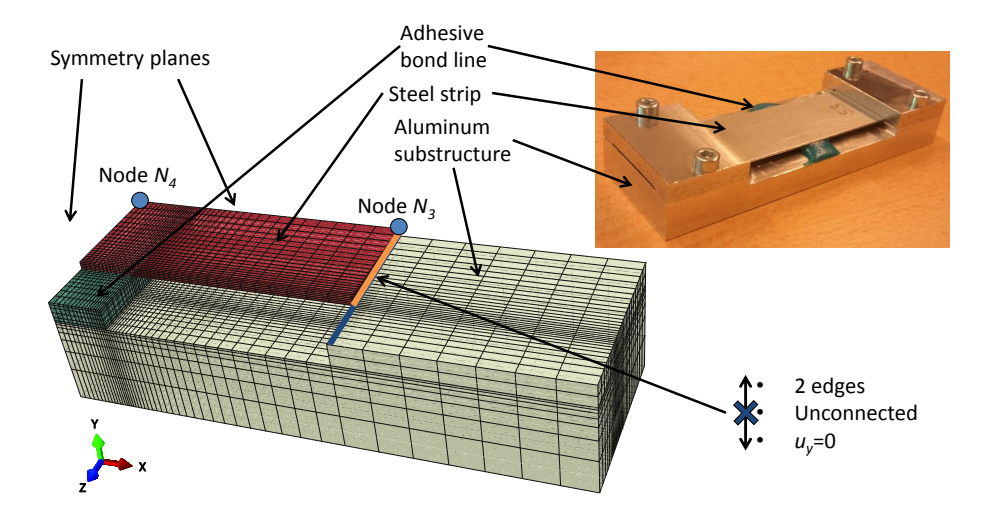


Figure 5.2: Finite-element model and photo of the specimen to monitor local panel distortions.

constant parameters listed in table 5.1. Properties of the adhesive are taken from literature, table 5.3, or obtained by the characterization tests below. The model consists of

Table 5.1: Properties of the steel and aluminium used in the simulation.

Material	E (GPa)	v (-)	$\alpha (10^{-6}/\text{K})$
Steel DX54D+Z	210	0.3	13
Aluminum 6082	69	0.33	23

16.190 brick elements of type C3D20R. Figures 5.3 and 5.4 show the different temperature profiles in experiment and simulation. The 6 cycles investigated are listed in table 5.2.

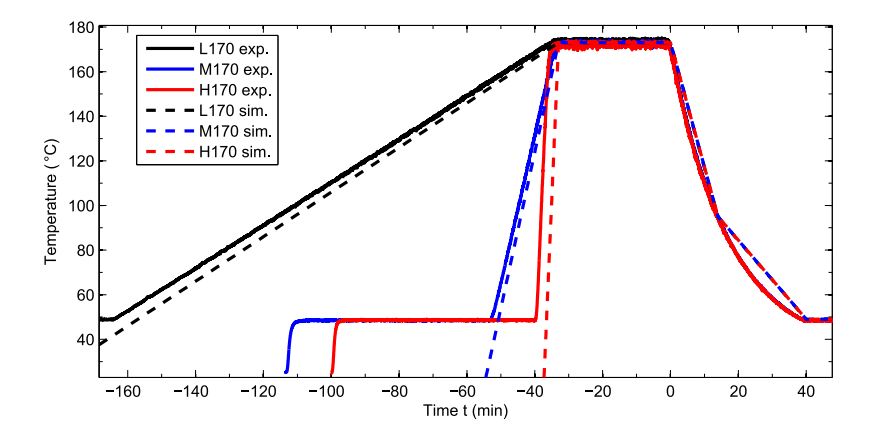


Figure 5.3: Temperature profiles with a cure temperature of 170 $^{\circ}$ C.

Table 5.2: Temperature cycles.

Name	Heating rate	Cure temp.	Dwell time
L170	1 K/min	170 °C	30 min
M170	7 K/min	170 °C	30 min
H170	35 K/min	170 °C	30 min
L155	1 K/min	155 °C	60 min
M155	7 K/min	155 °C	60 min
H155	35 K/min	155 °C	60 min

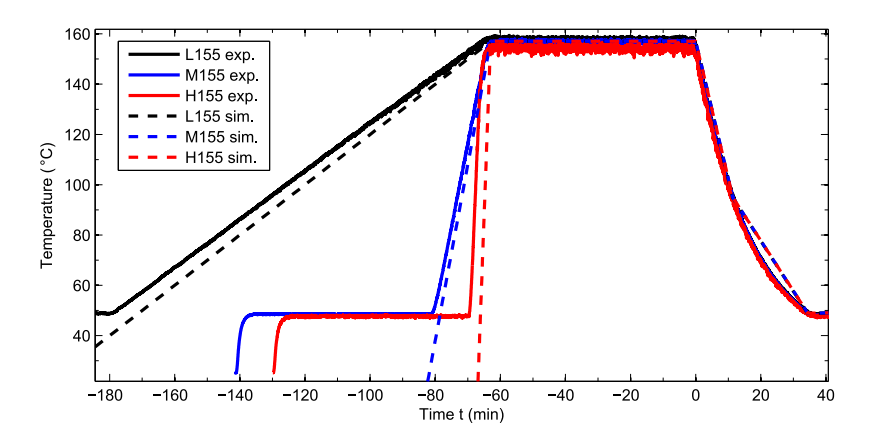


Figure 5.4: Temperature profiles with a cure temperature of 155 °C.

Table 5.3: Material constants for BM1496V from [33].

T _g (° C)	$v_0 ({\rm cm}^3/{\rm g})$	$\frac{v_4 - v_0}{v_0}$ (-)	q_{gel} (-)
85	0.862	$-1.44 \cdot 10^{-2}$	0.455

5.4. RESULTS AND DISCUSSION

5.4.1. CURE KINETICS

Table 5.4 lists the heat of reaction for each DSC run. 2 further DSC runs are added to the ones already done in chapter 3. The respective exothermic peaks in the heat flow curves are shown in figure 5.5. With the procedure described in section 5.2.1, the parameters in table 5.5 for equation 5.1 are found.

Assuming a cure evolution according to equation 5.1 leads to an overestimation of the cure rate or heat flow in case of the highest heating rate (see figure 5.5) while good agreement is reached for the lower heating rates. High rates can lead to an inhomogeneous temperature distribution in the DSC sample biasing the result. Values in that region may carry more error. Keeping that in mind, results are considered sufficient for the simulation model. It is desirable, however, to study the sensitivity of distortion predictions to small variations in the cure progress. See chapter 6 for that.

Table 5.4: H_{∞} for the different heating rates.

	1 K/min	4 K/min	7 K/min	10 K/min	35 K/min
H_{∞} (J/g)	224.2	217.8	207.0	210.8	202.0

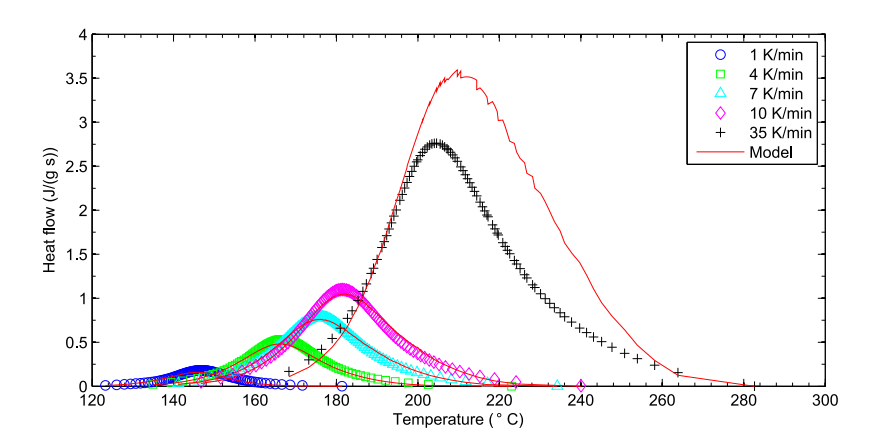


Figure 5.5: Exothermic peaks from DSC tests with different temperature rates compared to model predictions.

Table 5.5: Cure parameters.

$E_{\rm a}$ (J/mol)	k ₀ (1/s)	m (-)	n (-)
$8.877 \cdot 10^4$	$3.410 \cdot 10^8$	0.649	1.551

5.4.2. VOLUME CHANGES

The TMA curve for the fully cured adhesive is shown in figure 5.6. The material shows a linear expansion below and above the glass transition temperature with a greater CTE above. The value $T_{\rm g} = 85$ °C found in [33] agrees with TMA data here. The parameters k_1, k_2 and C_0 in table 5.6 and the dashed curve in figure 5.6 originate from fitting equation 5.11 to the TMA data.

The real chemical shrinkage $\varepsilon_{\text{tot}}^{\text{ch}}$ in table 5.6 is determined by equation 5.8, 5.9, 5.12 and 5.13. Parameters from tables 5.3, 5.3 and 5.6 are taken.

With the constants obtained, equation 5.7 can now be used to describe the volume change of the adhesive in cases in which the stress state stays unaltered. Figures 5.7 and 5.8 show curves of these volume changes for the experimental temperature cycles in figures 5.3 and 5.4, respectively.

It is noteworthy that for all cycles, the adhesives show the same amount of shrinkage after cycle completion. Differences only lie in cure evolution and, therefore, in the

Table 5.6: Parameters characterizing expansion and shrinkage of the adhesive.

<i>k</i> ₁ (1/°C)	k ₂ (1/°C)	C ₀ (1/°C)	$oldsymbol{\mathcal{E}}_{ ext{tot}}^{ ext{ch}}$
3.840e-04	1.990e-04	0.0871	-9.112e-3

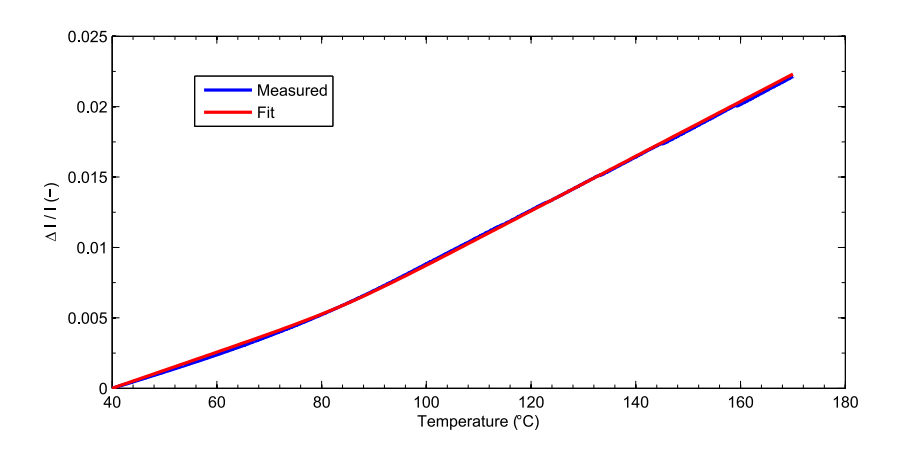


Figure 5.6: Thermal expansion of the fully cured adhesive.

development of cure-induced shrinkage. Figure 5.7 shows that with a low heating rate (continuous black curve), the cure and corresponding volume changes start already during the heating phase. In the fast heating experiment (dotted red line), on the other hand, the adhesive reaches the pre-set cure temperature essentially in an uncured state. The experiment with the medium heating rate shows a behaviour in between these two extremes.

The difference in cure evolution also influences the gelation process. While in cycles with medium or high heating rates the gel point is reached in the isothermal phase at cure temperature, gelation takes place at much lower temperatures for the L170 and L155 experiments. The gel point (*i.e.* the point when q reaches the value $q_{\rm gel}$ from table 5.3) is marked in figures 5.7 and 5.8.

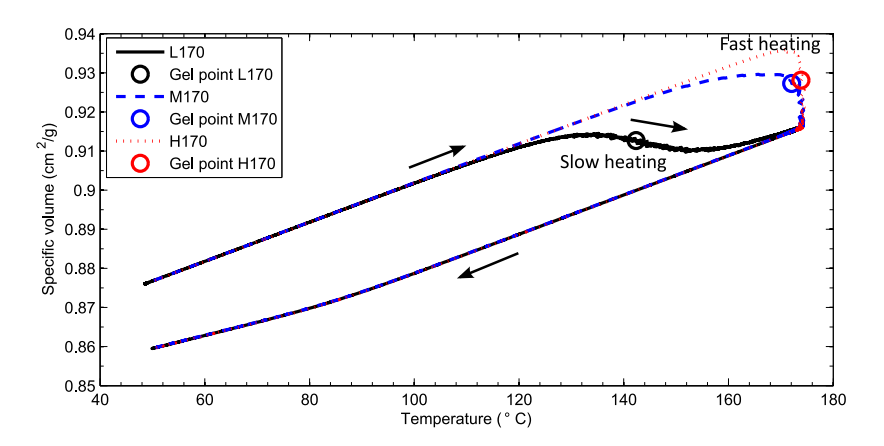


Figure 5.7: Predicted volume changes over the cure cycles L170, M170 and H170, and $q_{\rm gel}$ from table 5.3.

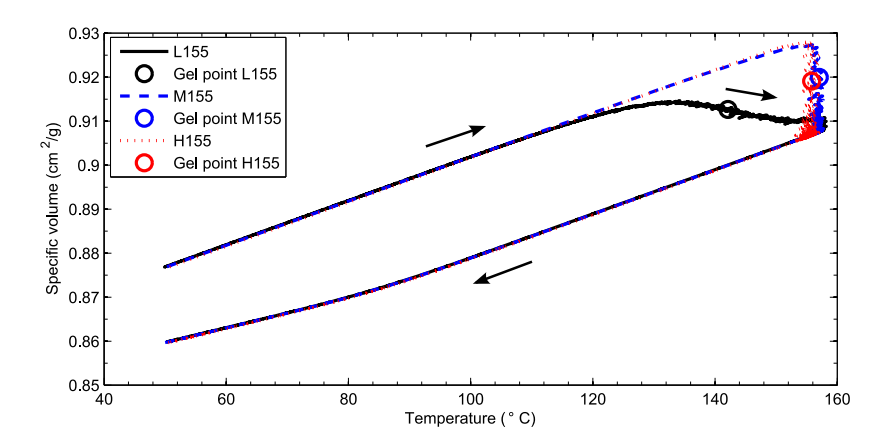


Figure 5.8: Volume changes over the cure cycles L155, M155 and H155, and $q_{\rm gel}$ from table 5.3.

5.4.3. MECHANICAL PROPERTIES

Figure 5.9 displays the DMA results in the form of storage modulus curves for the five different load frequencies versus temperature. By applying the time-temperature super-

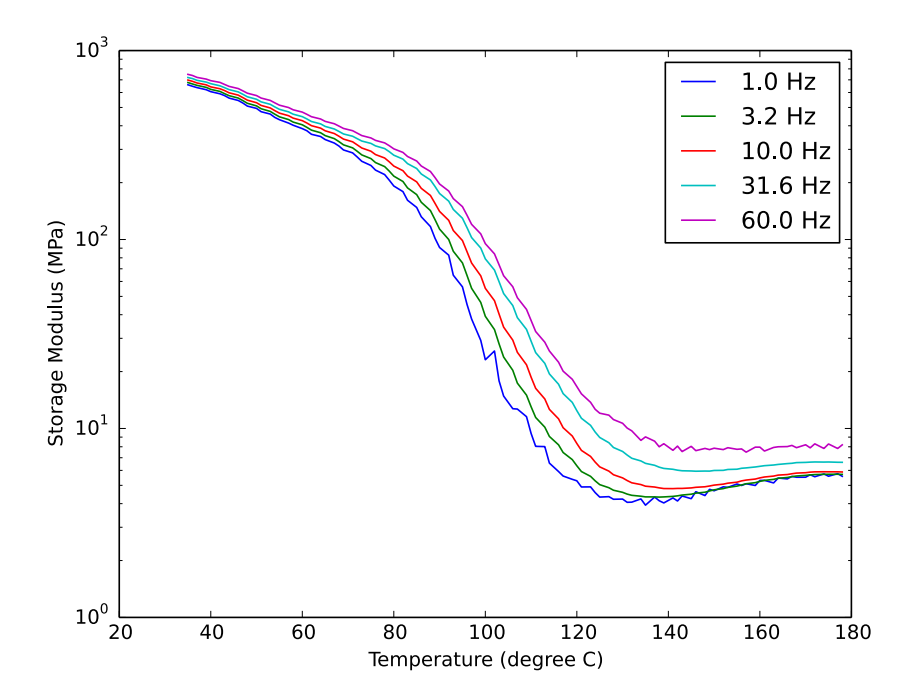


Figure 5.9: The storage modulus E' for different frequencies versus temperature.

position principle, a master curve for the storage modulus can be created. Figure 2.4 shows the curves measured and the assembled master curve. In figure 5.10, the shift factors used are plotted versus the temperature at which the respective partial curve was measured. The function in equation 5.14 with the fitted parameters in table 5.7 is depicted as well. Tables 5.8 and 5.9 list the obtained shear moduli, relaxation times and the bulk modulus.

Table 5.7: Shift factor parameters.

<i>C</i> ₁ (-)	C ₂ (K)	A (J/mol)
7.855	30.56	362900

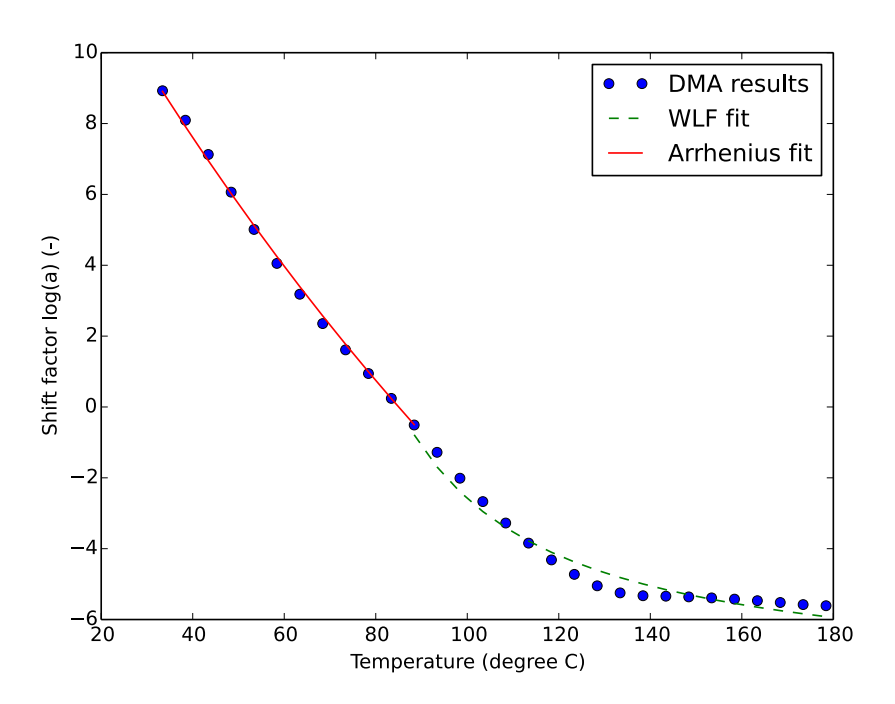


Figure 5.10: The shift factor from DMA data and fitted curves used in the model.

5.4.4. EXPERIMENT VERSUS SIMULATION

The simulation results presented here were obtained with the model described in section 5.3.2 and the values in tables 5.3, 5.5, 5.6, 5.7, 5.8 and 5.9. Displacement curves depict the difference between out-of-plane displacements of nodes N_3 and N_4 :

$$\Delta u_{\gamma} = u_{\gamma}(N_4) - u_{\gamma}(N_3) \tag{5.15}$$

(see figure 5.2). For better comparison, all curves are shifted on the time scale so that cooling down begins at t = 0 min.

Figure 5.11 shows the simulated and measured displacement of the steel strip for the cycles with a cure temperature of 170 °C. Curves for the medium and high heating rate (blue and red lines) resemble each other: the curves start to drop late in the heating phase or early in the dwell phase to a plateau level where they remain until the end of the isothermal phase. The second drop sets in with the cooling down. Predictions and experiments show good agreement for these curves. The simulation somewhat underestimates the first decrease, whereas it overestimates the second. The fact that the

Table 5.8: Shear moduli and relaxation times.

τ_m (s)	G_m (MPa)	τ_m (s)	G_m (MPa)
1E-10	3.228E+01	1E-02	2.535E+01
1E-09	1.415E+01	1E-01	2.383E+01
1E-08	2.274E+01	1E+00	1.953E+01
1E-07	1.847E+01	1E+01	1.061E+01
1E-06	1.899E+01	1E+02	3.776E+00
1E-05	1.778E+01	1E+03	1.391E+00
1E-04	1.822E+01	1E+04	2.307E-03
1E-03	2.126E+01	1E+10	3.254E-02

Table 5.9: Bulk and rubbery shear moduli.

G_{∞} (MPa)	G^{final} (MPa)	K (MPa)
1.608	1.608	2463

H170-curve shows less absolute final displacement than the M170-curve, however, is not reflected in the simulation results.

The simulation model allows further insights in the cure process. Figure 5.12 shows the development of the strain component ε^{th} for the steel, aluminium and the epoxy, and the strain components ε^{ch} and $\varepsilon^{\text{ch}} + \varepsilon^{\text{th}}$ for the adhesive. Furthermore, the black vertical line marks the gel point. Strain before the gel point cannot cause permanent shear stress and, consequently, no displacement of the strip. The gel point is reached in the isothermal phase; thermal strain components do not change in that phase. Hence, the first drop in strain of the M170- and the H170-curves in figure 5.11 is caused by the chemical strain component alone. As soon as ε^{ch} fades out, no further displacement is seen. Strain in the H170-cycle shows similar behaviour; the only difference is that the gel point is passed later in the dwell period. The second drop in displacement in all cycles is caused by the thermal shrinkage of the adhesive during cooling down, which exceeds that of the steel and aluminium.

The steel strip's slow rise early in the heating phase (continuous black line in figure 5.11) is not to be found in the corresponding simulation curve. From about t=-60 min on, however, both curves show similar shapes: a down-up movement before the cure temperature is reached, a constant level above zero during the isothermal phase and a larger drop during cooling.

The predicted strain contributions in figure 5.13 can help to interpret the experimental low heating-rate curve L170 in figure 5.11. The chemical strain development takes place entirely in the long heating phase. There, it causes first an overall shrinkage of the adhesive (mechanical strain neglected) and, consequently, the up-down movement of

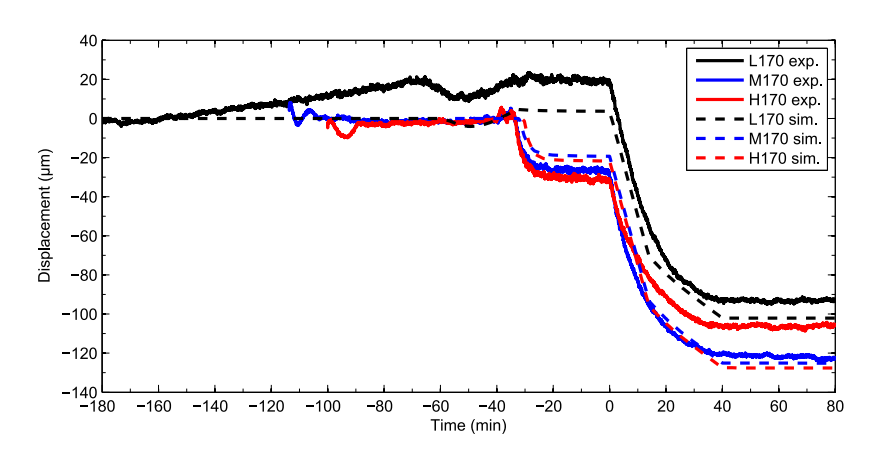


Figure 5.11: Measured (solid lines) and predicted (dashed) displacement of the steel strip for the cycles with 170 °C as cure temperature.

the steel strip. As displayed already in figure 5.7, the gel point is reached during heating. The development of $\varepsilon^{\text{ch}} + \varepsilon^{\text{th}}$ (green line) indicates that the adhesive tends to occupy more space in the dwell phase than at the gel point. That explains why the steel strip deflects in the upwards direction during the isothermal phase (see figure 5.11).

The experimental M155- and H155-curve in figure 5.14 show, similar to the $170\,^{\circ}$ C-curves, two distinguished, sudden drops in displacement. The simulation results reflect that behaviour but underestimate the depth of the first drop and, therefore, the absolute final displacement. The observed difference in displacement between the M155- and H155-cycles is not predicted by the simulation.

The L155-curve has a less pronounced first drop than the M155- and H155-curves, which also starts earlier in the cure cycle. The simulation reproduces that, but with smaller depth and with a few minutes delay. Also, the predicted first drops in the cycles M155 and H155 set in later than the ones observed. This might be due to deviations of the simulated gelation process from the actual one in the experiment. As in cycles with a cure temperature of 170 °C, the first drop in all 155 °C curves is linked to the strain components $\varepsilon^{\text{ch}} + \varepsilon^{\text{th}}$ (see figures 5.15 and 5.16).

While both simulated L-curves show the same amount of final displacement, the M170 and H170 graphs show more absolute final displacement than their 155 °C counterparts. The reason for that is the gel point, which is reached at different temperatures for the M- and H-curves but not for the L-curves (see figures 5.7 and 5.8). Only thermal strain from that point on contributes to panel distortions.

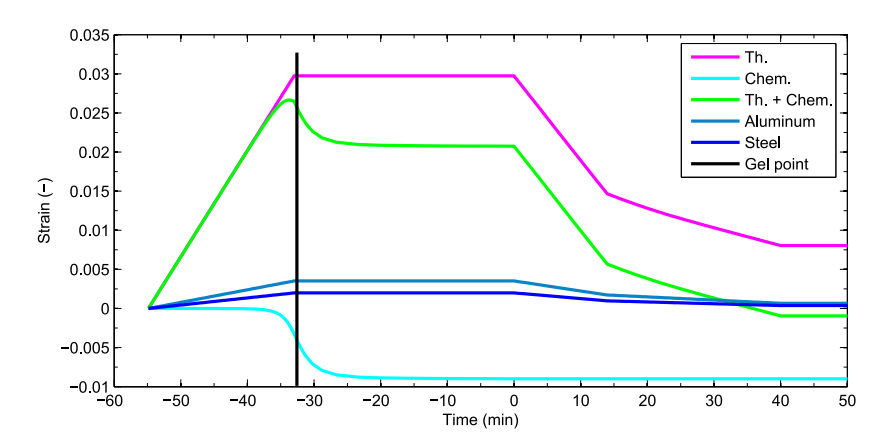


Figure 5.12: Predicted strain development in cycle M170.

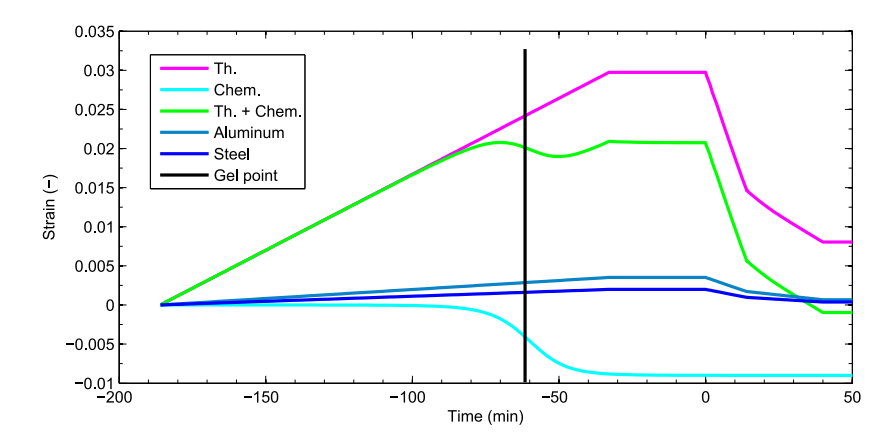


Figure 5.13: Predicted strain development in cycle L170.

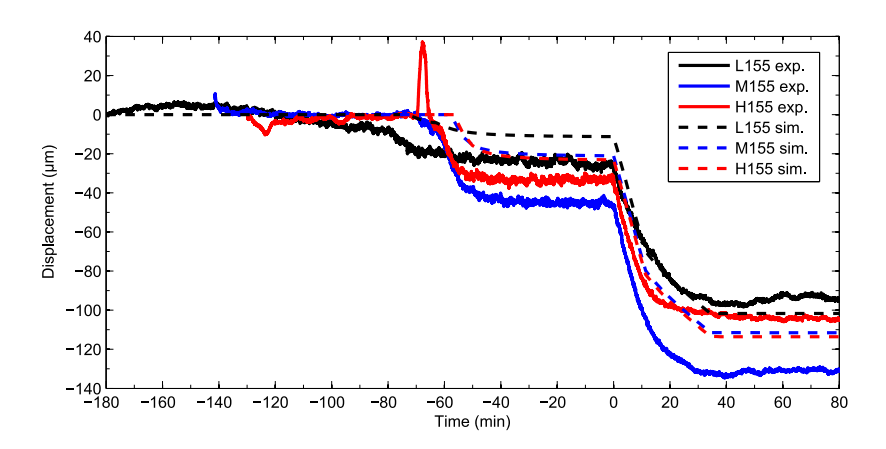


Figure 5.14: Measured (solid lines) and predicted (dashed) displacement of the steel strip for the cycles with $155\,^{\circ}\mathrm{C}$ as cure temperature.

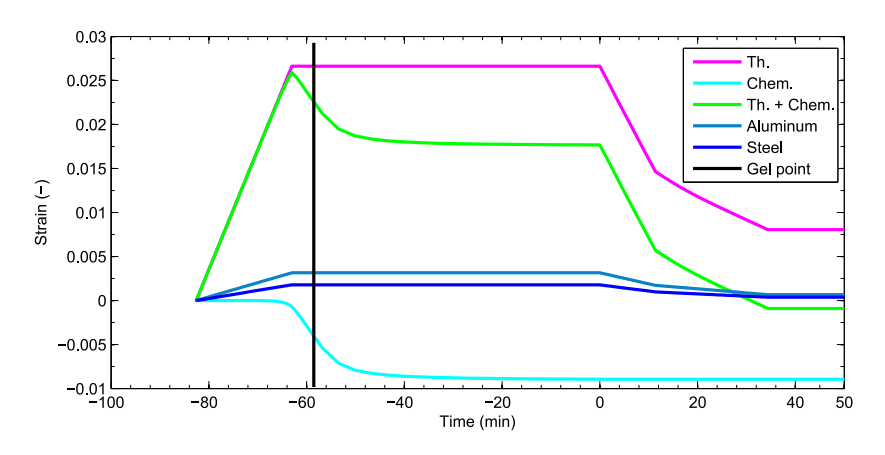


Figure 5.15: Predicted strain development in cycle M155.

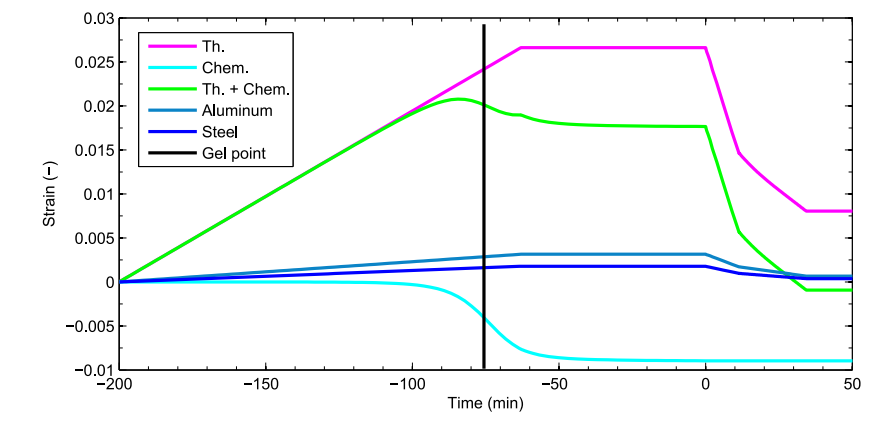


Figure 5.16: Predicted strain development in cycle L155.

5

5.5. CONCLUSIONS

In this chapter, the development of panel distortions measured in chapter 3 due to hotcuring adhesives was simulated. Material constants of a commercial, epoxy-based system were determined and incorporated in the model from chapter 4 making it possible to compare predicted panel distortions to experimental data.

The simulation reproduced many phenomena seen in experiments: the steel strip deforms already before the cooling down sets in; in case of low heating rate even before the cure temperature is reached. The final displacement depends on the entire temperature cycle.

To assure better quantitative predictions, further experiments are done in chapter 6. In a parameter study, the influence of the adhesives material constants on the simulation results are investigated.

REFERENCES

- K. Priesnitz, K. Jansen, J. Sinke, and R. Benedictus, Simulation of the development of local panel distortions due to hot-curing adhesives, Journal of Materials Processing Technology 225, 405 (2015).
- [2] T. Barnes and I. Pashby, *Joining techniques for aluminium spaceframes used in automobiles: Part II adhesive bonding and mechanical fasteners*, Journal of Materials Processing Technology **99**, 72 (2000).
- [3] A. Beevers, S. Steidler, J. Durodola, and M. Coackley, *Analysis of stiffness of adhesive joints in car bodies*, Journal of Materials Processing Technology **118**, 95 (2001).
- [4] C. Adderley, Adhesive bonding, Materials & Design 9, 287 (1988).
- [5] H. Fuchs, K. D. Fernholz, and P. Deslauriers, *Predicted and Measured Bond-Line Read-Through Response in Composite Automotive Body Panels Subjected to Elevated Temperature Cure*, Journal of Adhesion **86**, 982 (2010).
- [6] O. Hahn, A. Chudaska, and B. Hüsgen, *Influence of the process parameters on the quality of thermosetting adhesive joints*, Welding in the World, Le Soudage Dans Le Monde **31**, 277 (1993).
- [7] A. Chudaska and O. Hahn, Damages of bonded parts caused by the thermal and reactionary contraction of adhesives during the curing process, in Vide-Science Technique Et Applications (1994) pp. 223 –227.

[8] A. Chudaska and O. Hahn, *Influence of constructive factors and the process conditions during the curing of hot setting adhesives on the properties of bonded joints*, in *Special Joining Technologies - International Symposium* (1994) pp. 12 – 24.

- [9] O. Hahn and T. Orth, Avoiding bondline readthrough on thin steel elements by modification and optimization of processes, adhesives and sample shape, in International Body Engineering Conference (1997) pp. 111 115.
- [10] O. Hahn and J. Jendrny, Evaluation of simulation models for the estimation of deformation of adhesively bonded steel sheets during curing, Welding in the World **47**, 31 (2003).
- [11] K. A. Patankar, D. A. Dillard, and K. D. Fernholz, *Characterizing the constitutive properties and developing a stress model for adhesive bond-line readout,* International Journal of Adhesion and Adhesives **40**, 149 (2013).
- [12] D. Adolf and J. E. Martin, *Calculation of Stresses in Crosslinking Polymers*, Journal of Composite Materials **30**, 13 (1996).
- [13] M. Wenzel, *Spannungsbildung und Relaxationsverhalten bei der Aushärtung von Epoxidharzen*, Ph.D. thesis, Technical University of Darmstadt (2005).
- [14] A. Lion and P. Höfer, *On the phenomenological representation of curing phenomena in continuum mechanics*, Archives of Mechanics **59**, 59 (2007).
- [15] J. De Vreugd, K. M. B. Jansen, L. J. Ernst, and C. Bohm, *Prediction of cure induced warpage of micro-electronic products*, Microelectronics Reliability **50**, 910 (2010).
- [16] Dow Automotive Systems, BETAMATETM 1496V, data sheet.
- [17] M. Kamal and S. Sourour, *Kinetics and thermal characterization of thermoset cure*, Polymer Engineering and Science **13**, 59 (1973).
- [18] B. Prime, *Thermosets*, in *Thermal characterization of polymeric materials*, Vol. 2, edited by E. A. Turi (Academic Press, 1997) pp. 1380 1766.
- [19] K. M. B. Jansen, C. Qian, L. J. Ernst, C. Bohm, A. Kessler, H. Preu, and M. Stecher, Kinetic characterisation of molding compounds, in EuroSime 2007: International Conference on Thermal, Mechanical and Multi-Physics Simulation Experiments in Microelectronics and Micro-Systems, 2007 (2007).

[20] M. Starink, *The determination of activation energy from linear heating rate experiments: a comparison of the accuracy of isoconversion methods*, Thermochimica Acta **404**, 163 (2003).

- [21] P. Haupt, *Continuum mechanics and theory of materials*, 2nd ed. (Springer, Berlin, 2002).
- [22] W. H. Müller, Streifzüge durch die Kontinuumstheorie (Springer, 2011).
- [23] B. Yagimli and A. Lion, *Experimental investigations and material modelling of curing processes under small deformations*, ZAMM Zeitschrift für Angewandte Mathematik und Mechanik **91**, 342 (2011).
- [24] C. Liebl, M. Johlitz, B. Yagimli, and A. Lion, *Three-dimensional chemo-thermomechanically coupled simulation of curing adhesives including viscoplasticity and chemical shrinkage*, Computational Mechanics **49**, 603 (2012).
- [25] C. Li, K. Potter, M. R. Wisnom, and G. Stringer, *In-situ measurement of chemical shrinkage of MY750 epoxy resin by a novel gravimetric method*, Composites Science and Technology **64**, 55 (2004).
- [26] P. Gromala, J. Duerr, M. Dressler, K. M. B. Jansen, M. Hawryluk, and J. De Vreugd, Comprehensive material characterization and method of its validation by means of fem simulation, in 2011 12th Int. Conf. on Thermal, Mechanical and Multi-Physics Simulation and Experiments in Microelectronics and Microsystems, EuroSimE 2011 (2011).
- [27] J. de Vreugd, *The effect of aging on molding compound properties*, Ph.D. thesis, Technische Universiteit Delft (2011).
- [28] J. De Vreugd, K. M. B. Jansen, L. J. Ernst, and J. A. C. M. Pijnenburg, *Modelling of viscoelastic properties of a curing adhesive*, in *WIT Transactions on Engineering Sciences*, Vol. 57 (2007) pp. 241–251.
- [29] M. Sadeghinia, K. M. B. Jansen, and L. J. Ernst, *Characterization and modeling the thermo-mechanical cure-dependent properties of epoxy molding compound*, International Journal of Adhesion and Adhesives **32**, 82 (2012).
- [30] Y.-H. Li, *Equation of state of water and sea water*, Journal of Geophysical Research **72**, 2665 (1967).

[31] M. Williams, R. Landel, and J. Ferry, *The temperature dependence of relaxation mechanisms in amorphous polymers and other glass-forming liquids*, Journal of the American Chemical Society **77**, 3701 (1955).

- [32] J. López, C. Ramírez, A. Torres, M. Abad, L. Barral, J. Cano, and F. Díez, *Isothermal curing by dynamic mechanical analysis of three epoxy resin systems: Gelation and vitrification*, Journal of Applied Polymer Science **83**, 78 (2002).
- [33] S. Menzel, *Zur Berechnung von Klebverbindungen hybrider Karosseriestrukturen beim Lacktrocknungsprozess*, Ph.D. thesis, Technische Universität Dresden (2011).
- [34] A. Lion, *Einführung in die Lineare Viskoelastizität*, Vol. 4 (Universität der Bundeswehr München, 2007).



6

MODEL SENSITIVITY AND SURFACE MEASUREMENTS

Adhesive bonding is an established joining technique in automotive or aerospace applications. In case thin structures like car body panels are bonded, distortions can occur during the hot cure of the adhesive. Finite-element analysis can help to understand and prevent distortions. However, accurate models require a large number of material constants obtained in time-consuming experiments. Some of the parameters might have a great influence on panel distortions and need to be measured accurately while for others, a rough estimate may suffice. Understanding how much each material constant contributes to panel distortions allows to identify important parameters which require an accurate determination. In this chapter, the sensitivity of a finite-element simulation to varying material parameters is investigated. To that end, the model is run with different combinations of material coefficients; the results are fitted to regression models. In addition, the reduction of panel distortions due to an improved cure cycle is investigated. The deflections of a steel-aluminium strip originating from the bonding processes in a standard and an improved cure cycle are investigated. The process is simulated as well. From all parameters investigated, the chemical shrinkage shows the strongest influence on bonding deformations followed by the gel point. The improved cure cycle can reduce displacements of the structure. The simulation predicts well the displacements and the difference in displacements between those two cure cycles. However, with the strips not being flat before the bonding process, the improvement may be in the order of magnitude of their deviation

from flatness and may be equalized by that.

6.1. Introduction

In chapter 5, the constitutive equations from chapter 4 were combined with results from material characterization tests, thereby allowing to simulate the bonding processes studied in chapter 3. The simulations delivered deeper insight into the development of distortions in a specific structure under specific cure cycles. For the application engineer, further experimental data is desirable to verify the accuracy of the model or to learn more about its limitations.

The simulation model is based on certain assumptions about the adhesive's properties. Among other things, the bulk modulus was assumed to be constant, the chemical shrinkage was estimated by presuming the CTE of the curing adhesive is equal to that of the fully cured one above the glass transition temperature. Other material parameters, however, are determined in designated experiments rather than estimated. The questions may arise how the assumptions affect the accuracy of the model or if further simplifications can be applied to reduce the amount of experimental work in case the model is applied for another adhesive.

Apart from that, reducing distortions or the risk of distortions may be desired. White and Hahn [1] showed that residual stresses in composites can be reduced if the polymer dwells at an elevated temperature prior to the actual cure phase. Their findings indicate that a pre-cure step in the cure cycle would also reduce panel distortions due to hotcuring adhesives.

This chapter addresses these issues. The sensitivity of the simulation model to varying material properties is investigated. To that end, a set of material constants is identified. The model for cycle M170 from chapter 5 is run with different values for these constants. Linear and one-way interaction regression models are fitted to the simulation results with the material parameters as input variables and the absolute final displacement of the steel strip after the cure cycle as the response variable.

In addition, another experiment is performed. A steel strip and an aluminium strip are bonded in cure cycles with and without pre-cure step. The deflection is measured via Digital Image Correlation (DIC) before and after cure.

6.2. PARAMETER STUDY

The simulation model for cure cyle M170 in chapter 5 is investigated here. The simulation is run with different combinations of a chosen set of material parameters. As the

output (response) variable, the absolute final displacement of the steel strip after the cure cycle is chosen, that is the absolute value of the blue dashed line in figure 5.11 at about t = 40 min.

6.2.1. PARAMETERS AND RANGES

More than 40 material constants are used for the adhesive's constitutive model in chapter 5. Using all of them as varying input variables would lead to a vast amount of possible combinations and consequently to a large number of simulation runs needed. Therefore, to reduce simulation time, only 7 variables are selected here. This work focusses only on the impact these 7 variables have on the predicted displacement and the correlation they have to each other. For each variable, a variation range is defined. The material parameters, their original values from chapter 5 and their upper and lower bounds are listed in table 6.1. The shift factor $\log a(T)$ is varied above (C_1) and below (A) the glass transition temperature simultaneously (see equation 5.14). It is treated as a single variable in the regression model.

In the previous chapter, the bulk modulus K was not measured but estimated and assumed to be constant. Estimated values carry presumably a greater uncertainty than directly measured ones which only deviate from true values because of measurement errors. The glassy bulk modulus of the fully cured adhesive is about twice the rubbery one [2, 3]. Rabearison [4] assumes a factor of [2, 3] between the cured and the uncured bulk modulus. Taking these factors into account, the bulk modulus can vary in a range where the upper bounds is about [4, 2] times the lower one. Choosing an interval of that range and with the estimate from chapter [5, 3] as the centre leads to the limits listed in table [6, 1].

Table 6.1: Material parameters used as input variables, their original value and their variation ranges.

Mater. parameters	Original	Min.	Max.	Min./org.	Max./org.
K (MPa)	2463	947.3	3978.7	0.38	1.62
G_{∞} (MPa)	1.608	1.367	1.849	0.85	1.15
$G_{\rm g}$ (MPa)	248.4	211.1	285.7	0.85	1.15
$\log a(T) \colon C_1 (-)$	7.855	6.677	9.033	0.85	1.15
$\log a(T)$: A (J/mol)	362900	308465	417335	0.85	1.15
q_{gel} (-)	0.455	0.3	0.6	0.66	1.32
$k_0 (1/s)$	3.41E+08	2.90E+08	3.92E+08	0.85	1.15
${m \mathcal{E}}_{ ext{tot}}^{ ext{ch}}$ (-)	-9.112E-03	-4.800E-03	-9.112E-03	0.53	1.00

The degree of cure at the gel point $q_{\rm gel}$ for the adhesive BM1496V was measured in [5]. Lopéz *et al.* [6] find values for curing epoxies from 0.28 to 0.58. Here, limits of 0.3 and 0.6

6

are chosen.

The CTE of the fully cured adhesive is not integrated in the model. In cases (with other adhesives) where there is doubt if a simple estimate suffices or if experimental determination is needed, a measurement is fairly easy to accomplish. In that sense, the CTE differs from the chemical strain ε_{rot}^{ch} .

 $\varepsilon_{\text{tot}}^{\text{ch}}$ was not measured directly. Other researchers pointed out that an in-situ recording of volume changes is required to obtain the exact chemical shrinkage. Therefore, the value determined in [5], here referred to as effective chemical shrinkage, was corrected in section 5.2.2. That led to a significantly higher absolute value. Effective and real chemical strains are taken as lower and upper bounds.

For the following parameters, variation intervals of \pm 15% around their original value are chosen. The shear relaxation curve of the adhesive is determined by a set of moduli and relaxation times at each temperature. For simplicity reasons, only the equilibrium modulus G_{∞} , the glassy instantaneous modulus

$$G_{\rm g} = G_{\infty} + \sum_{m=1}^{M} G_m$$

and the shift factor $\log a(T)$ are chosen as input variables. Equation 5.1 determines the cure evolution of the adhesive. Here, only the cure rate \dot{q} is varied by varying the prefactor k_0 .

6.2.2. DESIGN PLAN

To keep the number of runs small, a two-level approach is chosen that is only simulation runs with variables at their maximum or minimum values are performed. Instead of all 2^7 possible combinations, a fractional factorial design with 16 runs is chosen. Simulations are only performed with input variables at their maximum or minimum values (2-level design) decoded as 1 or -1 in table 6.3. The test plan was designed with the software tool Minitab 16 [7]. The same software package is used for data analysis.

6.2.3. REGRESSION MODELS

The simulation results with their respective variable value combination are fitted to a linear model

$$\chi = \beta_0 + \beta_1 \chi_1 + \beta_2 \chi_2 + ... + \beta_7 \chi_7$$

6.3. BIMETAL STRIP 101

and a linear model with 2-way interactions

$$\gamma = \beta_0 + \beta_1 \chi_1 + \beta_x \chi_2 + ... + \beta_7 \chi_7 + \beta_{12} \chi_1 \chi_2 + \beta_{13} \chi_1 \chi_3 + ... + \beta_{67} \chi_6 \chi_7$$

where γ is the response variable (absolute displacement of the steel sheet $|\Delta u_y|$ after the cure cycle, see equation 5.15, figures 5.2 and 5.11), χ_i are the variables representing the material parameters on a coded scale from -1 (minimum value) to 1 (maximum), $\chi_i \chi_j$ represent the interaction of factor χ_i and χ_j . The fitted β_i are the main effect coefficients and β_{ij} are the interaction coefficients.

The null hypothesis for each coefficient is that the coefficient is zero and that the associated variable has no influence on the response. It is tested with a significance level of $\alpha=0.05$. That means the null hypothesis is rejected and the coefficient is significantly different from zero if the coefficient's P-value is less than α . The P-value calculated from the observation data represents the probability of incorrectly rejecting the null hypothesis when it is actually true [7, 8].

6.3. BIMETAL STRIP

6.3.1. SPECIMEN

A $100 \times 20 \times 0.25$ mm steel strip made of DC04+EZ is bonded to a $100 \times 20 \times 0.3$ mm aluminium 2024-T3 strip with 0.25 mm BM1496V adhesive layer. Table 6.2 lists the material properties of both metals. Figure 6.1 shows a drawing and a photograph of the bimetal specimen.

Table 6.2: Properties of the materials used.

Material	E (MPa)	v (-)	$\alpha (10^{-6}/\text{K})$
Aluminium 2024-T3	73.1	0.33	23
Steel DC04+EZ	210	0.3	13

6.3.2. SAMPLE PREPARATION AND EXPERIMENTAL PROCEDURE

On one side of the steel strip, a layer of white paint is sprayed on the degreased surface followed by a speckle pattern of black coloured paint (see figure 6.2). After a day of drying, the other side is bonded to the aluminium strip. To ensure a constant adhesive layer thickness of 0.25 mm, glass beads were spread in the adhesive film and the sample was weighted for several hours.

After cleaning the sample from squeezed out adhesive, a first set of DIC photographs

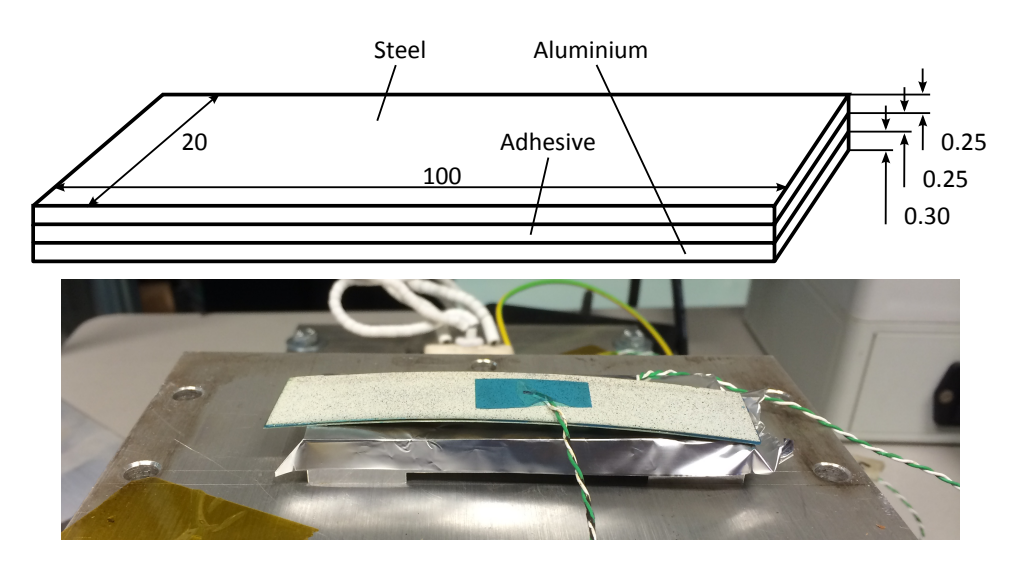


Figure 6.1: Top: drawing of the bimetal strip with different material layers; distances in millimetres. Bottom: photograph of the specimen with thermocouples taped to both the top (aluminium) and bottom (steel) side and speckle pattern on top.

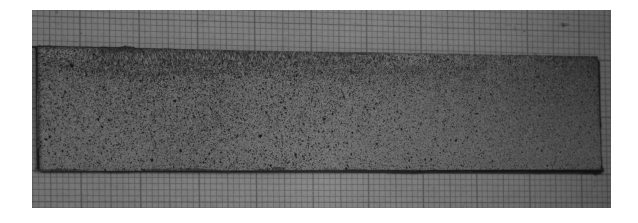


Figure 6.2: Photograph of the specimen's speckle pattern.

is taken. Afterwards, thermocouples are taped on both sides of the bimetal strip and the sample is placed in an oven and exposed to a cure cycle with (P170) or without (NP170) pre-cure step. For each cycle, one sample is taken. The cycle NP170 consists of a heating phase, an isothermal (dwell) phase of 30 minutes at 170 °C as recommended by the producer [9] and a cooling down phase. The cycle P170 has an additional isothermal phase of 60 minutes at 125 °C prior to the recommended one. The cooling down to room temperature is done passively by leaving the sample without further heating over night.

After cure, a second set of DIC photographs is taken. The DIC set-up has not been moved between the two shootings and the sample is placed on a marked position for both shootings. However, to avoid errors due to inaccurate positioning, the displacement field from the second shooting is ignored. Instead, the surface shapes from both shootings, before and after cure, are compared. The displacement is set to zero in the centre of the surface.

6.3.3. SIMULATION MODEL

The simulation model for the bimetal strip consists of 7371 brick elements of type C3D20R. Each material layer is built up of three layers of elements. The top layer of the model depicted in figure 6.3 represents the steel strip followed by the adhesive layer and the aluminium strip. Symmetries allow to reduce the model to one quarter piece of the

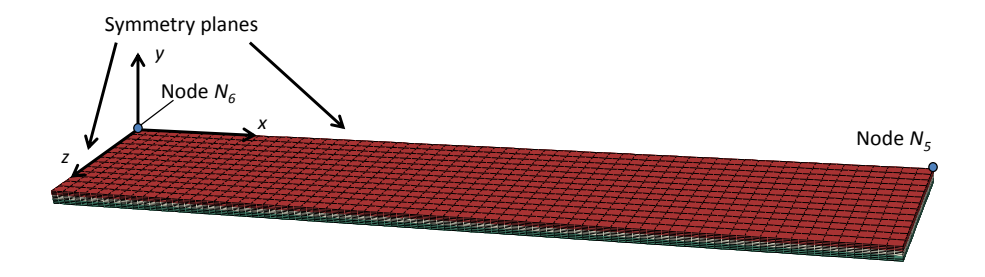


Figure 6.3: Mesh of the finite-element simulation model with three material layers: steel (red), adhesive (white) and aluminium (green).

specimen with the symmetry boundary conditions shown in figure 6.3. The coordinate system's origin is located in the centre of the specimen's top surface with *y* being the out-of-plane coordinate.

The material constants from table 6.2 are used to describe the metals in the simulation; the properties of the adhesive are the ones determined in chapter 5. The temperature profiles for the NP170 and P170 cure cycles are adopted from the experiments. For simplicity reasons, the curves are piecewise linear (see figures 6.6 and 6.9). A homogeneous temperature distribution through the entire sample is assumed.

6.4. RESULTS AND DISCUSSION

6.4.1. PARAMETER STUDY

Table 6.3 lists the simulation results with the combination of variable values used. Table 6.4 shows the *P*-values and coefficients of the designated material parameters for the linear regression model. The complete Minitab output for both regression models can be found in appendix B.

Only $\varepsilon_{\text{tot}}^{\text{ch}}$ and q_{gel} have a P-value below 0.05 in the linear model; they are the only parameters showing a significant influence on the steel strip displacement. Figure 6.4 shows a Pareto chart of the standardized effects (absolute values of the coefficients divided by their respective standard errors) of the linear model with the red line repre-

Table 6.3: Simulation runs with the according input coded input variable values and the results.

Run no.	K	G_{∞}	$G_{\rm g}$	$\log a(T)$	$q_{\scriptscriptstyle m gel}$	k_0	$oldsymbol{\mathcal{E}}_{ ext{tot}}^{ ext{ch}}$	Result (µm)
1	1	-1	1	1	-1	-1	1	128.5
2	-1	-1	1	-1	1	1	1	119.2
3	-1	-1	-1	1	-1	1	1	126.6
4	-1	-1	1	1	1	-1	-1	112.0
5	1	1	-1	1	-1	-1	-1	118.7
6	1	-1	-1	-1	1	-1	1	121.1
7	1	1	1	-1	1	-1	-1	114.7
8	-1	1	1	-1	-1	-1	1	128.6
9	1	-1	-1	1	1	1	-1	113.5
10	1	-1	1	-1	-1	1	-1	117.4
11	-1	1	-1	1	1	-1	1	120.8
12	1	1	1	1	1	1	1	121.6
13	-1	1	1	1	-1	1	-1	116.4
14	-1	1	-1	-1	1	1	-1	113.2
15	1	1	-1	-1	-1	1	1	129.5
16	-1	-1	-1	-1	-1	-1	-1	116.7

Table 6.4: Coefficients and P-values of the linear regression model.

Coefficient	P-value
119.868	0.000
0.719	0.061
0.531	0.145
-0.106	0.755
-0.144	0.674
-2.894	0.000
-0.231	0.502
4.581	0.000
	119.868 0.719 0.531 -0.106 -0.144 -2.894 -0.231

senting the cut-off significance level for $\alpha = 0.05$. The chemical strain has the strongest influence on the steel strip displacement followed by the degree of cure at the gel point. The bulk modulus K has, even though given a larger variation interval, no significant correlation with the response variable. The standard distance of data points from the regression line is $S = 1.32 \, \mu \text{m}$ for the linear model.

A better fit is achieved by the linear model with two-way interactions ($S=0.03~\mu m$). Table 6.5 shows the effects, regression coefficients and P-values for that model. The limited number of simulation runs does not allow to model all two-way interactions. Minitab automatically removes those which are totally confounded.

Several regression terms show coefficients significantly different from zero. The standardized effects in figure 6.5 show that more terms have a significant effect on the model response. With $\varepsilon_{\text{tot}}^{\text{ch}}$ and q_{gel} showing by far the strongest influence on the steel strip displacement, the interaction term of shift factor and equilibrium shear modulus has an affect, too. All main effect coefficients are significantly different form zero in that model.

Table 6.5: Coefficients and P-values of the linear regression model with two-way interactions.

Term	Coefficient	P-value
Constant	119.868	0.000
K	0.719	0.006
Ginf	0.531	0.007
Gg	-0.106	0.037
loga	-0.144	0.028
qgel	-2.894	0.001
qdot	-0.231	0.017
ech	4.581	0.001
K*Ginf	-0.031	0.126
K*Gg	0.031	0.126
K*loga	0.094	0.042
K*qgel	-0.006	0.500
K*qdot	0.106	0.037
K*ech	-0.031	0.126
Ginf*loga	-0.919	0.004

6.4.2. MEASURED AND PREDICTED STRIP DEFORMATIONS

Time plots are shifted on the time scale so that cooling down starts at t = 0. Figure 6.6 shows the temperature profiles measured on both sides of the bimetal strip. The temperature overshoot in the beginning of dwell phase was adopted in the simulation temperature profile. It is caused by the reacting adhesive. The sensor for the temperature

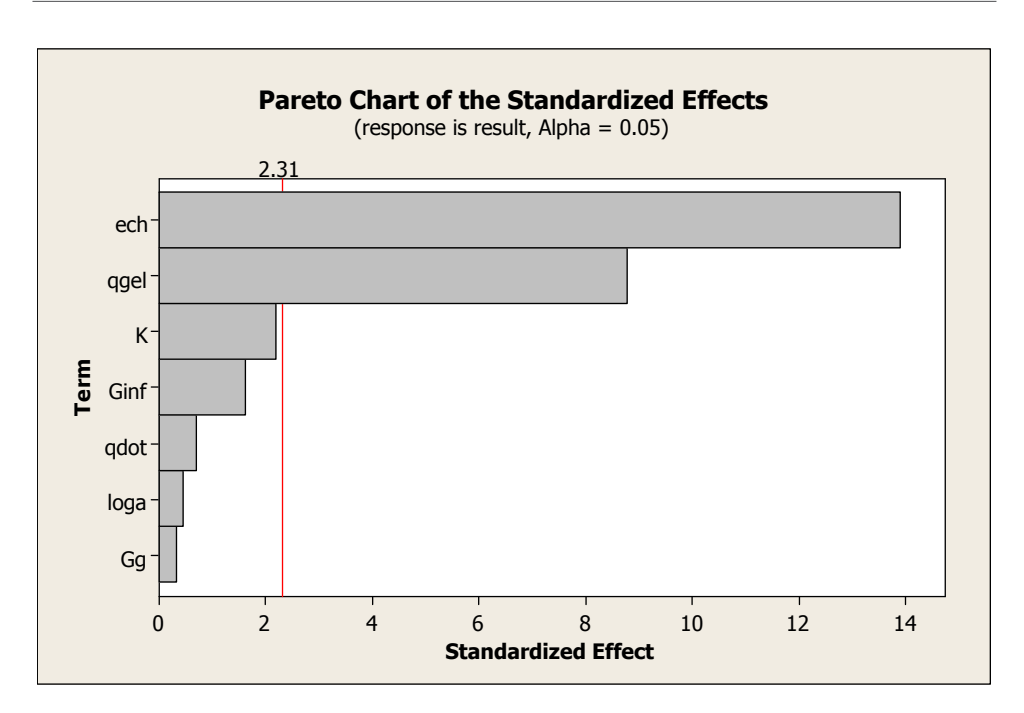


Figure 6.4: Pareto chart of the standardized effects for the linear regression model.

control is placed directly at the heating element so that it captures the highest temperature in the oven unless another heating source increases the temperature at another location. The degree-of-cure curve in figure 6.6 shows that a significant amount of the cross-linking reaction takes place in the heating phase.

Figure 6.7 shows the measured and simulated sample temperature in the cycle P170. The simulation of the cure reaction for that cycle reveals that the gel point shifts to the pre-cure step and, therefore, to lower a temperature.

Figures 6.8 and 6.9 show the measured contour maps of the bimetal strips before and after the cure cycle NP170 and P170, respectively. Note that left and right contour plots have different colour scales. While showing a very similar deflection after both cure cycles, the strips deviate from an intent flat surface before cure in both cases. The way they deviate is quite different. Plots along the *x*-axes illustrate that difference (figure 6.10).

The simulation model does not account for any curvature before the cure cycle, but assumes a flat strip in the reference state.

The development of the strip's deflection becomes apparent when looking at $\Delta u_y = u_y(N_6) - u_y(N_5)$, the difference between out-of-plane displacements of nodes N_5 and N_6 depicted in figure 6.3. Figure 6.11 shows the plots of Δu_y over time for both cure cycles.

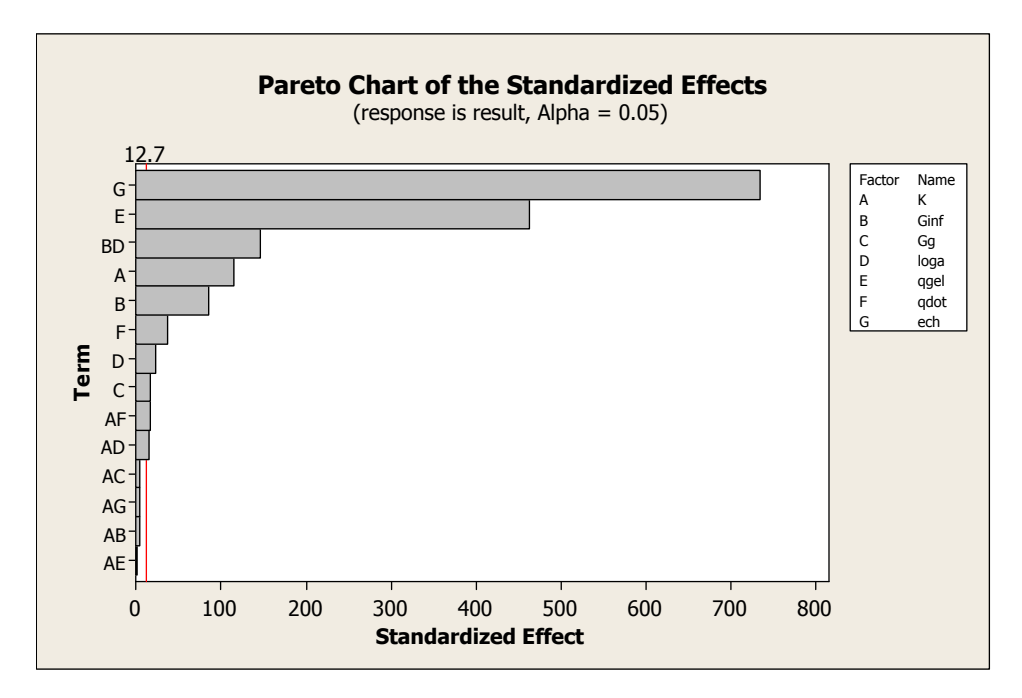


Figure 6.5: Pareto chart of the standardized effects for the regression model with two-way interactions.

The deflection of a bimetal strip usually originates from different CTEs of both metals and temperature change. Looking at the bonding process of two metal strips, additional factors need to be accounted for. The compound strip can deflect only if the adhesive is able to transfer loads between both metals. The gel point can be seen as the point from which on that is the case. Moreover, the expansion and shrinkage of the adhesive might contribute to deflections as well.

The deflection in the P170 cycle starts at about t=-30 min with an increase in Δu_y (see figure 6.11). Before that point in time, no deflection is observed. However, the gel point has been passed and the degree has increased from 0.5 to about 0.7. Since the cure shrinkage grows linearly with the degree of cure in the model (see equation 5.10), 20% of the chemical shrinkage occurred in the time period between the gel point and the first deflection. Evidently, that shrinkage did not contribute to any deflection. Keeping the geometry of the specimen depicted in figure 6.1 in mind, that is not surprising. The adhesive layer is close to the neutral line and has a by some order of magnitude smaller modulus than the metal strips. Therefore, volume changes of the adhesive contribute less to deflections than volume changes of the metals.

The first increase of Δu_y in cycle P170 can be explained by the temperature raise from the pre-cure step to the 170 °C cure temperature; the drop is caused by the cooling

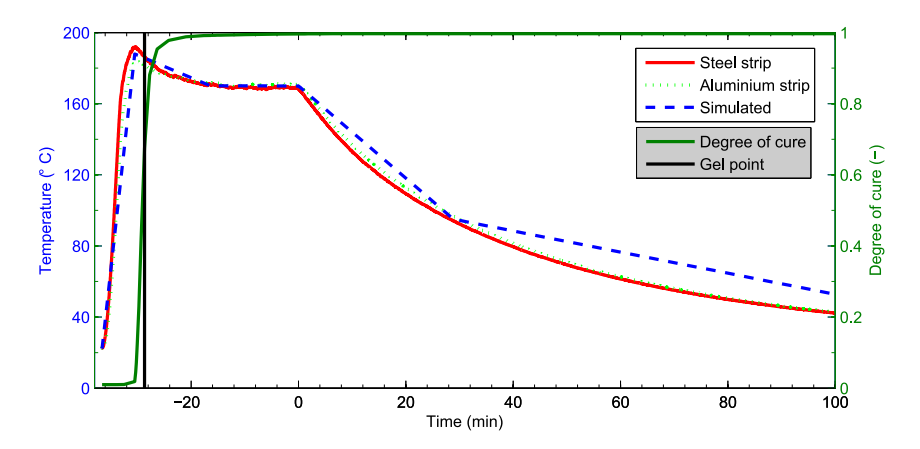


Figure 6.6: Cure cycle NP170: measured (continuous red and dotted green line) and simulated (dashed blue line) temperature together with the predicted degree of cure (continuous green line). The gel point is marked with a vertical black line.

down (see figures 6.7 and 6.11). The first drop of Δu_y in cycle NP170 is caused by the temperature decay from the overshoot peak. During that displacement drop, there is also quite some cure shrinkage taking place (see figure 6.6), but, as seen in the other cure cycle, that will hardly cause any deflection.

The difference in Δu_y between both cure cycles does not change much more during cooling down. Figure 6.12 shows the displacement along the x-axis after both cure cycles for both experiment and simulation. The simulation predicts well the final displacement for both cycles. The difference in displacement at the outer edges of the strip between the two cure cycles of about .5 millimetres agrees well with the measured one. However, because the simulation model starts from a flat strip, that difference is also to be found in the predicted final shape of the strip, while for the measurement, the difference in displacement is compensated by the difference in deviation from a flat reference state (see figure 6.10).

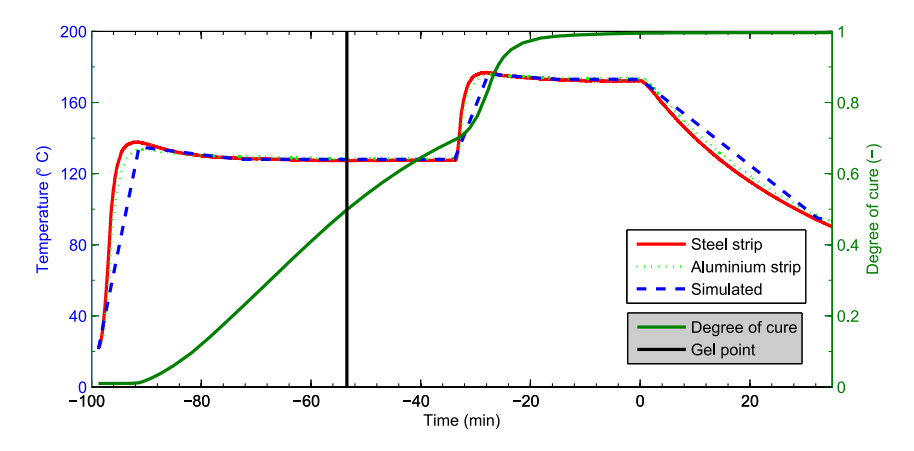


Figure 6.7: Cure cycle P170: measured (continuous red and dotted green line) and simulated (dashed blue line) temperature together with the predicted degree of cure (continuous green line). The gel point is marked with a vertical black line.

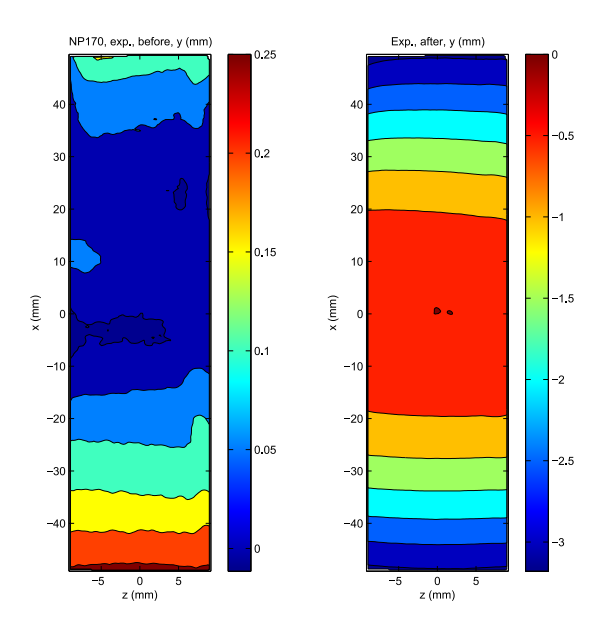


Figure 6.8: Contour map of the bimetal strip before (left) and after (right) the cure cycle NP170 measured with DIC.

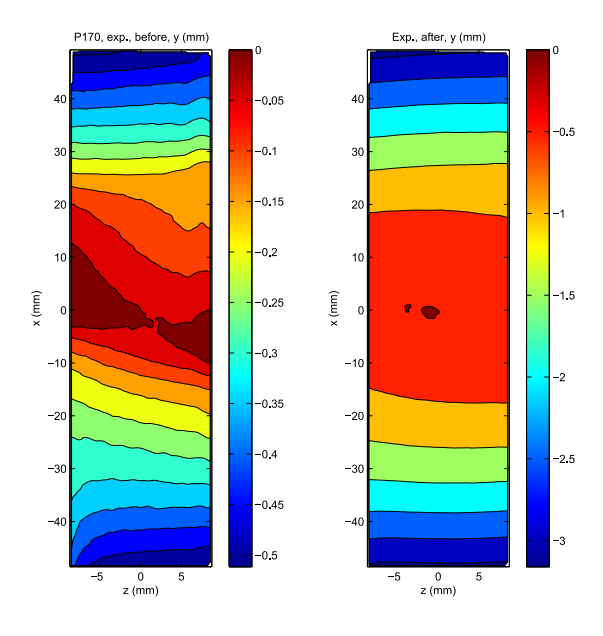


Figure 6.9: Contour map of the bimetal strip before (left) and after (after) the cure cycle P170 measured with DIC.

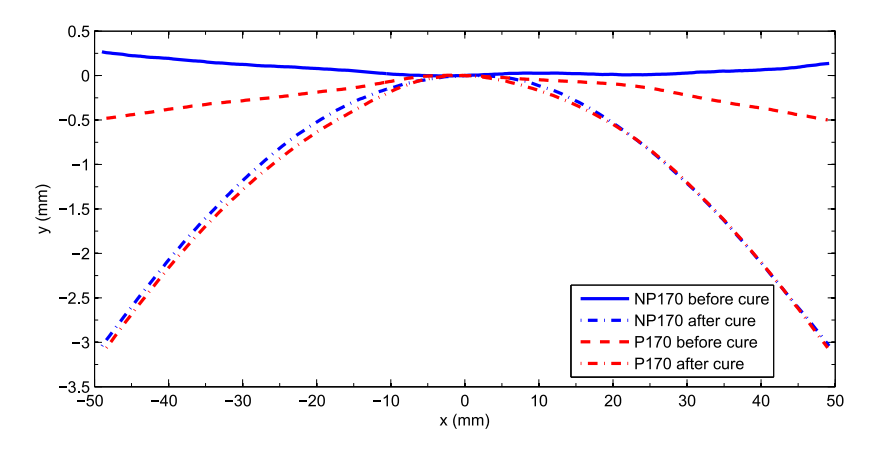


Figure 6.10: Measured position of the bimetal strip before and after cure at position z = 0.

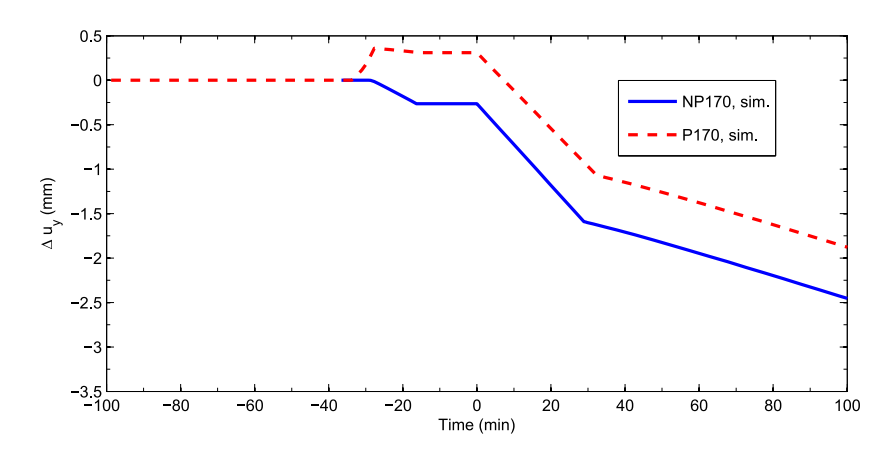


Figure 6.11: Predicted displacement of the bimetal over time.

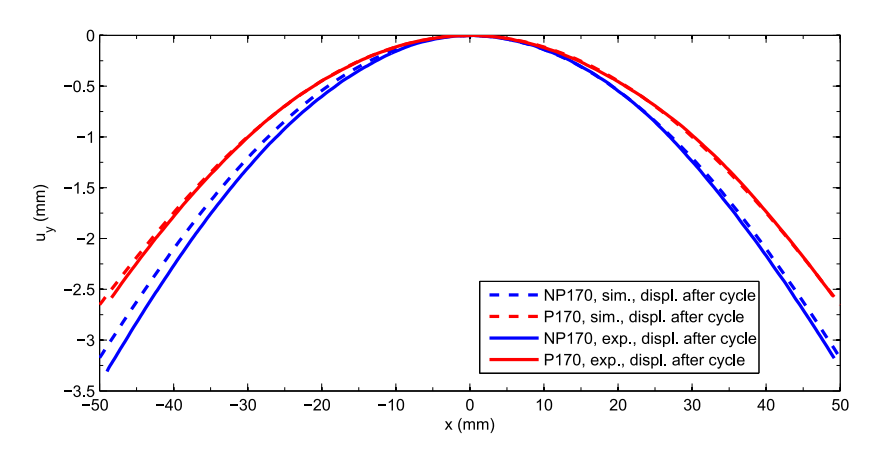


Figure 6.12: Predicted and measured displacement of bimetal strip after cycle NP170 and P170.

6.5. CONCLUSIONS

The chemical strain $\varepsilon_{\text{tot}}^{\text{ch}}$ should be determined with great care. With variation interval from the effective to the real strain, it showed a greater influence on the steel strip displacement than all other material constants investigated. In addition, the point of gelation is of importance too. An estimate with the common region from 0.3 to 0.6 might not be sufficient; an experimental determination is required. The bulk modulus only shows a significant affect in one of the regression models. An estimate might suffice. The other mechanical properties G_{∞} , $G_{\rm g}$ and $\log a(T)$ as well as k_0 show a weaker relationship with the displacement. Their determination does not require more effort as there is no evidence that this would improve the prediction quality of the model.

A cure cycle with a pre-cure step at a lower temperature than the cure temperature can reduce panel distortions. The simulation model is capable of predicting the improvement. For accurate predictions, however, a simulation with the real part shape instead of the intent geometry is recommended.

REFERENCES

- [1] S. R. White and H. T. Hahn, *Cure cycle optimization for the reduction of processing-induced residual stresses in composite materials*, Journal of Composite Materials **27**, 1352 (1993).
- [2] D. Adolf and J. E. Martin, Calculation of Stresses in Crosslinking Polymers, Journal of Composite Materials 30, 13 (1996).
- [3] J. Ferry, Viscoelastic properties of polymers (Wiley, 1980).
- [4] N. Rabearison, C. Jochum, and J. Grandidier, *A FEM coupling model for properties prediction during the curing of an epoxy matrix*, Computational Materials Science **45**, 715 (2009).
- [5] S. Menzel, Zur Berechnung von Klebverbindungen hybrider Karosseriestrukturen beim Lacktrocknungsprozess, Ph.D. thesis, Technische Universität Dresden (2011).
- [6] J. López, C. Ramírez, A. Torres, M. Abad, L. Barral, J. Cano, and F. Díez, *Isothermal curing by dynamic mechanical analysis of three epoxy resin systems: Gelation and vitrification*, Journal of Applied Polymer Science **83**, 78 (2002).
- [7] Minitab[®] StatGuideTM.
- [8] D. C. Montgomery, Design and Analysis of Experiments, 6th ed. (Wiley, 2005).

[9] Dow Automotive Systems, $BETAMATE^{TM}$ 1496V, data sheet.



7

DISCUSSION

7.1. SIMULATION APPROACH

In this work, a model is proposed that predicts well panel displacement measured during cure in different temperature cycles. It can be used to predict local panel distortions that are caused by the evolving properties of the adhesive. Some characteristics of the model were proven to be essential for accurate predictions and should be taken into consideration for similar modelling approaches.

Describing the stress-strain relation in form of rate equations as it is done in equation 4.6 turned out to be of importance. As described in the respective section, the hypoelastic formulation implies that cross links that lead to an increase in the modulus only contribute to stresses through strain that occurs after the cross link is formed. Since the evolving equilibrium shear modulus depends on the cure process which, in turn, depends on the temperature history, stress development in the adhesive depends on the temperature history. As a consequence, the model predicts different levels of distortions for different cure cycles as it was also seen in the experiments. The rate equations were essential for that.

The bulk modulus was not measured but roughly estimated. The research on the sensitivity of predictions to the bulk modulus confirmed the preceding assumption that the bulk modulus has little influence on deformations as long as the adhesive is not applied in a confined space. This simplifies material characterization. The bulk modulus is usually not as easy to determine as other mechanical constants such as shear or ten-

116 7. DISCUSSION

sile modulus for instance, especially when it depends on time, temperature and degree of cure. In addition, using measurements of other properties to calculate *K* yields inaccurate results. Doing a rough estimate rather than measurements of the bulk modulus saves time and effort. A more accurate determination is required in cases where the adhesive has no space to spread.

The chemical strain showed a significant influence on panel distortions and needs to be determined accurately. The difference between the effective chemical shrinkage found through density measurements at room temperature before and after cure and the real one occurring at elevated temperature can be large enough to affect the prediction of local distortions. An in-situ measurement is desirable. However, if that is not possible, then the correction procedure as described in chapter 5 may be used to improve predictions.

Adhesives that are glassy in their operative range pass the glass transition temperature during cooling from the cure temperature. The drastic change in properties need to be accounted for by temperature-dependent material parameters. In this work, the shear relaxation modulus of the adhesive investigated is a temperature-dependent function. The assumption of thermorheological simplicity reduced significantly the experimental effort while providing sufficient accuracy in the predictions. Shifting the relaxation curve did not show any significant impact on predictions in the sensitivity analysis. However, the relaxation behaviour may vary from material to material and needs to be evaluated separately for each adhesive. The investigations do not show any necessity to describe the bulk modulus as temperature-dependent. Quite the contrary, a constant bulk modulus may suffice. The CTE changes significantly at the glass transition temperature. The effect chemical strain has on distortions suggests that thermally induced volume changes are of equal importance. Therefore, the CTE should be measured below and above the glass transition temperature, which is a simple procedure and should not cause any problems.

The constitutive description of the adhesive is based on a small-strain assumption. It has been mentioned in this work that finite-strain models are available as well as models including plasticity or other phenomena. These models allow to extend the applicability to cases where these effects play a role. A thorough testing, in which deformation is monitored in various temperature cycles as it is done in this work, is needed to ascertain accurate predictions.

The results of a simulation may be processed further to evaluate the severity of distortions. In case a scale is used that is based on the deviations of curvature, the discretization of the finite-element model can be important. Changes in the slope of the

7.2. DISTORTIONS

panel's surface may appear less abrupt in a simulation due to a wider mesh. Estimates on the severity need to take that into account. The robustness of the severity value to changes in mesh size may need to be examined.

The model can be applied to other one-part adhesives which cure at an elevated temperature. However, if the cure mechanism is a different one, the model needs to reflect that. In cyanacrylic adhesives for instance, the distance to adherends might need be included in the setting rate equation since ions diffusing from the substrate initiate the setting process.

7.2. DISTORTIONS

The occurrence of distortions in the bonding process is usually an exception. However, light-weight design will also promote more diverse combinations of materials and thinner panels in the future. While the use of dissimilar materials suggests adhesive bonding as a joining method, the use of thinner panels increases the risk of bonding distortions. If occurring distortions can be linked to the changing properties of the adhesive, simulations similar to the ones done in this work can help to study them and find measures to prevent them (as for example modifying the temperature cycle). It is noteworthy, however, that simulations based on an ideal geometry can under-predict distortions. Deviations of the adherends from the intended shape can lead to an inconsistent adhesive layer thickness, which, in turn, can cause visible defects. Therefore, simulations might need to incorporate manufacturing tolerances.

If relative movements of the adherends cause distortions, the entire structure and the real bonding process need to be examined. The complex temperature field during cure needs to be determined. But even if that is accomplished and the distortions can be explained by the adverse temperature development in the oven, the temperature of the assembly is usually not in direct control of the engineer. Controllable parameters in a cure oven might be the temperature and speed of the hot air at the inlet nozzles to the oven, the orientation of the nozzles and the movement and position of the structure in the oven. How a modification of these parameters improves the temperature field can be quite complex. A study on the correlation of control parameters and panel distortions is necessary to provide directly applicable guidelines for the avoidance of distortions. Such a study needs industrial investigations and cannot be limited to laboratory research. It requires a detailed knowledge on the heat transfer during cure. The current model is based on a known temperature field. In future works, the model should be expanded to also cover heat conduction; the balance equation of linear momentum needs to be solved in conjunction with the balance equation of energy.



8

CONCLUSIONS AND RECOMMENDATIONS

8.1. CONCLUSIONS

The goal of this research was to study the development of local panel distortions during the hot cure of an adhesive, to understand the correlation between changing properties of the adhesive and the occurrence of distortions, to derive a mathematical description of the bonding process that can be used in a simulation model to predict distortions and the comparison of simulation results and experiments.

Local panel distortions can arise in early stages of the cure cycle, even before the cure temperature is reached. In order to analyse the origins of distortions, the temperature history over the entire bonding process needs to be looked at. Investigations on the cure temperature only are insufficient; changing the cure temperature might not affect the (amount of) distortions. For accurate predictions, a degree-of-cure and temperature-dependent model is needed that factors in chemical shrinkage, thermal deformation and stress relaxation. In order to be able to predict differences in distortions that arise from different heating rates or pre-cure dwelling periods, the model has to take into account that the cross links formed in the adhesive material contribute to stresses only via subsequent mechanical deformation. A hypo-elastic constitutive model meets that demand.

To assure accurate predictions but keep the effort small, different material constants need different treatment. The chemical shrinkage and the gel point should be deter-

8

mined with good accuracy as they have a strong influence on the distortions predicted. To measure a time-, temperature- and cure-dependent bulk modulus is not necessary if bond lines are not confined. A constant value or an estimate suffice for these cases.

By providing a tool to compare the distortions from different cure cycles, the model can help to design robust bonding processes in which distortions are kept underneath a defect threshold.

8.2. RECOMMENDATIONS FOR FUTURE WORK

The constitutive equations for the adhesive can be used to describe other types of adhesive or other cross-linking polymers if the cure mechanism and the correlation between the state of cure and the mechanical properties are the same. Otherwise, adjustments are needed. The model assumes that the temperature field is known beforehand. However, it is desirable to predict the temperature development for a given heating set-up. Therefore, future work should focus on solving equations for the heat transfer along with the stress calculations. For distortions that originate from the relative movement of adherends, these calculations must incorporate the entire assembly and even the air flow in the oven. To provide directly applicable guidelines to reduce distortions, the correlation between distortions and controllable process parameters such as nozzle direction, inlet air temperature and position and movement of the structure in the oven has to be investigated. Future work on that topic must exceed laboratory studies and focus on specific industrial bonding processes.

The prediction model at hand can be used to study bonding processes of complex structures in a complex temperature field. The experimental validation of the model that has been obtained here ensures that the correlation of distortions and evolving properties of the adhesive are represented correctly. Extending the model for use in more complex processes requires validation of these modifications. For example, if processes with larger displacements such as global distortions are studied, finite strain, plastic deformation and/or damage to the adherends or the adhesives might occur and should be integrated in the model; they need additional validation.



MATERIAL PARAMETERS FOUND IN LITERATURE

From [1] the following material properties have been retrieved:

E _a (J/mol)	m (-)	n (-)	k ₀ (1/s)	k ₁ (1/°C)	k ₂ (1/°C)
$71.28 \cdot 10^3$	0.272	1.125	$7.98\cdot10^6$	$3.31\cdot10^{-5}$	$6.1\cdot10^{-5}$
C ₀ (1/°C)	C (-)	T_g (°C)	$oldsymbol{\mathcal{E}}_{ ext{tot}}^{ ext{ch}}$ (-)	<i>b</i> ₁ (-)	b ₂ (-)
0.0777	0.0894	91.7	$-2.0 \cdot 10^{-3}$	2568	$4.33 \cdot 10^{-3}$
G ^{final} (MPa)	$q_{ m gel}$ (-)	s ₀ (°C/MPa)	$T_{ m trans}$ (°C)		
590	0.4	0.394	10		

The Prony terms of the tensile relaxation modulus E(t) in [1] are used to determine the shear relaxation modulus:

$$G(t) = \frac{3K_{60}E(t)}{9K_{60} - E(t)},$$

where $K_{60} = 17136$ MPa is the bulk modulus at 60 °C(see equations 4.7, 4.8, and 4.9). By fitting equation 4.15 to that function, the following parameters are obtained with $G_{\infty} = G^{\text{final}} = 590$ MPa:

i	τ_i (s)	G _i (MPa)	i	τ_i (s)	G _i (MPa)
1	1.00E-20	6.56E+00	19	1.00E-02	5.77E+02
2	1.00E-19	1.49E+02	20	1.00E-01	3.86E+02
3	1.00E-18	9.61E+01	21	1.00E+00	2.70E+02
4	1.00E-17	8.37E+01	22	1.00E+01	2.06E+02
5	1.00E-16	7.22E+01	23	1.00E+02	1.70E+02
6	1.00E-15	7.11E+01	24	1.00E+03	1.53E+02
7	1.00E-14	7.52E+01	25	1.00E+04	1.42E+02
8	1.00E-13	8.19E+01	26	1.00E+05	1.39E+02
9	1.00E-12	1.02E+02	27	1.00E+06	1.40E+02
10	1.00E-11	1.23E+02	28	1.00E+07	1.49E+02
11	1.00E-10	2.12E+02	29	1.00E+08	1.54E+02
12	1.00E-09	3.78E+02	30	1.00E+09	1.78E+02
13	1.00E-08	8.45E+02	31	1.00E+10	1.45E+02
14	1.00E-07	1.12E+03	32	1.00E+11	2.16E+02
15	1.00E-06	1.07E+03	33	1.00E+12	2.26E+01
16	1.00E-05	1.24E+03			
17	1.00E-04	1.11E+03			
18	1.00E-03	8.28E+02			

REFERENCES

[1] J. de Vreugd, *The effect of aging on molding compound properties*, Ph.D. thesis, Technische Universiteit Delft (2011).



REGRESSION MODELS FITTING RESULTS

Minitab output for the linear regression model:

Factorial Fit: result versus K, Ginf, Gg, loga, qgel, qdot, ech

Estimated Effects and Coefficients for result (coded units)

Term	Effect	Coef	SE Coef	T	P
Constant		119.868	0.3292	364.08	0.000
K	1.438	0.719	0.3292	2.18	0.061
Ginf	1.062	0.531	0.3292	1.61	0.145
Gg	-0.213	-0.106	0.3292	-0.32	0.755
loga	-0.288	-0.144	0.3292	-0.44	0.674
qgel	-5.787	-2.894	0.3292	-8.79	0.000
qdot	-0.462	-0.231	0.3292	-0.70	0.502
ech	9.162	4.581	0.3292	13.91	0.000

S = 1.31693 PRESS = 55.4980

R-Sq = 97.21% R-Sq(pred) = 88.85% R-Sq(adj) = 94.77%

Analysis of Variance for result (coded units)

Source	DF	Seq SS	Adj SS	Adj MS	F	P
Main Effects	7	483.918	483.918	69.131	39.86	0.000
K	1	8.266	8.266	8.266	4.77	0.061
Ginf	1	4.515	4.515	4.515	2.60	0.145
Gg	1	0.181	0.181	0.181	0.10	0.755
loga	1	0.331	0.331	0.331	0.19	0.674
qgel	1	133.976	133.976	133.976	77.25	0.000
qdot	1	0.856	0.856	0.856	0.49	0.502
ech	1	335.794	335.794	335.794	193.62	0.000
Residual Error	8	13.874	13.874	1.734		
Total	15	497.792				

Minitab output for the linear model with two-way interactions:

Factorial Fit: result versus K, Ginf, Gg, loga, qgel, qdot, ech

Estimated Effects and Coefficients for result (coded units)

Term	Effect	Coef	SE Coef	T	P
Constant		119.868	0.006250	19178.86	0.000
K	1.438	0.719	0.006250	115.00	0.006
Ginf	1.062	0.531	0.006250	85.00	0.007
Gg	-0.213	-0.106	0.006250	-17.00	0.037
loga	-0.288	-0.144	0.006250	-23.00	0.028
qgel	-5.787	-2.894	0.006250	-462.99	0.001
qdot	-0.462	-0.231	0.006250	-37.00	0.017
ech	9.162	4.581	0.006250	732.99	0.001
K*Ginf	-0.062	-0.031	0.006250	-5.00	0.126
K*Gg	0.063	0.031	0.006250	5.00	0.126
K*loga	0.188	0.094	0.006250	15.00	0.042
K*qgel	-0.012	-0.006	0.006250	-1.00	0.500
K*qdot	0.212	0.106	0.006250	17.00	0.037
K*ech	-0.063	-0.031	0.006250	-5.00	0.126
Ginf*loga	-1.837	-0.919	0.006250	-147.00	0.004

S = 0.025 PRESS = 0.16

R-Sq = 100.00% R-Sq(pred) = 99.97% R-Sq(adj) = 100.00%

Analysis of Variance for result (coded units)

Source	DF	Seq SS	Adj SS	Adj MS	F	Р
Main Effects	7	483.918	483.918	69.131	110609.82	0.002
K	1	8.266	8.266	8.266	13225.00	0.006
Ginf	1	4.515	4.515	4.515	7224.29	0.007
Gg	1	0.181	0.181	0.181	289.03	0.037
loga	1	0.331	0.331	0.331	529.06	0.028
qgel	1	133.976	133.976	133.976	214361.59	0.001
qdot	1	0.856	0.856	0.856	1368.96	0.017
ech	1	335.794	335.794	335.794	537270.82	0.001
2-Way Interactions	7	13.874	13.874	1.982	3171.17	0.014
K*Ginf	1	0.016	0.016	0.016	25.00	0.126
K*Gg	1	0.016	0.016	0.016	25.01	0.126
K*loga	1	0.141	0.141	0.141	225.02	0.042
K*qgel	1	0.001	0.001	0.001	1.00	0.500
K*qdot	1	0.181	0.181	0.181	288.99	0.037
K*ech	1	0.016	0.016	0.016	25.00	0.126
Ginf*loga	1	13.505	13.505	13.505	21608.18	0.004
Residual Error	1	0.001	0.001	0.001		
Total	15	497.792				



ACKNOWLEDGEMENTS

This thesis would not have been possible if it was not for the help of others. I would like to express my sincere gratitude to everybody whose support brought me here.

I would like to thank Rinze Benedictus, head of the Structural Integrity and Composites Group (SI & C) at TU Delft, for promoting the PhD project and for believing in me. Thank you Jos Sinke for your calm and steady guidance, especially during the turbulent times. Thank you Ian Richardson for staying involved in the PhD project the entire time. Your ideas and remarks were invaluable. I thank Kaspar Jansen for the stimulating discussions and the support with the DSC and the DMA. I would also like to thank the industrial partners inpro Innovationsgesellschaft für fortgeschrittene Produktionssysteme in der Fahrzeugindustrie mbH (inpro, Berlin, Germany) for initiating the project and Tata Steel for joining the project later on. I thank Kim Kose (inpro) for the visits to Delft, valuable discussions and the support with the UMAT subroutine, and Jurgen Vrenken (Tata Steel) for the helpful remarks on my research and for providing materials. I thank Dow Automotive for providing the adhesive system. I also thank Andreas Zeiser (inpro) who sparked my interest in UMAT unit testing.

I would like to thank the Materials innovation institute (M2i), for creating an excellent environment that facilitates your research and lets you focus on it, and for the assistance in overcoming all the obstacles that come with a PhD abroad. Special thanks go to Monica Reulink who gave my worries and requests always the highest priority. Pursuing a PhD comes with many non-research related hurdles to take. I thank Gemma van der Windt who solved most of these issues and offered great support for handling the others.

I thank the technicians from the TU Delft laboratories who helped me with my experimental work, especially Johan Boender, Berthil Grashof, Misja Huizinga, Ben Norder, Frans Oostrum, Kees Paalvast, Ed Roessen, Bob de Vogel, Hans Weerheim and Lijing Xue. I thank my colleagues from the SI & C Group and the Delft Aerospace Structures & Materials Laboratory for many precious discussions, on and off topic, and for the coffee breaks at the *koffietafel* or outside while enjoying the Dutch weather: Adrian E, Adrian L., Alfonso, Bea, Bernhard, Cory, Daniel, Derek, Dimitrios, Eduardo, Fabricio, Freddy, Freek, FX, Greg R., Greg W., Gustavo, Helena, Huajie, Ilhan, Ilias, Jarret, John-Alan, Lei, Lucas, Marcelo, Maria Luisa, Maro, Mayank, Milan, Mladen, Morteza, Nat, Nicholas, Niels,

128 ACKNOWLEDGEMENTS

Nikos, Patricio, Riccardo, Sofia, Srikanth, Tian, Wandong, Yao and Zahid.

I also thank my Delftian friends for making my stay such a fun and memorable experience: Alejandra, Christina, Elta, Jesus, Joana, Jörn, Marie, Maruti, Mina, Pooja, Romain, Sarav and Yaiza. I thank Maria for listening and for the nightly discussions in front of the Board of Honour. And last but not least, thank you Danai for your patience, support and cheerfulness. You helped me putting my work back into perspective when I was running the risk of losing my head over it ("if your thesis is your only problem, your life is perfect"). Thank you for that.

CURRICULUM VITÆ

Konstantin Priesnitz

28-10-1982 Born in Berlin, Germany.

WORK EXPERIENCE

2015–present Researcher

Karlsruher Institut für Technologie, Germany

2010–2014 PhD researcher

Materials innovation institute (M2i)

Technische Universiteit Delft

2010 Development engineer

inpro Innovationsgesellschaft mbH, Berlin, Germany

2002–2003 Alternative civilian service

Vereinigung für Jugendhilfe gGmbH, Berlin, Germany

EDUCATION

2003–2009 Diploma

Physikalische Ingenieurwissenschaft Technische Universität Berlin, Germany

1995–2002 Secondary school

Katholische Schule St. Marien, Berlin, Germany



LIST OF PUBLICATIONS

- K. Priesnitz, K.M.B. Jansen, J. Sinke, and R. Benedictus, Simulation of the development of local panel distortions due to hot-curing adhesives, Journal of Materials Processing Technology 225, 405 (2015).
- 4. **K. Priesnitz, J. Sinke, and R. Benedictus**, *On the simulation of panel distortions due to hot curing adhesives*, International Journal of Solids and Structures **51**, 2470 (2014).
- 3. **K. Priesnitz, J. Sinke, and R. Benedictus**, *Influence of the temperature cycle on lo- cal distortions in car panels caused by hot curing epoxies*, International Journal of Adhesion and Adhesives **50**, 216 (2014).
- 2. **K. Priesnitz, J. Sinke, and R. Benedictus**, *Distortion in polymer-metal hybrids due to adhesive bonding*. M2i Conference 2013, oral presentation.
- 1. **K. Priesnitz, J. Sinke, and R. Benedictus**, *Simulation of chemically and thermally induced distortions in adhesive bonds*, Adhesive Bonding 2013, oral presentation.